European **S**ynchrotron **R**adiation **F**acility
INSTALLATION EUROPEENNE DE RAYONNEMENT SYNCHROTRON

Beamline Review, November 4-5, 2008

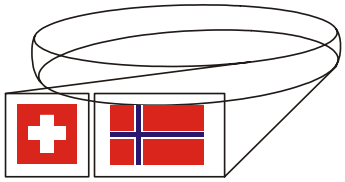

Swiss-**N**orwegian **B**eam **L**ines

●

Multifunctional beam lines for complex in-situ XRD and XAFS experiments

September 2008

The present report provides an overview of the Swiss-Norwegian Beam Lines, its activity during the three-year period 2005-2007 and the options for the future development of the project. Two key factors account for the success of this bi-national facility. First of all, there is the proactive role of the users in helping to shape the strategy of its development: both in terms of the technical specifications and equipment of the beamlines and also in defining the ideology and goals of the facility. The second definitive factor is the competence and motivation of the beamline staff in making technical improvements, analysing the trends in the evolution of the user community, suggesting solutions to ensure further progress, and, last but not least, providing a high-quality service on the beam lines.

Contact with the user community in Switzerland and Norway has been a high priority throughout this period. Several SNBL workshops have been organized in Grenoble covering the interests of our users. These workshops have provided an ideal opportunity for us to listen to the present and future needs of our users, and to promote SNBL as a forum for information exchange between user groups. The last of these workshops attracted over 80 participants, and will be followed up by another meeting on the same theme which will take place in two years at SOLEIL.

It is our goal to provide a facility which can both fulfil the existing requirement of our users, and can offer opportunities to carry out new, exciting and technically challenging experiments. With the aid of the strong financial support from our funding agencies, and with the availability of additional resources coming directly from our users, we have been able to deliver a reliable and attractive pool of equipment well-matched to the needs of our users.

Our users and partners have had many occasions to benefit from and to appreciate the “team style” of working at SNBL. This report is also the result of collective work, and the full list of the authors is given in the chapter “SNBL staff”.

V. DMITRIEV, P. PATTISON, H. EMERICH

BEAM LINES REVIEW PANEL 2004:
Recommendations and Actions

The preceding review of SNBL took place in 2004. The principle recommendations of the Review Committee and the actions taken after review were:

- **Reduce the variety of experimental activities at the beamline and concentrate on the high-energy experiments.**

  The question of the optimal configuration of the beam lines and the direction of further development, together with its technical and financial aspects, were considered in detail by the SNBL management following the beamline review. The final decision was formed after discussions with our user community; it had strong links to their research strategy, and aimed to providing the most appropriate assistance to their projects, both those already running and others still in planning. The beam lines were seen as multifunctional, dedicated to complex in situ experiments requiring a combination of diffraction and spectroscopic techniques. This approach received full support from both the SNX Council and national science foundations. The decision taken three years ago seems to be bearing fruit both in terms of the quantity and the quality of publications emerging from SNBL. The trend towards high energy experiments was recognised, and appropriate steps have been taken to extend the spectral range of the optics on the beamlines.

- **Continue development of combined techniques.**

  We have been able to purchase and install our own dedicated Raman spectrometer on the beamline in 2007. Fibre-optic connections to both experimental hutches make it possible to collect in-situ Raman data simultaneously with X-ray diffraction and XAS under a wide variety of experimental conditions. The availability of a dedicated and complex gas mixing system, together with an on-line mass spectrometer, facilitate in-situ experiments.

- **A stronger in-house program should be established.**

  SNBL staff members are successfully developing several strong programs in material science and instrumentation. The SNBL team are actively following both possible routes to develop an in-house program of research, i.e. by submitting proposals for peer-review (SNBL and ESRF) and also by using effectively the limited beam time allocated for in-house research. Some of the results of this activity are presented in the section "V.2 In-House Research".

- **Better relationships should be established, and maintained, with SLS and MAXLAB.**

  Close collaboration has been established with SLS, including exchange of expertises in research and instrumentation. SLS and SNBL are considered as complimentary facilities for Swiss users with the accent on using the advantages of ESRF machine as a source of hard X-rays. First steps toward linking SNBL and MAXLAB have been made: SNX representatives took part in several MAXLAB events (see section "IV.5 SNBL Collaborations").

CONTENTS

I. INTRODUCTION

The mission of the Swiss-Norwegian Beam Lines at ESRF (SNBL) is to provide scientists from both Norway and Switzerland, from both academia and industry, with increased access to synchrotron radiation. A user on SNBL has access to state-of-the-art, custom-designed instrumentation for diffraction and absorption experiments. Both partner countries have relatively large and exceptionally active scientific communities using X-ray diffraction and absorption as their main probes; for these groups the amount of public beamtime offered by ESRF was insufficient from day one, and this is the *raison d'être* of the Swiss-Norwegian Beam Lines at ESRF. To circumvent this potential bottleneck, the Swiss and Norwegian scientists formed in 1990 a consortium and applied for access to a bending magnet port at ESRF.

Strong, long-term financial support was pledged by the Norwegian Research Council and the Swiss National Science Foundation, with substantial contributions coming from universities concerned. On the Swiss side, the foundation's support was intended to raise interest amongst the Swiss scientific community in the benefits of hard synchrotron radiation, with the goal to contribute to the creation of a SR user community and to prepare it for the use of a Swiss synchrotron light source. The realization of this bi-national facility aimed as well at providing scientists from the two partner countries with instruments custom-built for their own specific needs. Initially, the Swiss-Norwegian facility was planned as a single multi-purpose line. However, in the interest of increased operational efficiency and to attract an even wider user community, the consortium soon decided to split this single line into two branch lines: one dedicated to single-crystal diffraction and the other to powder diffraction, EXAFS and topography. The split-beamline design also permitted to optimize the x-ray optical configuration for the two types of experiments, scattering and absorption.

The facility started to operate in the fall of 1994. First on-line was the high-resolution powder diffractometer, and then followed: a single-crystal diffractometer, an image plate system, an EXAFS spectrometer, and, finally, a newly developed high-resolution single-crystal diffractometer, specially conceived to carry heavy loads. All of this instrumentation was commissioned with users.

The SNBL currently has four different experimental techniques, which are distributed over two beamlines, and include:

- High-resolution single-crystal diffractometry
- Large-area imaging for x-ray diffraction and scattering
- High-resolution powder diffractometry
- XAFS spectrometry.

II. FUNDING and ORGANISATION

II.1 Funding and Governing Bodies

The two funding organisations of the SNBL project are Swiss State Secretariat for Education and Research (SER) and Norwegian Research Council (NSR) who contribute equally to the operation costs. The Norwegian contribution consists of two equal parts providing by NSR itself and by Norwegian universities. Until and including the year 2007, the SNBL budget was considered and approved by the funding agencies on annual base. In the three-year period 2005-2007 it was €3'610'000 in total, including €2'900'000 according to the Swiss-Norwegian contract and an additional €710'000 outside the contract. The latter contains contributions from several Swiss and Norwegian institutions and was earmarked for specific projects (such as the Raman project, for example). Since 2008, both funding agencies, SER and NSR, opted for a 4-year budget, and the current SNBL budget under the terms of the Swiss-Norwegian contract is €4'400'000 for the four-year period 2008-2011.

The Cooperation Agreement and Memorandum of Understanding signed by Swiss and Norwegian sides, which is reconsidered and renewed every 4 years, is a legal basis for the existence of SNBL and its funding. The current Agreement is valid for the period 2008-2011. The organisation chart of the bi-national facility is shown in Fig. II.1.

The *Swiss-Norwegian Foundation for Research with X-rays (SNX)* is a federally registered Swiss foundation established in 2004. The foundation is a governing body for SNBL. It also acts as the legal body *vis-à-vis* the ESRF. The SNX affairs are handled by a seven-member council (SNX Council) consisting of three Swiss and three Norwegian members, with one member, the SNBL Director, functioning as the Executive Director of the foundation but having no voting right. One observer each from SER and NSR attend the council meetings which take place twice a year.

The *Association Swiss-Norwegian Grenoble* is a French association, which employs all Grenoble-resident staff. It is run by a three-member board, with the SNBL Director as its President, and SNX Chair and Vice-Chair as members.

II.2 Beam time allocation procedure

The SNX Council also acts as a Proposal Review Committee to SNBL. It allocates 2/3 beam time available for users at any run. Decision on a proposal is taken on the basis of a report communicated by one of the SNX Council members and a report submitted by an independent anonymous referee (non-Swiss, non-Norwegian), selected by the BL Director. The 1/3 of the beamtime that has, in accordance to the ESRF-SNX contract, to be made available to general ESRF users falls under the remit of the general ESRF beamtime allocation panels and ESRF directors.

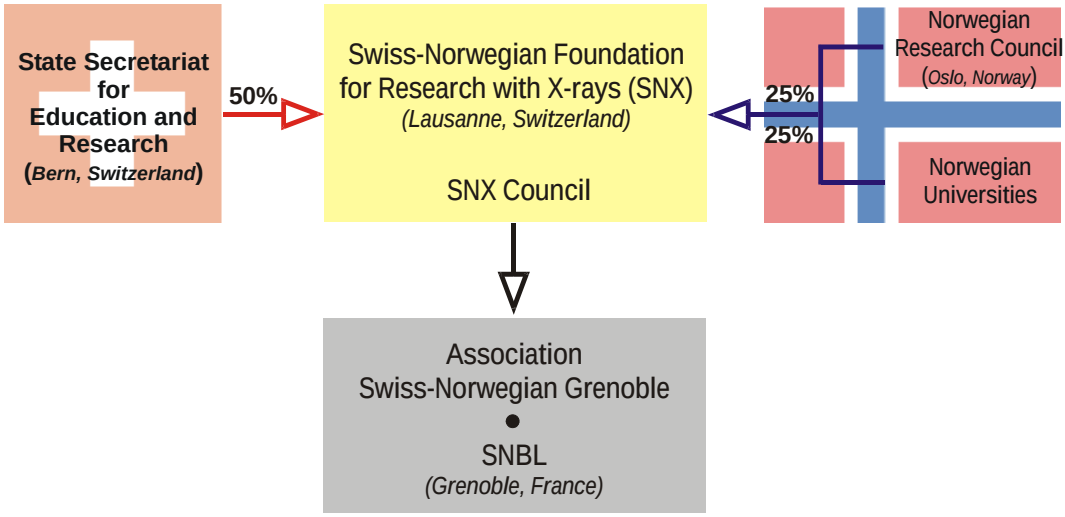

***Figure II.1**. Block diagram of the organisational structure of SNBL.*

The SNX Council established three classes of proposals for SNBL in 2005:

- *Standard Research Proposals*
- *Long Term Project Proposals*
- *Urgent Research Proposals*

In addition to the standard proposals typical for ESRF and other CRGs, SN users may request a long-term commitment from the SNBL to provide beamtime during up to four successive scheduling periods (two years). A given user group cannot operate more than one Long-Term Proposal (LTP) in the same period. The percentage of LTPs is limited to 1/3 of beamtime available for SNBL.

SN users may request as well an urgent commitment to provide beamtime within a maximum of three months of submitting a proposal. The special status of an Urgent Proposal should be clearly justified. Time requested should not exceed 6 shifts. The percentage of Urgent Projects is limited to 5% maximum of the beamtime available for SNBL and is designated as Director's discretionary beamtime. No fixed deadlines are made for such proposals. If approved, beamtime is normally allocated within 2 months of the proposal date. The UP undergoes a two-step appraisal procedure, the first step being performed by the SNBL Director, who makes a preliminary evaluation as to the urgency of the project, and its scientific quality, and the second step carried out by the competent SNX Council member.

III. TECHNICAL DESCRIPTION OF THE BEAM LINES

III.1 General Layout and X-ray Optics

The ESRF delivers a 6mrad wide fan of synchrotron radiation to SNBL from bending magnet BM01. A water-cooled aperture plate at the entrance to the Optics Hutch (26m from the source point) divides this beam into two parts of width 2.5mrad and 1.0mrad, with a gap of 2.5mrad between the two beams. The fan of 2.5mrad width supplies the photons to BM1A, while the 1.0mrad beam provides the synchrotron radiation to BM1B. SNBL has been designed from the onset to allow both lines to operate simultaneously, and with a minimum of interaction between the X-ray optics, vacuum system, shielding and controls for each branch line. There are three leaded hutches in series. The first hutch (Optics) contains the majority of the optical components for both branch lines (Figs.III.1-2). These include two mirrors and a monochromator for BM1A, two separate monochromators for BM1B, as well as various slits, beam position monitors, station shutters, valves and other vacuum components. Although the X-ray optical configurations of both beamlines are fairly conventional, the space restrictions have been a major technical challenge. The available space between the two fans of synchrotron beam which pass through the Optics Hutch is only about 70mm, yet our goal is to operate the two beamlines independently. The two Experimental Hutches are arranged sequentially down the beamline, with the vacuum pipework for BM1A passing through the BM1B Hutch (and through the data acquisition cabin). Two major instruments are positioned in each of the two Experimental Hutches. In BM1A, there is a heavy duty multi-axis diffractometer followed by a large-area image plate detector. BM1B is equipped with a high resolution powder diffractometer and an EXAFS spectrometer. A detailed description of the instrumentation is given below.

The optical configuration of BM1A is a conventional arrangement of vertically collimating mirror, followed by a double crystal Si(111) monochromator and a vertically focusing mirror. The beamline can be configured to operate without mirrors (in order to access higher X-ray photon energies, for example), although some manual realignment of the beamline components is necessary for the changeover. In normal operation, the Rh-coated mirrors provide vertical focusing and harmonic rejection while a sagittally bent second crystal makes the horizontal focusing. It is also possible to interchange the second crystal bending mechanism with a flat crystal mount, if a highly parallel beam is required. The first crystal of the monochromator is water-cooled, as is the first mirror. The mirrors both have a fixed radius of curvature, and the optimum focal spot is roughly circular with a FWHM of about 300 microns. The excellent mechanical and thermal stability of the X-ray optics (at least up to the present maximum current of 200mA) allows us to operate the beamline without a feedback mechanism. Most experiments are carried out in the spectral range from about 10 keV – 20 keV, although higher energies can be accessed if the mirrors are removed. In line with the recommendations of the last beamline review, and following the requests of our user groups, we aim to extend the spectral range of the beamline while maintaining the focussing option. This goal can be achieved by reducing the grazing angle of incidence of the synchrotron beam onto the

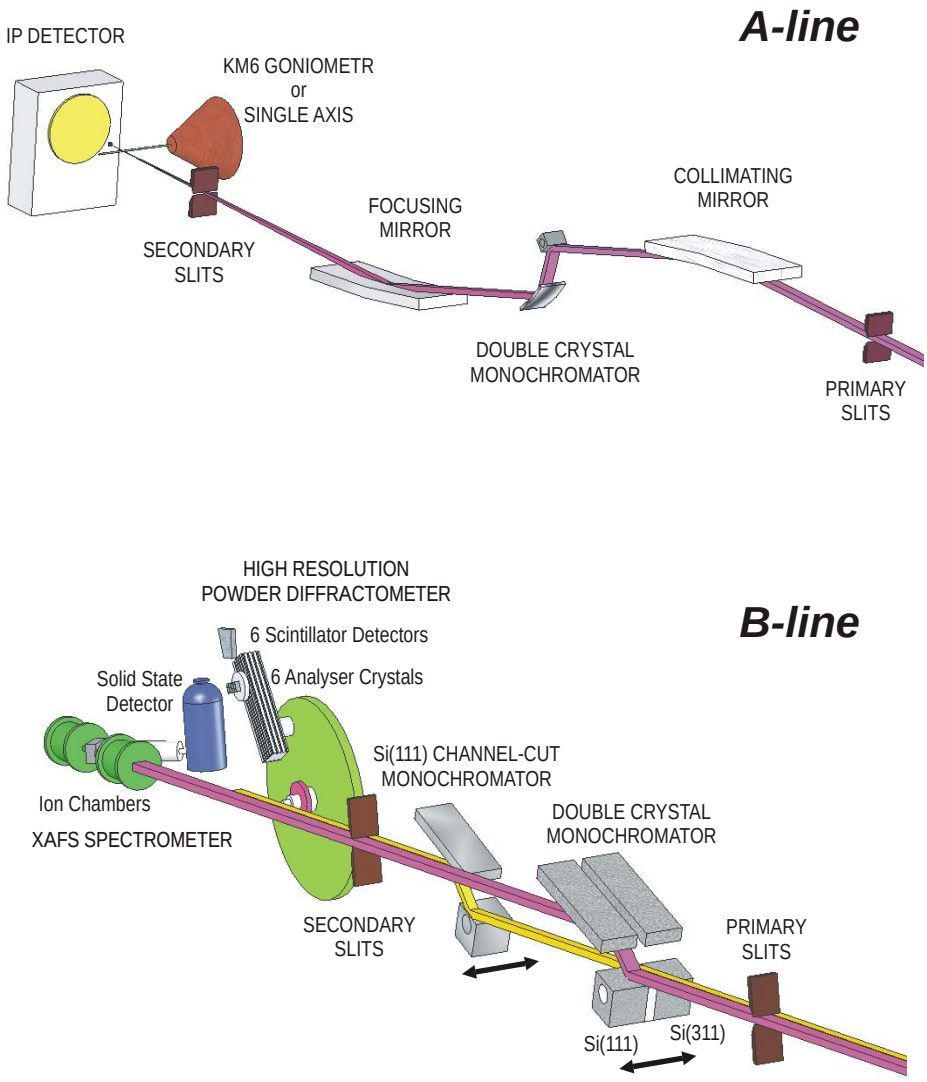

Figure III.1. *Schematic layout of the SNBL Optics*

Figure III.2. *General view of the Optics Hutch*

mirrors from the present value of 3mrad down to 2.5mrad or possibly lower. Although this will involve some loss of total flux in the focussed beam (because of the reduced fraction of the synchrotron beam intercepted by the mirrors), these losses will be offset by the gain in spectra range delivered to the users. It is our goal to extend the spectrum of the focussed beam up to at least 25 keV, and if possible to 30 keV. After several years of operation within the high radiation environment of the monochromator, the motors which drive the sagittal bending mechanism failed due to radiation damage. These DC motors have now been replaced with mechanically more precise (and more reliable) micro-stepping actuators. The more accurate control of the crystal bender has already allowed us to improve the focal quality and hence increase the flux density in the focussed beam.

BM1B is dedicated to High Resolution Powder Diffraction (HRPD) and EXAFS experiments. A considerable effort has been devoted to the goal of combining these two techniques into quasi-simultaneous measurements. In order to achieve this aim, we have built and integrated two independent, water-cooled monochromators into the optics enclosure (Fig.III.3). This allows us to

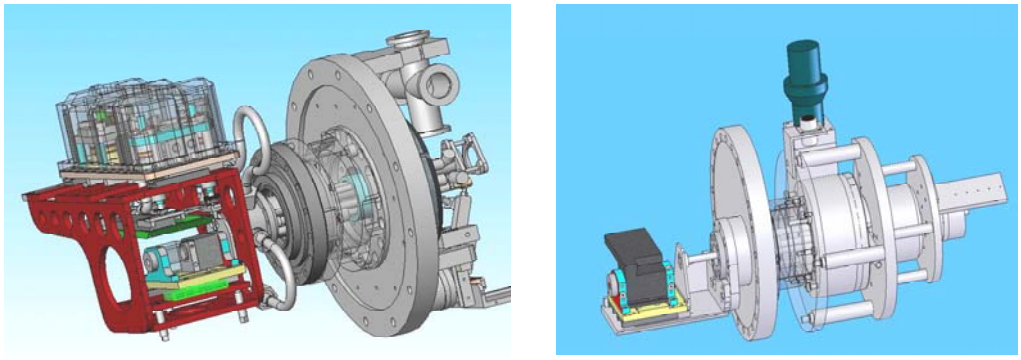

Figure III.3 *Schematic drawings of the two monochromators on the BM1B branch line*

automatically swap between the respective monochromators and hence from HRPD to EXAFS (and vice versa) within a few seconds.

The first monochromator is an unfocused double-crystal monochromator dedicated to EXAFS measurements. It consists of two crystal pairs, Si (111) and Si (311) orientation, mounted on a slide transverse to the incoming beam. By means of this slide, one can quickly choose between the Si(111) and the Si(311) crystal pair, or alternatively select a position that lets the white beam pass by between the two crystals. It is in this configuration that the white beam can reach the following monochromator, which is a Si(111) channel-cut dedicated to High Resolution Powder Diffraction. This channel-cut crystal is again mounted on a transverse slide such that it can be easily moved out of the beam in case that the beam from the first monochromator for EXAFS experiments is required. When using the EXAFS monochromator, one can quickly choose between the Si(311) high resolution and Si(111) high flux crystal pair. A swap can be performed within a few minutes only (including calibration).

III.2 Beamline BM1A

After passing through a set of secondary slits within the experimental hutch, the focused synchrotron beam can be delivered to either a multi-axis heavy-duty single crystal diffractometer (KM6 supplied by Oxford Diffraction Ltd) or to the MAR345 Image Plate manufactured by MarResearch GmbH. The MAR345 instrument allows only a single rotation axis for the sample, and a slide provides variable distance between sample and detector. The diameter of the X-ray sensitive plate is 345mm, and a pixel resolution of either 100 or 150 microns can be selected by the user. The KM6 instrument is a κ-diffractometer with the conventional 3 sample rotations (κ, ω and φ) and the detector angle θ. In addition, the diffractometer is mounted on two further rotation tables (ω' and θ') giving an additional degree of freedom to the orientation of both the sample and the detector.

Figure III.4. *Example of an in-situ experiment carried out on the KM6 diffractometer*

The KM6 multi-axis diffractometer incorporates both a point detector and a large area CCD detector onto the detector arm. The combination of movements available on the KM6 allows us to position the sample in an arbitrary orientation relative to the incoming synchrotron beam (and hence also to its polarization vector), and also to choose freely the angular coordinates of either of the X-ray detectors. This instrument provides a completely generalized platform on which to collect diffraction data. It can be configured either as a vertical or as a horizontal diffractometer, or indeed anywhere in between these scattering planes. Complete surveys of reciprocal space can be rapidly completed using the area detector, while the point detector provides the opportunity to investigate the profiles of individual reflections with high angular resolution. Information concerning the crystal orientation matrix and the diffractometer parameters can be passed smoothly from point detector to area detector configurations. The relatively open architecture of the kappa diffraction geometry is well-suited for the installation of ancillary equipment around the sample. The Figure III.4 illustrates an in-situ diffraction experiment involving laser excitation of a photo-induced structural phase transition observed at He temperatures.

Apart from a refurbishment of the MAR345 detector, together with some improvements to the optical microscope setup, our image plate system has remained relatively unchanged over the last 5 years. We are now approaching the impressive statistical threshold of 500,000 readout cycles of the image plate. Our efforts have concentrated rather on developing and improving the infrastructure around the sample environment for in-situ experiments. Several types of gas-mixing and gas flow controllers have been used in combination with the image plate detector and the Raman spectrometer. Our upper limit, at present, for gas pressures is around 100 bar (Fig. III.5), but we wish to extend this pressure range up to at least 200 bar in the near future (with our ultimate goal of reaching 700 bar H_2 pressure).

Figure III.5*. Instrumentation for high gas pressure experiments*

Amongst the most successful and productive of the techniques which the advantage of the high efficiency and sensitivity of the image plate detector are the high pressure experiments using diamond anvil cells (DACs). These experiments already take up about

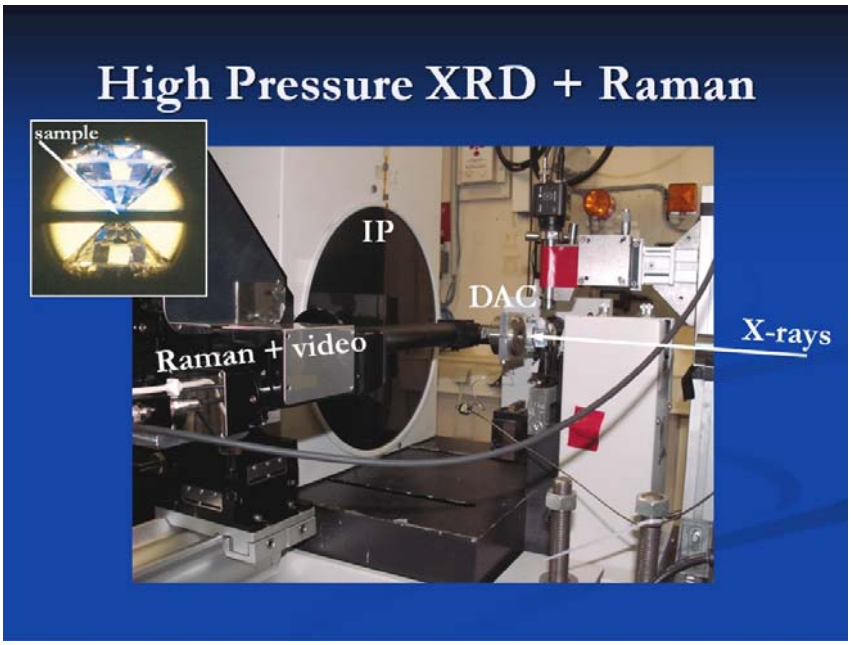

Figure III.6*.Combined high pressure powder diffraction and Raman experiment on the MAR345*

10% of the available beamtime on BM1A, and the demand is increasing. A very interesting development concerns the combination of high pressure DAC experiments with the Raman spectrometer, as illustrated in Fig. III.6.

III.3 Beamline BM1B

III.3.1. The Two Axis High Resolution Powder Diffractometer (HRPD)

The workhorse of the B-station is a two circle powder diffractometer (theta being the outer arm and omega being the inner circle to which the sample is attached. The theta circle is fitted with an array of 6 Si(111) analyzer crystals in front of a second array of 6 scintillation counters (Fig.III.7). An analyzer crystal/photomultiplier pair forms one channel. Great care has been taken in order to reduce the angular distance between the channels to a minimum. To do so, the scintillation counters had to be tailor-made (OD 12mm) to allow for a close spacing of 1.1 degrees between two adjacent channels. A second point of consideration was the possibility to reach energies above 30keV. Therefore the scintillator crystals of NaI(Tl) were optimized for efficient photon absorption at high energies. The analyzer set-up consists of a supporting plate holding all six crystals which can be mounted and rotated individually. The supporting plate itself is fixed onto a precision rotary table in order to adjust the Bragg-angle of all analyzer crystals in one rotary motion only. The scintillation counters are assembled to one block, which is mounted onto a second rotary table. Changing the wavelength implies therefore a change of the Bragg-angle of the analyzer array, and a subsequent change of the detectors of twice the Bragg-angle of the analyzer crystals. It takes typically a less than one hour to change from one wavelength to another including a silicon calibration run.

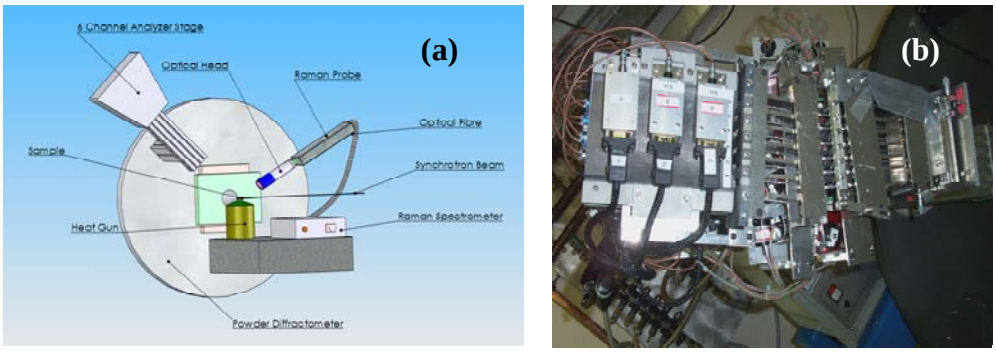

Figure III.7*. (a) Schematic set-up of the Diffractometer when used in combination with our Raman Spectrometer. (b) Close-up of the analyzer crystal/photomultiplier array. All channels are separated by Soller slits*

Both circles can be run individually (i.e in a HRPD run where the sample is spun by an independent sample spinner (omega table stationary) – or in a synchronized way (omega/2theta) which is mainly used for measurements in reflection mode.

III.3.2. The EXAFS Spectrometer

A) Transmission Measurements

Presently BM1B is equipped with a set of three ion chambers (Hasylab design) for I_0, I_t, I_{ref} respectively. We also possess a small, dedicated gas mixing rack that allows us to change the gas fillings of the ion chambers within a few minutes.

B) Fluorescence Measurements

With additional joint funding from the Swiss and Norwegian partners, we could acquire a 13-element Ge(Li) solid state detector, including the digital acquisition electronics (XIA), in 2003 [Fig.III.8(a)]. This detector is frequently used for highly diluted or non-transparent samples.

III.3.3. Raman

A strong point of SNBL lies in the use of a combination of techniques. This is particularly important for in-situ experiments. In order to understand complex dynamic processes, a maximum of information has to be collected simultaneously. With HRPD being a technique allowing us to measure the long range order and EXAFS being a tool for probing the local structure, vibrational spectroscopy is an ideal non-destructive tool for probing length scales in between these two extremes. Obviously there are additional complementarities to be exploited depending on the system studied. One could cite the different sensitivities of these techniques on surface/bulk or particle size properties. Furthermore, Raman spectroscopy can be applied simultaneously and independently from EXAFS and PD and adds valuable information to a vast number of experiments. The acquisition of a two color (green, red) research grade Raman spectrometer in 2007 made this dream come true. The spectrometer

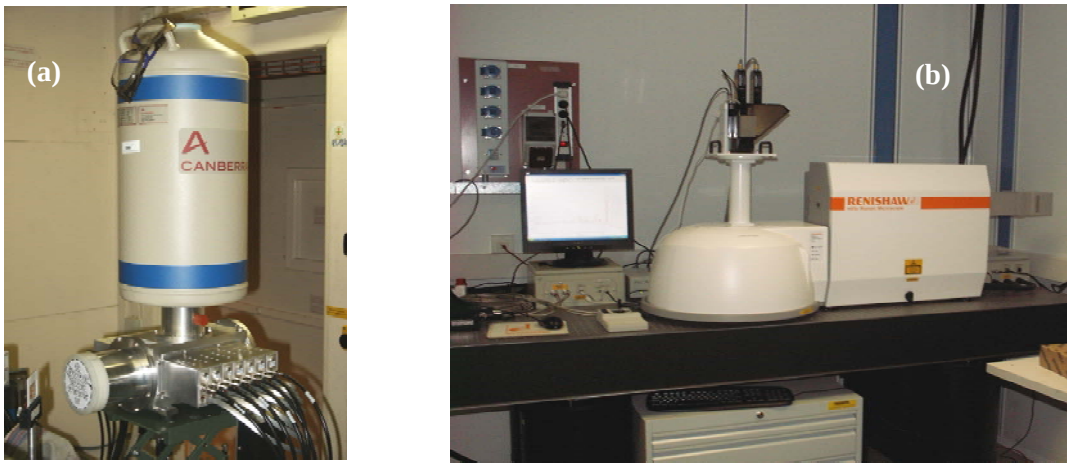

Figure III.8. *(a) The 13 element solid state detector*
(b) The Raman spectrometer as mounted in the sample preparation room

resides in our sample preparation room at the end of the beamline [Fig.III.8(b)]. Long optical fibers allow us to link the lasers and the spectrometer to the optical heads in both Experimental Hutches, or, alternatively in the sample preparation room as a stand alone device.

III.4. Auxiliary equipment available for both beamlines

A. Cryostats

As far as possible we try to adapt our equipment to the need of combining different techniques. As a practical consequence we design our sample environment to be as open and accessible as possible. One example is our He-flow cryostat. By designing the cryostat around our needs, we are in a situation where we can apply all our techniques (Diffraction+EXAFS+Fluorescence+Raman) down to temperatures of 4.5K. An additional, miniature He-flow cryostat has recently been purchased for the KM6 diffractometer, and this cryostat is now being commissioned.

B. Gas mixing and gas flow control

The last year we have also developed together with our user community a gas mixing, flow and measuring system. This system is also fully integrated in the beamline and can distribute gasses to both of our experimental stations. It is a very flexible system capable of adapting to the needs of our wide user community. All gas bottles are stored outside the Experimental Hutches, and a total of 6 different gasses can be supplied via stainless steel pipework to both beamlines. The gas mixing and control system can be completely remote controlled (Figs.III.9-10). A mass spectrometer is permanently installed to characterize the gases released after the in-situ reaction. A variety of micro-reaction cells are available for gas pressures up to 100 bar. The majority of the funding for this equipment came from the Catalysis Initiative sponsored by the Norwegian Research Council.

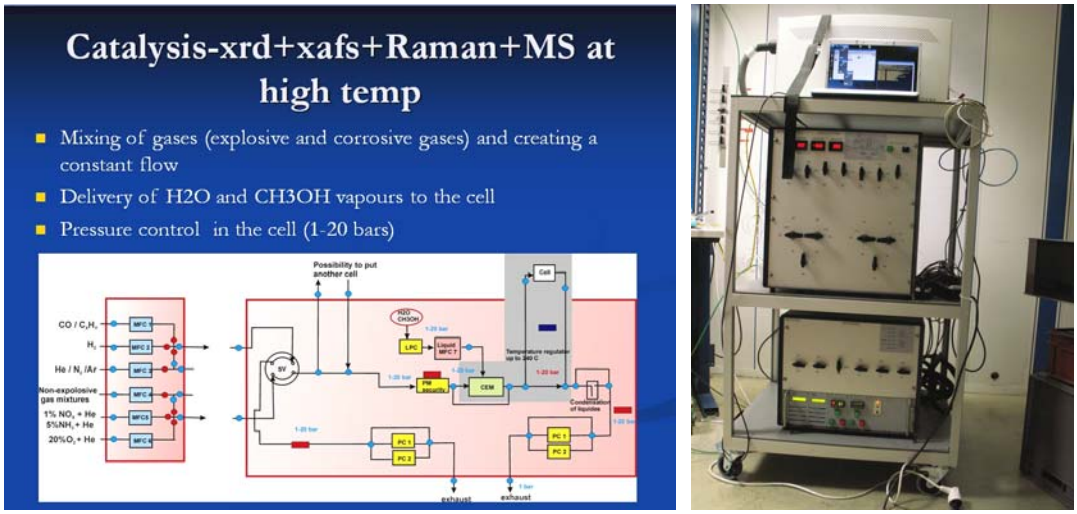

Figure III.9. *Gas mixing and flow control system (including mass spectrometer).*

Figure III.10. *The array of gas bottles outside the experiment hutches, and the gas mixing system designed for high gas pressures installed on the MAR345 image plate setup*

III.3.5 Acquisition Software

The increasing complexity of experiments and the flexibility needed to cater for quicker and combined experiments lead us to adopt SPEC as data acquisition software on BM1B in 2004. It also brought the advantage to have direct support from the ESRF software group in order to integrate new instruments and devices. This choice has turned out to be extremely fruitful be it in terms of recently added functionalities (speed, data logging, scanning modes) or in the light of speeding up and synchronizing different measurements or external parameters. As part of the general refurbishment of the beamline, BM1A has now also adopted SPEC for beamline instrument control.

IV. SNBL OPERATION: on the beamlines and beyond

IV.1 BL staff

A beamline operation depends to a large extent on the staff – its flexibility, motivation, expertise and scientific interests. The following list introduces the SNBL team members and indicates their functions.

Dr. Vladimir DMITRIEV - *Project Director* - Has overall responsibility for and authority over SNBL's daily operation, as executive director of the SNX Foundation, member of its Council and chairman of ASNG (at SNBL since 1999, from January 2005 as a Director). Assists users in the performance of their experiments. Scientific interests include experimental (x-ray diffraction and Raman spectroscopy) and theoretical (symmetry analysis and phenomenological theory) study of phase transitions in condense matter; high-pressure/high-temperature study of metals, minerals and inorganic compounds.

Dr. Philip PATTISON - *Senior Beamline Scientist (A-Station), Deputy Director of SNBL* - Responsible for all scientific and technical aspects of the operation, planning, scheduling and development of beamline BM1A (1991). Assists users in the performance of their experiments. Scientific interests: Applications of synchrotron radiation to crystal chemistry and solid state physics; Design and development of X-ray optics for synchrotron beamlines.

Dr. Dmitry CHERNYSHOV – *1st Beamline Scientist at BM1A* - Assists users in the performance of their experiments, participates in the development of beamline BM1A (2005). Scientific interests cover field of phase transitions in molecular crystals induced by temperature, pressure, light irradiation, and physics of neutron and synchrotron scattering on periodic structures in general.

Dr. Yaroslav FILINCHUK – *2nd Beamline Scientist at BM1A* - Assists users in the performance of their experiments, participates in the development of beamline BM1A (2006). Scientific interests are in the field of materials for hydrogen

storage such as metal hydrides and light chemical hydrides, coordination compounds, diffraction studies (powder and single-crystal) of their structure, phase transitions and reactivity.

Mr. Herman EMERICH - *Senior Beamline Scientist (B-Station*) - Responsible for all scientific and technical aspects of the operation, planning, scheduling and development of beamline BM1B (1993). Assists users in the performance of their experiments. He has strong interest in development and instrumentation and applying these advancements in collaboration with independent research groups. Amongst other collaborations is an ESRF LTP for the study of ancient art pieces by means of powder diffraction, EXAFS and Raman.

Mr. Wouter Van BEEK - *1st Beamline Scientist at BM1B* - Assists users in the performance of their experiments, participates in the development of beamline BM1B (1997). Has a strong track record in instrumental developments, e.g. multiple technique approaches under a wide variety of external stimuli. His research interests are focused on the study of phase transitions, synthesis and catalytic processes with the aim to use the newly created opportunities to its full scientific potential.

Dr. Olga SAFONOVA – *2nd Beamline Scientist at BM1B* - Assists users in the performance of their experiments, participates in the development of beamline BM1B (2006). Scientific interests: mechanisms of reactivity of heterogeneous catalysts (supported metal nanoparticles, mixed oxide catalysts for selective oxidation) and gas sensor materials under *in situ* conditions using XAS, XRD, and Raman spectroscopy.

Dr. Olga BANDILET – *Computer Engineer* (0.25).

Mrs. Chantal HEURTEBISE - *Administrative manager* - Handles general office work; administrates all accounting operations; secretary of the SNX Council (1999).

Technician – Position vacant (selection procedure in progress)

Former members (2000-2008)

Dr. Hans-Peter WEBER – Project Director (1990-2004)
Dr. Jon Are BEUKES – PostDoc (2000-2004)
Dr. Silvia CAPELLI – PostDoc (2000-2003)
Dr. Denis TESTEMALE – PostDoc (2003-2005)
Mr. Olexii KUZNETSOV – PhD Student (2001-2004)
Mr. Denis MACHON – PhD Student (2001-2004).
Mr. Marc PISSARD – Senior Technician (2000-2008)

IV.2 SNBL In-house research activity

Several programs in scientific research and instrumentation development are currently being carried out at SNBL by its staff. In the technical description of the beamline, some aspects of the innovative solutions in instrumentation and beam line design were presented. Two EU collaborative projects, with the participation of several groups from European universities, aim to design, construct and commission new high-pressure/high-temperature diamond anvil cells for studying the transport properties of material under extreme conditions, and for single-crystal X-ray diffraction at high pressure and temperature.

The research programs in the study of new materials for energy storage and the chemistry of storage processes in framework structures, as well as new classes of multiferroic materials have been successfully carried out by the SNBL team. The staff has published their own original research in 20 papers in the period 2005-2008 in peer-reviewed international journals (underlined in the list of Appendix A), as well as participating as co-authors in many other publications. Some of the publications by in-house staff have been highlighted by reviewers and editors: the papers no. 2008-14 and 2008-17 (see Appendix A), reported on crystal structures, their stability, and the phase diagram of $LiBH_4$ were published as a *Very Important Paper* in Angewandte Chemie Int. Ed., and as an *Editors' Suggestion* in Physical Review B. The paper on colossal, pressure-induced lattice expansion of graphite oxide [2008-58] appears as a *Hot Paper* in Angewandte Chemie Int. Ed. Two publications [2007-17 and 2008-19] were announced on the cover pages of the Physical Chemistry – Chemical Physics journal and European Journal of Inorganic Chemistry. The corresponding scientific highlights are presented in the section IV.2.

IV.3 SNBL Upgrade and Scientific Perspectives

IV.3.1 Refurbishment and infrastructure

The beamline has recently undergone a major refurbishment of its infrastructure and controls. This refurbishment will be completed in 2008, and it has involved the following items:

- Complete renewal of the vacuum hardware (pumps, gauges, controllers including flow meters for cooling water).
- Replacement of the old vacuum control and interlock system by the latest ESRF standard.
- Complete exchange of the old error prone air-conditioning modules against modern more reliable standard ESRF units.
- Entire rewiring of the mains in order to comply with ESRF standards and French safety regulations.

- Complete replacement of the old UPS power supply (including wiring) against a modern system.

- Replacement of all stepper-motor cards against the new ESRF cards (ICEPAP)

- The latter point induces also a change of the stepper motor control by using the ESRF system (SPEC).

- New floor covering and complete repainting of the radiation enclosures.

In addition to the beamline itself, the experimental equipment has all been checked and serviced (KM6 diffractometer + Onyx CCD and the MAR345 image plate and base). In the case of the computing and motor controls for the experiments, the hardware has been completely replaced. Normal operation of SNBL has been maintained during the entire refurbishment. SNBL is now one of the most up-to-date beamlines at the ESRF concerning all aspects of motor controls and software for instrumentation. One of our major goals is now to automate as many procedures as possible on the beamline (e.g. wavelength change and intensity optimisation, switch between different instrumentation such as powder-to-EXAFS, KM6-to-MAR345 etc.). Despite all of our efforts to maintain the efficiency of the beamline operation, time is inevitably lost when switching between the different instrumentation and functionality of the beamline. In addition, our manpower resources can be heavily committed during such changeover periods. The introduction of more automatic procedures will minimize lost time, reduce the chances of operator error, and release some effort for other tasks.

The SNBL management is following closely the plans for the ESRF Upgrade. Although the CRG bending magnet beamlines are not directly involved in the upgrade, SNBL may well be able to profit from the increased space available when the experimental hall is extended. We have therefore made a preliminary request for additional floor space along the beamline, which would be used to construct an additional laboratory. The need for more space has become particularly pressing since we have now a permanent installation for the Raman spectrometer in our sample preparation laboratory at the end of the beamline. In addition, of course, an increase in the current in the storage ring from the present value of 200mA up to 300mA and beyond would bring a welcome additional flux. Tests with our X-ray optics has demonstrated that we would have no difficultly in taking advantage of the extra photon flux in the incident synchrotron beam.

IV.3.2 Developments and Scientific Perspectives

A. Secondary focussing

Both the KM6/CCD and the MAR345 are routinely used for structure solution from single crystals. Generally, the samples are either too small for lab data collection, or else the crystallography is complex (e.g. incommensurate and

modulated structures, twinning, phase transitions). The MAR345 is still used by the Norwegian groups in Oslo and Tromso for data collection on protein crystals. The Oslo group is interested to continue on SNBL with PX measurements because they also use the optical and Raman spectrometers available on BM01. In order to extend further the capabilities for measurements on very small and weakly scattering crystals, we have recently purchased a doubly-curved, graded multi-layer mirror from XENOXS (Grenoble). This mirror can be inserted into the beam close to the sample (Fig. IV.1), and provides a secondary focus of about 30 microns size (compared to the standard focal spot of about 300 microns). The gain in flux density is about a factor of 30 times. The mirror has a fixed radius, and therefore functions only at photon energies of about 17 keV. This optical configuration will be ideal for working with very small crystals, where the present flux density is too low. It will also be very useful to increase the flux onto samples within a diamond anvil cell, where a beam size of 30 microns will be ideal. A precision multi-axis alignment stage will be required, in order to align the mirror relative to the incoming beam. Test results with this mirror have already shown very promising results, and the plan is to install the mirror on a commercial, muti-axis motorized table in the coming months.

The integrated flux transmitted though the XENOXS mirror will inevitably be reduced by imperfect reflectivity and figure errors, but nevertheless the gain in flux density of a factor of 30 times onto a 30 x 30 μm^2 spot is dramatic (although in practice well within the expected specification). The only drawback of such a secondary focussing device, apart from the limited operational wavelength range, is an increase in the divergence of the beam arriving on the sample. However, the divergence of the focussed beam increases only to about 1 mrad FWHM, which is quite acceptable for most diffraction experiments. We

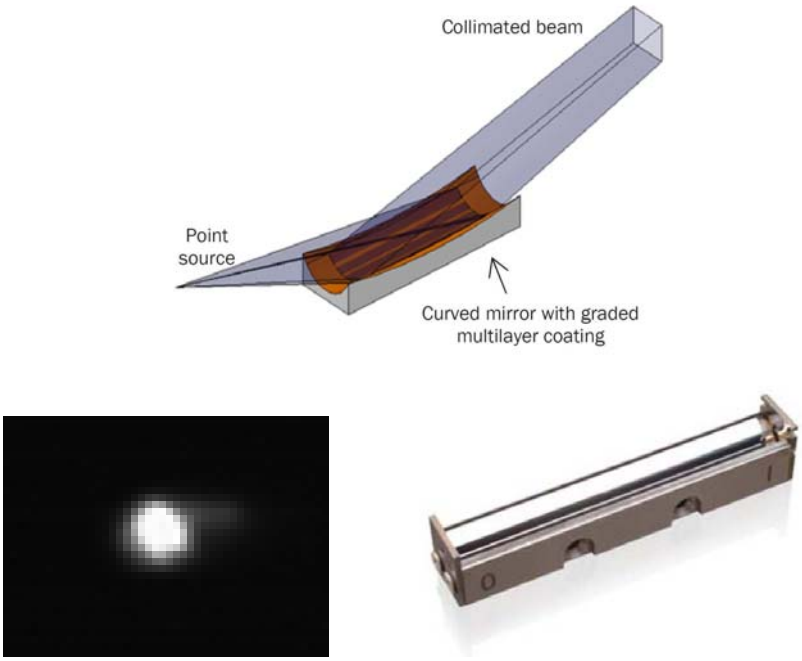

Figure IV.1. *The black rectangle corresponds to the dimensions of the incoming beam arriving on the mirror (about 400 x 600 μm^2), whereas the white spot shows a true image of the focussed beam.*

have found many cases where a sample which was originally planned for measurements on our powder diffraction facility in fact consisted of very small, single crystal grains. Such tiny crystals could until now be measured only with difficulty on SNBL, but the availability of secondary focussing will improve this situation significantly. Similarly, our high pressure experiments using diamond anvil cells, where the typical beam size is about 50 μm, will profit enormously from the increase in flux density on the sample.

B. Powder diffraction with a strip detector

Over the last few years, more and more powder diffraction experiments have been carried out on BM01A, even though this station was originally designed exclusively for single crystal diffraction. In 2007, for example, about 40% of the experiments on BM01A were in fact measurements on powder samples. There are good reasons for the shift in emphasis towards powders:

- When the samples are weakly scattering, or else only very small sample volumes are available, then the combination of focussed beam and highly efficient area detector (MAR345) make some experiments feasible which would otherwise be completely impossible on SNBL. High pressure measurements for samples contained in diamond anvil cells is a good example of this type of experiment. Represents typically about 10% of the total beamtime on BM01A.

- The time resolution of the powder diffraction experiments can be reduced to about 30s using the MAR345 (for some experiments, even shorter times are possible when using a motorized mask placed in front of the image plate). This time resolution matches well the type of experiment in which the temperature is ramped over a wide range (say 120ºC over 2 hours) and a powder pattern collected every 60s. The major drawback of this data collection strategy is the relatively poor angular resolution. Represents typically about 30% of the total beamtime on BM01A.

While the first reason given above will always be valid (unless a complete change in the optical design of BM01B is envisaged), the second reason represents rather a problem with the type of detector system available on the powder diffractometer. Our present arrangement of a set of scintillation detectors positioned behind an array of analyser crystals is intrinsically a relatively slow data collection instrument. The collection times are typically several hours for a full pattern with good statistics. The slow speed of data collection on high resolution diffractometers has long been recognized as a problem at other powder diffraction facilities (e.g. at the SRS, Daresbury, the NSLS Brookhaven and, more recently at Diamond, UK and the Australian Synchrotron) and considerable effort has gone into the development of rapid and efficient X-ray position sensitive detectors. Fortunately, one of the best technical solutions to this problem has emerged from the detector group at the Paul Scherrer Institute in Switzerland. Their electronic strip detector (MYTHEN) has been operating very successfully on the Materials Science beamline at the Swiss Light Source. The narrow width and fine spacing of the individual strips on this detector (50μm pitch with 1280

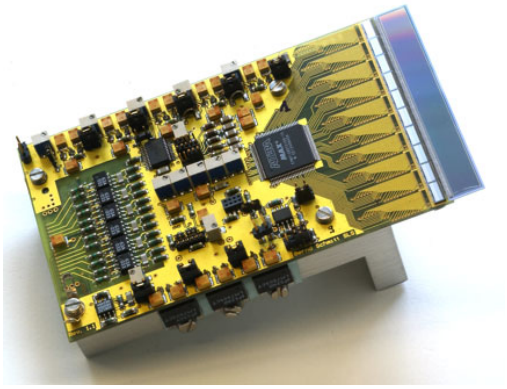

Figure IV.2. *The MYTHEN II detector unit.*

strips/unit) implies that a dramatic improvement in data collection speed can be achieved without a significant loss in angular resolution. We are very pleased to acknowledge the generous gift to SNBL from the Paul Scherrer Institute of three of their latest MYTHEN II detector units. Each unit (as illustrated in Fig. IV.2) covers about 60mm × 8mm, and the three units will be mounted on the SNBL high resolution powder diffractometer. Depending on the distance from the sample, our array of MYTHEN II units can cover either a wide angular range with reduced resolution, or else a more restricted angular range with improved resolution. The time resolution of the powder measurement can be defined by the user in the range between msec to minutes, depending on the goal of the experiment and the required statistics. Completely new types of experiment will become feasible, such as rapid pump-probe, fast switching of electric or magnetic field, polarization switching of liquid crystals and the investigation many other time-resolved physical phenomena which are currently not possible on SNBL.

Silicon sensor:

- 1280 strips
- 8 mm long
- 50 μm pitch
- 300 μm thick.

Read out chip:

- 128 channels
- low noise preamp (noise ≈ 230 e-)
- 18 bit counter
- Read-out time: 250 μs
- Count rate: 1 MHz per channel

IV.4 SNBL Workshops (2006 – 2008)

As part of our policy of seeking way to facilitate the exchange of information between the SNBL team and our synchrotron user community, the SNBL management has organized a series of workshops at the ESRF based on themes of current and future interest both to the SN community and a wider scientific audience. The first of these meetings on the topic of nanoscale materials was held in 2006, followed by a workshop on the subject of high gas pressures for *in-situ* experiments in 2007. Both of these meetings were attended by 30-40 participants, including participants from various synchrotron beamlines as well as external users. The recent meeting, which took place in June 2008, continued the theme of *in-situ* experiments, but specifically includes the use of our new Raman spectrometer in combination with x-ray absorption and diffraction measurements. 80 participants, coming from 14 countries, created a very stimulating, constructive and friendly environment for exchanging both scientific and technical know-how and creating new ideas.

- ***Synchrotron Radiation in Studies of Nanoscale Materials***

A workshop of the use of synchrotron radiation in studies of nanoscale materials was held on June 22-23, 2006 at ESRF, Grenoble, France. The two-day seminar was attended by around 40 participants coming from Norwegian and Swiss universities and research institutes, including 7 scientists representing synchrotron facilities (SNBL, SLS, DUBBLE, ESRF). Seven speakers from Denmark, Germany, the Netherlands, France, Switzerland and Russia were invited to this seminar to present review talks. Furthermore, 6 talks from project leaders and 4 talks from beam line scientists were also presented.

The seminar aimed at strengthening bi-national cooperation in some strategically important fields of scientific research that have considerable industrial potential. The general objective of the Swiss-Norwegian Seminar was to place into focus the role of synchrotron radiation in studying nanoscale materials, hereby stimulating the search for new effects and new technological applications based on the size-controlled properties of materials. The seminar topics included studies of nanoscaled materials for hydrogen storage, the search for new, efficient nanocrystalline oxides for gas sensoring and catalytic applications, methods for production and characterization of semiconducting materials for nanoelectronics, investigation of the structure of nanometric thin films, and *in situ* studies of mechanisms and kinetics of switching processes in such films. Besides facilitating an exchange of ideas, knowledge, and experience, the seminar was also aimed at attracting new users to the national synchrotron facilities. Feedback from the participants revealed that the program impressed them and they very much enjoyed the atmosphere of the seminar.

- ***In-situ experiments at SNBL using high gas pressures***

A proper understanding of structure-property relationships plays a central role in the design and discovery of novel materials. In many cases, developing the relationship between the structure of a new material and its physical and chemical properties requires that measurements be made under exactly the same *in-situ* conditions of temperature, pressure and atmosphere that match the performance environments of the materials of interest. Examples of research at SNBL leading to a better understanding of materials properties already include catalysis, battery and fuel-cell studies, and solid-state hydrogen storage technology.

The SNBL, in collaboration with our Dutch-Belgian colleagues from DUBBLE, organized a 2-day workshop at the ESRF on 8 and 9 November 2007 on the theme of "High gas pressure experiments". A total of 20 external participants and 10 members of the SNBL and DUBBLE teams attended the Workshop. The external participants came in roughly equal numbers from Norway, Switzerland and the Netherlands, together with some additional invited speakers from the United Kingdom and France.

The main themes of the Workshop included the present status and progress in the field of *in-situ* catalysis experiments, and the current activities in solid-state hydrogen storage research. Both of these subject areas have become the subject of intensive research and development over the last few years, and currently contribute to roughly 50% of the total activities at SNBL. These developments have been driven by the very successful work of the ETHZ groups in Technical Chemistry and the recent Catalysis Initiative led by teams from the Universities of Oslo and Trondheim. In addition, catalysis is supported strongly in the Netherlands (for example in the University of Utrecht and at the Energy Centre of the Netherlands, Petten). Another major area of activity at SNBL concerns energy storage techniques, and in particular solid state hydrogen storage. Several presentations described both the current activities in this field, and the targets for future research. Another research area which was covered during this workshop concerns the use of metal-organic-framework structures (MOFs), which has recently resulted in several very high profile publications from SNBL.

Interestingly, MOFs can find application both as catalysts and as hydrogen storage materials. In all of these activities, the extension of the current capabilities of SNBL toward experiments under much higher gas pressures is of great topical interest. The various fields of research which require high gas pressures are moving forward rapidly at SNBL. The in-house team has recognized the importance of these techniques, and we have received strong encouragement and financial support from our user community.

- ***SNBL Workshop on simultaneous Raman-X-ray diffraction/absorption studies for the in situ investigation of solid state transformations, and reactions at non ambient conditions.***

X-ray diffraction (XRD) and absorption spectroscopy (XAS) are the principal techniques used to investigate long and short-range order of atoms and molecules in the solid state, respectively. The Raman technique, in contrast, has the ability to probe the length scale between these two extremes. The synergy between these methodologies has attracted application to many scientific studies where the Raman and XRD or XAS techniques have been performed *ex-situ* and independently *in-situ.* The SNBL has further developed their beamline such that these three fundamental probes (XRD-XAS and Raman) can be combined under a wide range of external sample stimuli. This new approach has opened up many new avenues of research and offers vital new detail in the study of materials and solid state sciences. Similar initiatives have recently also been undertaken at other Synchrotrons: APS, SOLEIL, SLS, DIAMOND, BESSY, ANKA, other ESRF beamlines and even in home laboratories. The time was right for a first meeting on combining methods at synchrotrons.

All above mentioned laboratories were represented within the 80 participants as well as industrial partners. The participants, coming to Grenoble June 18-19, 2008, from 14 countries divided over all continents, created a very stimulating, constructive and friendly environment for exchanging both scientific and technical know-how and creating new ideas. Among the speakers were experts in Raman scattering from Biology, Physics and Chemistry. Excellent presentations were for instance given on identification of ligand-bound or intermediate states in Macromolecules, surface versus bulk sensitivity, structure dynamics in combination with computational chemistry, nanostructured ferroelectrics, structure activity relationships on supported oxide catalysts, catalysts in general, micro-focus applications, high throughput screening and possible future developments on sensitivity enhancement. All of the speakers exploited in one form or another the almost endless complementarities between the different techniques dependent on their specific case. The need to combine techniques became with every presentation more and more obvious to anyone in the audience. Many of the presented studies were performed under complex and multiple external stimuli making it impossible to reproduce the experiments on individual machines. It was also extremely stimulating to observe that excellent science has already been performed on the freshly installed installations around the world, consequently indicating a long and bright future for the *in situ, time resolved combination of techniques*.

The participants were finally very happy to hear the announcement that a follow up workshop will be organized by the people from SOLEIL in 2010. The SNBL Workshop Proceedings from our 2008 meeting will be published in a special issue of ***Phase Transitions*** (Guest Editors: V.Dmitriev/SNBL and M.Milanesio/Univ. Piemonte Orientale - Italy).

IV.5 SNBL Collaborations

Active cooperation of efforts, in different fields, with user's institutes and similar facilities is an important aspect of the SNBL management policy. The collaborations had a significant impact affecting the beam line configuration, priorities in its technical development and financial issues. It helps us in ensuring the SNBL's current solid equipment and financial base, and gives confidence in its successful future.

Cooperation with Swiss and Norwegian institutes has the highest priority in the "external" affairs of SNBL. An active role of the SNBL in seeking and establishing close relations with bi-national research groups, institutes and centres is a key part of the strategy of the management team.

A. Interaction with national institutions

An example of such interaction is the involvement of SNBL in the long-term Norwegian Natural Gas Processes and Products program (*inGAP*). Partners in the project are both academic, such as the University of Oslo, NTNU Trondheim, SINTEF, as well as industrial: Statoil ASA, Hydro Polymers AS, Norsk ASA, and Borealis. The Research Council of Norway launched, on March 2007, the *inGAP* center. During the first year, the focus of its activity has been set on laying the basis for later achievements through construction of in-situ characterisation installations, especially at SNBL. The aim of the project "In-situ@SNBL" was to build up a state-of-the-art facility for synchrotron X-ray based in-situ studies of catalysts. As in situ studies will play a key role in many of the projects in *inGAP*, the construction of this facility was prioritised in the early stages of the *inGAP* collaboration. The construction of the facility at SNBL is now completed and operational. Following the conclusion of our partners, "it is truly state-of-the-art equipment for in situ studies. To our knowledge, no similar system exists at a synchrotron facility, and there is already significant international interest in utilising the equipment. The good collaboration with the beam line personnel has been very important for the success" (see *inGAP* 2007 Annual report[1]). On the one hand, the above project had the immediate effect of injecting an additional €120'000 into the SNBL budget. On the other hand, it also ensures a long-term perspective for the SNBL operation in the field of catalysis.

Another initiative, coordinated by the SNX Council representatives, was the purchasing and installation on the beam line of a Raman spectrometer for simultaneous in situ measurements of molecular vibration spectra along with X-ray diffraction and absorption data. A joint request submitted by the group of Swiss and Norwegian universities and technological institutes received full support from the Swiss National Science Foundation and the Research Council of Norway. The latter contributed, in equal parts, to the Raman project at SNBL with a total sum of €350'000.

[1] <http://www.ingap.uio.no/about/reports/ingap_annualreport07-11-screen.pdf>

B. Links to SLS/PSI

Collaboration with Swiss Light Source (SLS/PSI) is developing in a very constructive and stable manner. For example, SNBL has benefited from the excellent experience accumulated in PSI in the design and construction of detectors. The microstrip-type detector MYTHEN 2 for ultra-fast measurement of diffracted X-rays was designed and installed on the materials beamline of the SLS for high-resolution powder diffraction. Several MYTHEN 2 modules were generously offered to SNBL by the SLS management. The superlative performance of these modules will significantly improve the time resolution of our powder diffractometer. On the other hand, the SNBL staff members share their expertise in X-ray optics and combined measurement techniques (Raman+XRD+EXAFS) with colleagues from SLS. Dr. P.Pattison (SNBL) works part-time as an adviser in the working group on the PSI Free Electron Laser project; SNBL director, Dr. V.Dmitriev, is a member of the Proposal Review Committee at SLS.

It is well recognised by the Swiss users community that SNBL is complimentary to SLS facility since it can cover the hard X-ray range of the synchrotron spectrum. In order to give a full picture of accessible facilities to our users, SNBL regularly presents reports on its status at SLS User Meetings in Villigen – a practice requested by the SLS management since 2005. The active role of Prof. Friso van der Veen and Dr. Rafael Abela in establishing close relations between two facilities should be stressed and is gratefully acknowledged.

C. SNBL and MAXLAB

Until recently, there were no direct links between these two facilities which are oriented in part towards the Norwegian synchrotron community. The reason lies mainly in the significantly different energy ranges in which SNBL and MAXLAB operate. While the former uses a bending magnet source of the ESRF optimised for hard X-rays, the latter is an excellent facility for studies with low energy synchrotron radiation. The corresponding user groups usually belong to different research fields, and their interests rarely overlap. The new MAX-IV project envisages the extension of the energy range available to the MAXLAB users towards higher energies. Although the project is only in the early stage of discussion and concept design, management groups from MAXLAB and SNBL started regular contacts in order to establish a collaboration. The SNX Council representatives took an active role in founding the Nordic Synchrotron Radiation Initiative whose first meeting was organised by Prof. D.Nicholson, SNX Vice Chair, on April 2008 in Norway. SNBL has already been presented by its Director, in October 2007, at the MAXLAB User Meeting in Lund (Sweden). The program of the next meeting in October 2008 includes an invitation to the SNBL management to present a status report on the Swiss-Norwegian Beamlines. The relationship between two facilities seems to be developing in right way, and our users will benefit from these close contacts.

D. On-site collaborations

SNBL has a privilege being installed at the ESRF, in an exceptional environment of modern synchrotron beam lines operated by experienced instrument scientists. Regular contacts with ESRF and other CRGs staff members are realised in several forms.

SNBL has a well-established collaboration with the Dutch-Belgium CRG (DUBBLE). This collaboration has been formalized since November 2005 with a Memorandum of Understanding (MoU) which regulates the cooperation between the two facilities. The agreement provides beamtime access to both facilities for user groups from Norway, Switzerland, Belgium and the Netherlands. In addition, the MoU foresees the exchange of equipment and personnel between the two CRGs, and provides access to in-house research time on both beamlines. In practice, it means an enlargement of the instrumentation toolbox for the Swiss and Norwegian synchrotron user communities. The agreement provides a route for access to the SAXS technique as well as an XAFS set-up which is optimised in a different energy range than at SNBL. This agreement allows SNBL to economise resources and concentrate these resources more effectively on a limited number of topics.

Numerous other collaborations exist, such as a very fruitful scientific collaboration with a ESRF beam line ID-28 (BL responsible Dr. M.Krisch, BL scientist Dr. A.Bosak) specialised in inelastic X-ray scattering. The combination of X-ray diffraction under extreme conditions, or diffuse scattering method presented at SNBL, with the state-of-the-art inelastic scattering technique developed at ID-28, proved to be very efficient and informative. It was appreciated by our users, and already resulted in several joint publications [2006-37, 2007-61, 2008-6].

To complete the picture of SNBL contacts and links, the participation of SNBL as an independent research group, based on the in-house research activity, should be mentioned. The SNBL team is already sharing a part of the project “Mineralogy and Chemistry of Earth's core (MCEC)” in the framework the ESF EUROCORES EuroMinScI Programme. Two proposals in which SNBL is participating have been submitted to the European 7th Research Framework Programme (FP7), with the aim of creating: (a) Special high-pressure/high-temperature diamond anvil cells for studying transport properties of material under extreme conditions, and (b) Purpose-designed diamond anvil cells for single crystal X-ray diffraction at high-PT.

Another project, based on the study of amyloid fibrils and amyloid-like microcrystals under extreme conditions, based on collaboration of groups from University College of London (UK), Katholieke Universiteit Leuven (Belgium), and SNBL, was submitted to the Engineering and Physical Sciences Research Council of UK by our British partners. The later project envisages financing a PostDoc position at SNBL.

V. SCIENTIFIC HIGHLIGHTS

V.1 Users contributions

Structural Studies of Peroxide-Derived Myoglobin Intermediates.

Hans-Petter Hersleth and K. Kristoffer Andersson
University of Oslo, Department of Molecular Biosciences, P.O. Box 1041 Blindern, N-0316 Oslo, Norway

The main function of myoglobin (Mb) is oxygen storage and transportation in heart and skeletal muscle. However, Mb exhibit peroxidase-activity during oxidative stress with involvement in scavenging of reactive oxygen species or oxidising lipids. When Mb reacts with peroxides it goes through similar intermediates as found in peroxidases and oxygenases. Our interest is concentrated around the peroxidase function of Mb to gain further knowledge of this process and its intermediates. A summary of the reactions we have been studying with protein crystallography are described in the reaction scheme *Scheme 1*.

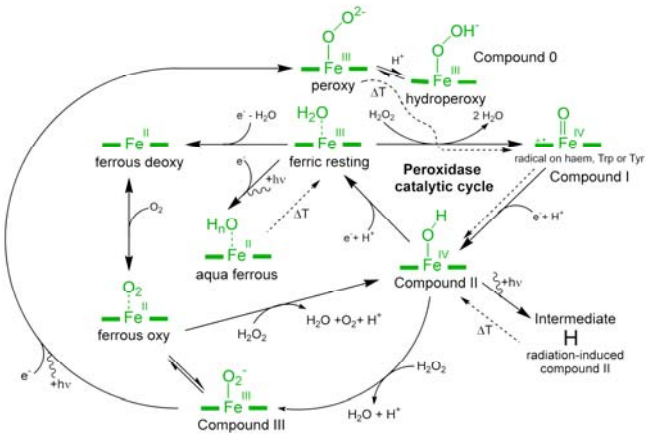

Scheme 1: *Reaction cycle studied in Mb*

Radiation damage

In recent years the awareness of potential radiation damage of metal centres in protein crystals during crystallographic data collection has received increasing attention. The radiation damage can lead to radiation-induced changes and reduction of the metal sites. For our studies on Mb we have observed this, and have therefore regularly used microspectrophotometry to monitor the influence of X-ray on our different states during X-ray diffraction data collection. Mb can nicely be monitored with light absorption because the different Mb states have characteristic absorptions in the 350-700 nm range. We have mainly studied three of the Mb states: resting ferric metMb, Mb compound II, Mb compound III and their corresponding radiation-induced states.

Radiation-induced resting ferric metMb

The ferric metMb is the resting state in the peroxidase reaction of Mb, and due to its ferric oxidation state it can potentially be reduced. This undesired radiation-induced change is observed for the ferric metMb state during crystallographic data collection. The radiation-induced reduction reduces the Fe^{III} to Fe^{II}, but at this low temperature the water that

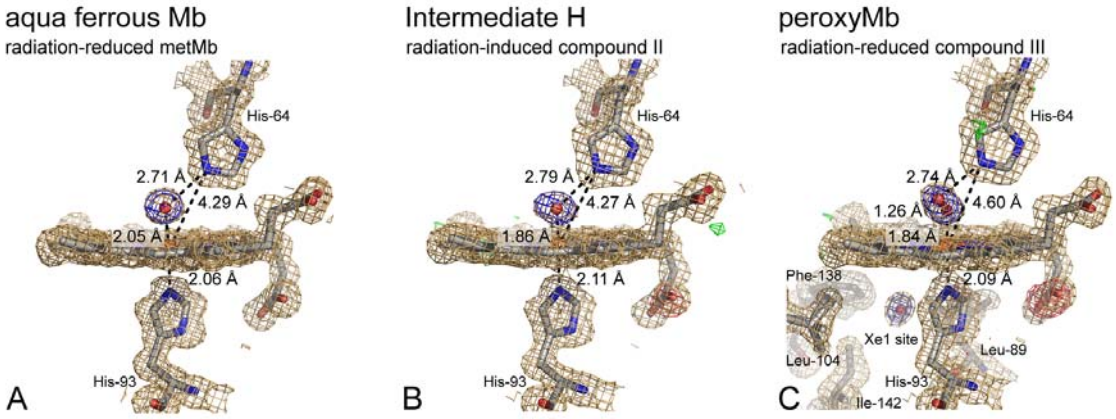

Figure 1: *The Crystal structures of the haem regions*

ligates to the iron is unable to move away to generate the normal ferrous deoxy. The crystal structure of the aqua ferrous low-spin state can be seen in *Fig. 1A* with a Fe-O bond of 2.1 Å, which is about 0.1 Å shorter than in the high-spin ferric metMb state. The cryoradiolytic-induced conversion from ferric metMb to aqua/hydroxy-ferrous Mb can in crystals be followed with single-crystal microspectrophotometry as seen in *Fig. 2*. The reduction is characterised by the reduction of the original ferric metMb peaks at 500, 540, 580 and 635 nm, with new peaks at 525 and 567 nm. When we carry out a short annealing of the aqua-ferrous state in crystals it seems that it is the high-spin ferric Mb state that is regenerated and not the ferrous deoxy state *(Fig. 2)*.

Radiation-induced Mb compound II

Single-crystal microspectrophotometry on Mb compound II shows radiation-induced changes during crystallographic data collection. The peaks at 540 and 580 as well as the shoulder peak at 595 nm decreases with increasing dose, while a new peak at 567 nm of unknown origin appears. The structure of this radiation-induced Mb compound II has a Fe-O bond of 1.85-1.90 Å, which indicate a single-bond *(Fig. 1B)*. The observation of a single-bond in compound II is supported by crystallographic studies on peroxidases. Fe-O bond distance of 1.85-1.90 Å is about 0.3 Å longer than expected for an oxoferryl (Fe^{IV}=O) species and about 0.2 Å shorter than in the radiation-induced ferric Mb structures. We have also collected datasets with shorter exposure time, and only partially radiation-induced structures as shown from single-crystal light absorption spectra. These structures show similar Fe-O bond distances of 1.85-1.90, which indicates that the unaffected compound II and the radiation-induced compound

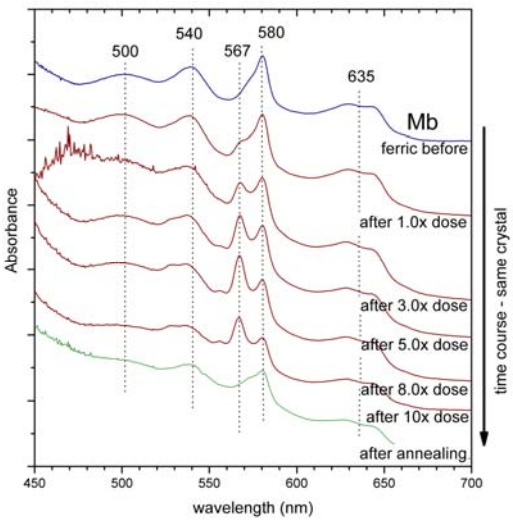

Figure 2: *Single crystal-light absorption spectra of the Build up of aqua ferrous Mb from ferric Mb during increased X-ray dose.*

II may have similar structures. Quantum refinement showed that at least in the radiation-induced Mb compound II crystal structure, the oxygen atom bound to the iron is protonated (Fe-OH). We believe, as mentioned above, that the structure of the Mb compound II and radiation-induced Mb compound II are similar, and thereby both Fe-OH states. Due to the shown protonation of the radiation-induced Mb compound II it has also been referred to as Mb intermediate H.

Radiation-induced generation of peroxyMb from Mb compound III

Mb compound III, which is similar to a ferrous-oxy (or ferric-superoxy) state (*Scheme 1*) has been generated in Mb crystals *(Fig. 1C)*. As with the other Mb states, Mb compound III also experiences a fast one-electron reduction by the synchrotron radiation during the crystallographic data collection. A one-electron reduction of the compound III leads to a peroxy intermediate that is isoelectronic with compound 0. The formation of compound III from compound II in Mb crystals can be seen by the disappearance of the 595 nm light absorption shoulder peak, resulting in only two quite sharp peaks at 540 and 580 nm *(Fig. 3)*. This is typical for low-temperature oxyMb spectra. The Mb compound III peaks at 540 and 580 nm decrease, while a new small peak at 567 nm appears showing the formation of peroxyMb *(Fig. 3)*. The peroxyMb structure have O-O bonds of ~1.3 Å and Fe-O distance of ~1.8-1.9 Å. The overall structure is quite similar to both radiation-induced ferric Mb and radiation-induced Mb compound II structures *(Fig 1)*. Quantum refinement on peroxyMb generated from compound III shows that the major unpaired spin density resides on the O-O, indicating a Fe^{II}-O-O^{-}, superoxy state.

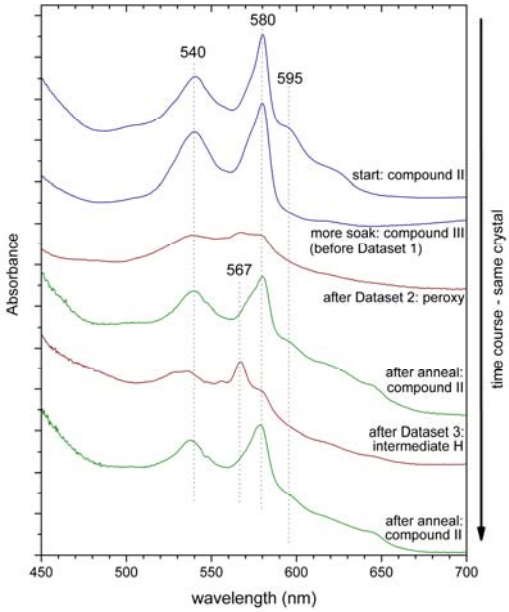

Figure 3: *Single crystal-light absorption spectra to monitor the changes experiences by the crystal subjected to collection of Datasets 1, 2 and 3.*

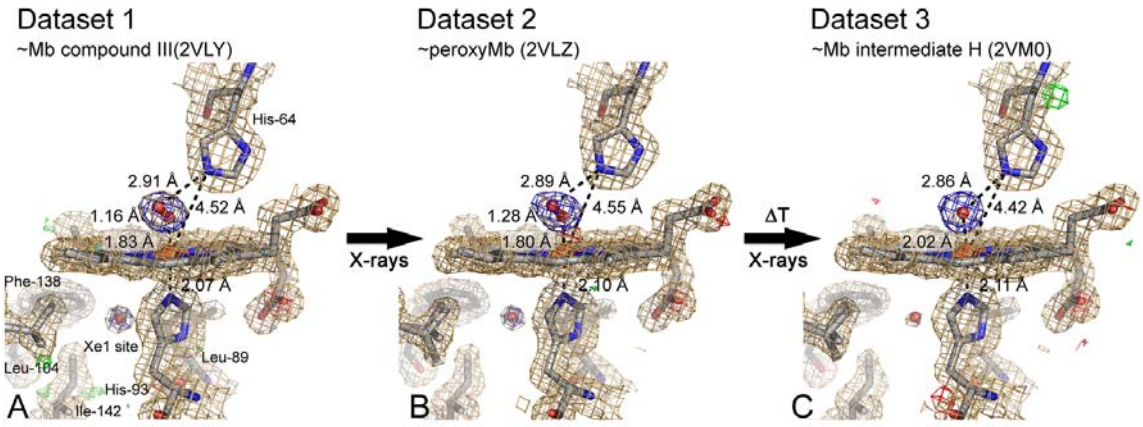

Figure 4: *Crystal structures of the haem regions of Mb shown with the electron density $2F_o$-F_c map (contoured at 1σ in golden), the final F_o-F_c map (at +3σ in green and at -3σ in red) and difference F_o-F_c map with the peroxy/hydroxy atoms and extra water molecule omitted for map calculation (at 4σ in blue). Consecutive datasets collected on the same crystal.*

Consecutive datasets and breaking of the oxygen-oxygen bond

We have collected two consecutive datasets on a Mb compound III crystal, the first one with a dose of ~3 MGy (Dataset 1), and the second one with a dose of ~10 MGy (Dataset 2). The light absorption spectrum collected after Dataset 2 shows the characteristic peroxyMb features *(Fig. 3)*. The structures resulting from Dataset 1 and Dataset 2 are shown in *Fig. 4A and 4B*, and indicate a shorter O-O bond for the former. The trend indicates that Dataset 1 is mostly compound III (oxy) with a shorter O-O bond, while Dataset 2 is mostly peroxyMb, but the resolution is not high enough to give conclusive results. A short annealing of 1 sec. of the peroxyMb crystal (Dataset 2) resulted in the formation of Mb compound II *(Fig. 3, after annealing)*. The characteristic shoulder at 595 nm can be seen, but it has a relative lower intensity than normal, so the conversion might not be complete. The structure of the dataset collected on this state (Dataset 3) can be seen in *Fig. 4C*, and will during data collection result in the radiation-induced compound II as indicated by the light absorption spectra *(Fig. 3)*. From *Fig. 4B and 4C* it is clearly seen by the electron density difference maps that the molecular oxygen has changed into a single oxygen atom. These results show that compound III can be cryoradiolytically reduced to a peroxyMb state that after protonation is analogous to the proposed compound 0 precursor in the reaction with hydrogen peroxide.

Summary

The structural studies on Mb have shown that most oxidised states of Mb experience some radiation-induced changes during crystallographic data collection from interactions with X-rays, and similar observations have been made for other haem proteins. The ferric metMb, Mb compound II and Mb compound III experiences undesired X-ray radiation-induced changes/reductions. The X-ray induced reduction during crystallographic data collection can also be used to add an electron to a state at low temperatures, generating intermediates that are otherwise unattainable. For Mb the crystal structure of peroxyMb has been generated in this way from Mb compound III. An annealing of the peroxyMb has shown that the oxygen-oxygen bond is broken in the crystal resulting in Mb compound II. This shows a way of trapping such intermediates, and that the peroxy/hydroperoxy state is an important intermediate in Mb peroxidase reaction cycle.

Acknowledgements

Our investigation has been supported by funding from the Norwegian Research Council: grant 177661/V30 (to K.K.A) and grant 138370/V30 (Synchrotron related research in the Oslo-region, SYGOR).The team at the Swiss-Norwegian Beam Line (BM01) is thanked for their valuable help.

Publications:

1. Hersleth, H.-P., Hsiao, Y.-W., Ryde, U., Görbitz, C.H. & Andersson, K.K. (2008) The crystal structure of peroxymyoglobin generated through cryoradiolytic reduction of myoglobin compound III during data collection. *Biochem. J.* **412**, 257-264

2. Hersleth, H.-P., Uchida, T., Røhr. A.K., Teschner, T., Schünemann, V., Kitagawa, T., Trautwein, A.X., Görbitz, C.H. & Andersson, K.K. (2007) Crystallographic and Spectroscopic Studies of Peroxide-Derived Myoglobin Compound II and Occurrence of Protonated Fe^{IV}-O. *J. Biol. Chem.* **282**, 23372-23386.

3. Hersleth, H.-P., Ryde, U., Rydberg, P., Görbitz, C.H., Andersson, K.K. (2006) Structures of the high-valent metal-ion haem-oxygen intermediates in peroxidases, oxygenases and catalases. *J. Inorg. Biochem*. **100**, 460-476.

4. Hersleth, H.-P., Varnier, A., Harbitz, E., Røhr, Å.K., Schmidt, P. P., Sørlie, M., Cederkvist, F.H., Marchal, S., Gorren, A.C.F., Mayer, B., Uchida, T., Schünemann, V., Kitagawa, T., Trautwein, A.X., Shimizu, T., Lange, R., Görbitz, C.H. & Andersson, K.K. (2008) Reactive complexes in myoglobin and nitric oxide synthase. *Inorg. Chim. Acta* **361**, 831-843.

5. Hersleth, H.-P., Hsiao, Y.-W., Ryde, U., Görbitz, C.H. & Andersson, K.K. (2008) The Influence of X-Rays on the Structural Studies of Peroxide-Derived Myoglobin Intermediates. *Chem. Biodiv.* In press.

Tyrolite: from 1817 to 2006

Sergey V. Krivovichev[1,2], Dmitry Yu. Chernyshov[3], Nicola Döbelin[4], Thomas Armbruster[4], Volker Kahlenberg[2], Reinhard Kaindl[2], Giovanni Ferraris[5], Richard Tessadri[2], and Gerard Kaltenhauser[2]

[1] *Department of Crystallography, Faculty of Geology, St.Petersburg State University, St.Petersburg (Russia)*
[2] *Institut für Mineralogie und Petrographie, Universität Innsbruck (Austria)*
[3] *SNBL at the ESRF (France)*
[4] *Laboratorium für chemische und mineralogische Kristallographie, Universität Bern, Freiestrasse 3, CH-3102 Bern, Switzerland*
[5] *Dipartimento di Scienze Mineralogiche e Petrologiche Università di Torino (Italy)*

Copper arsenates are common minerals in oxidation zones of sulfide ore deposits. There are more than 70 different copper arsenate mineral species reported so far. The restricted stability of arsenic-bearing minerals such as the copper arsenates may play a significant role in the mobility of arsenic in the near-surface environment. Structural investigations of secondary As-bearing phases may lead to a better understanding of the geochemical behavior of As and thereby help to elucidate mechanisms of transportation and accumulation of As under natural conditions.

Tyrolite, a complex copper arsenate carbonate hydrate, was first described by A.G. Werner in 1817 from Schwaz-Brixlegg, Tyrol, Austria. The mineral is widely distributed and has been reported to be found at more than 128 localities worldwide. Crystal structure of tyrolite was unknown, primarily due to the poor quality of their platy and flexible crystals. Recently, we have reported the crystal structures of two tyrolite polytypes, which were solved using the experimental advantages provided by modern area detector technologies and high-intensity synchrotron radiation.

The samples of tyrolite used in this study originate from the tyrolite type locality (Brixlegg, Schwaz, Tyrol). One of the samples represented a dolomite rock covered by greenish-blue flexible tyrolite crystals (Fig. 1). All attempts to collect indexable X-ray diffraction data from relatively large crystals extracted from this sample were unsuccessful. In all cases, only two unit-cell parameters could be reliably determined, whereas the third could not be found. Close inspection of the sample revealed two visually

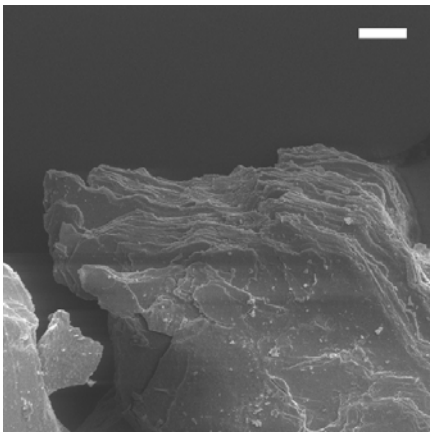

Fig. 1. *Crystals of tyrolite from Brixlegg-Schwaz, Tyrol. Scale bar is 50 μm.*

different aggregates: light blue plates and aggregates of greenish-blue elongated platy crystals. One of the greenish-blue aggregates was split and several strongly birefringent plates were selected under a polarization microscope. X-ray diffraction experiments were performed under ambient conditions at the Swiss – Norwegian beamline BM01A of the European Synchrotron Radiation Facility (ESRF) using an imaging plate area detector (Mar345) with a crystal-to-detector distance of 150 mm. Data were collected for the crystal with dimensions of 11 × 14 × 2 μm^3. Diffraction data were measured using monochromatic radiation (λ = 0.80000 Å) in an oscillation mode by rotating the crystal in φ by 2^o in 2 min per frame; 179 frames were measured. The structure was solved using SHELXS program. The agreement factor for the final model is $R_1 = 0.089$ for 2522 unique observed reflections with $|F_o| \geq 4\sigma_F$.

Structure description

Fig. 2 shows projection of the structure of tyrolite-1*M* along the *b* axis. It is based upon complex slabs consisting of Cu, As, and Ca coordination polyhedra. The slabs are about 26 Å = 2.6 nm thick and thus can be considered as nanolayers. This feature of the structure of tyrolite is very
specific and has not been previously observed in oxysalt minerals. The architecture of the nanolayers can be understood in terms of separate sublayers. The core of the nanolayer is a copper arsenate substructure consisting of the **A** and **B** sublayers specified in Fig. 3. The **B** sublayer represents a series of chains of edge-sharing Cu octahedra running along the *b* axis. Within the chain, three $Cu^{2+}\varphi_6$ octahedra form trimers by sharing the common OH group. Similar trimeric units constitute an important part of the **A** sublayer. However, in this case, the trimers do not form chains but share corners with AsO_4 tetrahedra to produce a complex 2-dimensional topology. The copper arsenate substructure consists of two **A** sublayers linked by the octahedral chains from the **B** sublayer resulting in formation of the 18Å-thick **ABA** slab. The **ABA** copper arsenate slab is sandwiched between the sublayers of the Ca^{2+} cations and H_2O molecules. The adjacent nanolayers are connected by hydrogen bonds to the interlayer species.

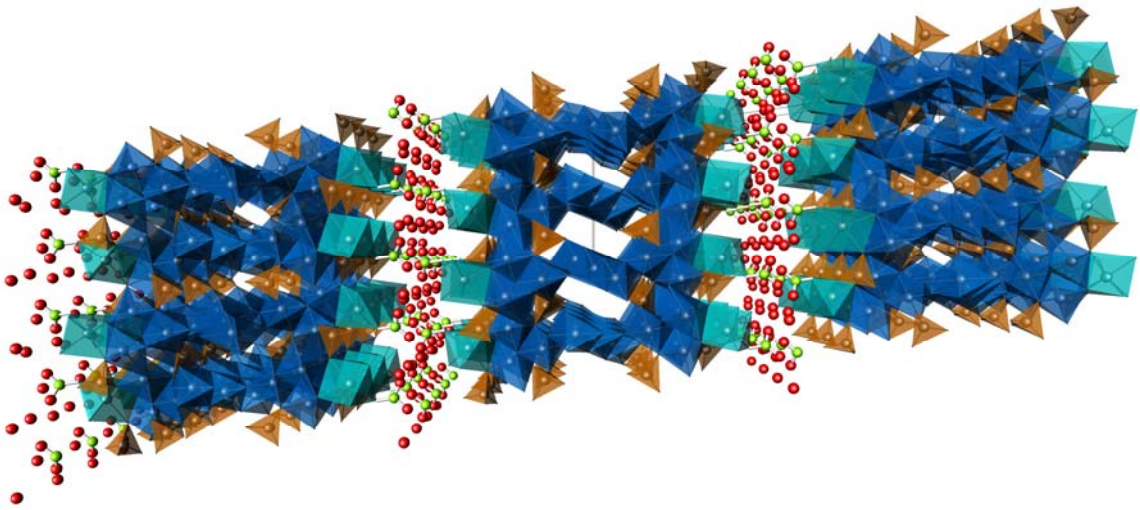

Fig. 2. *Crystal structure of tyrolite viewed parallel to the b axis (perspective view). Cu, As, and Ca polyhedra are blue, brown, and light-blue, respectively; O and H_2O groups are red, C atoms of the carbonate groups are light-green.*

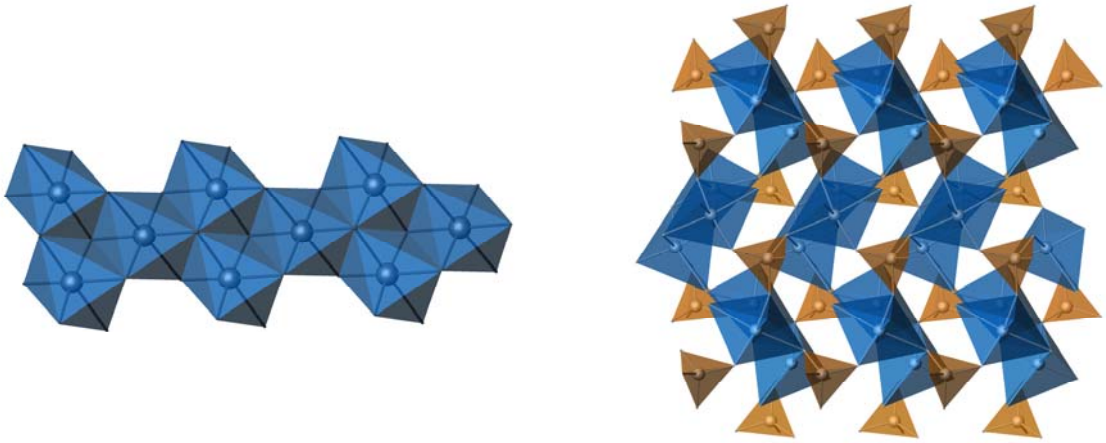

Fig. 3*. Chains of trimeric units of Jahn-Teller distorted Cu octahedra (left) constituting the* ***B*** *sublayer and layer of Cu octahedral trimers interlinked through AsO_4 tetrahedra (****A*** *sublayer) (right).*

The structure of tyrolite-2*M* is very similar to that of tyrolite-1*M* and differs from the latter by the stacking sequence of the nanolayers. In both structures, adjacent nanolayers are translationally equivalent. The adjacent nanolayers in tyrolite-2*M* are shifted by *b*/2 = 2.8 Å in comparison to the relative position of the nanolayers in tyrolite-1*M*. This shift is quite subtle compared to the thickness of the nanolayers (26 Å). Perhaps, this feature of the tyrolite polytypes explains the difficulties associated with the structural characterization of this mineral.

The unique character of the structures of tyrolite polytypes described here (nanometer-sized layers linked by weak hydrogen bonds) makes it interesting from the viewpoint of material science. Recently, much attention as been attracted by the layered materials with

weak interlayer bonding. Using specific experimental procedures, these materials can be exfoliated into nanosheets with subsequent fabrication of nanomaterials (e.g. by rolling nanosheets into nanotubes or by intercalating of organic molecules in between the layers and fabrication of organic/inorganic nanocomposites). Tyrolite polytypes are especially interesting in this regard owing to the magnetism of the Cu^{2+} cations. In tyrolites, 2-dimensional nanosized substructure of transition metal ions (Cu^{2+}) is sandwiched between the layers of dielectric Ca^{2+} cations and H_2O molecules. This peculiarity of the tyrolite structure makes it very interesting from the viewpoint of physical properties, which are currently under investigation.

Publication:

Krivovichev, S.V., Chernyshov, D.Y., Döbelin, N., Armbruster, Th., Kahlenberg, V., Kaindl, R., Ferraris, G., Tessadri, R., Kaltenhauser, G. *Crystal chemistry and polytypism of tyrolite* American Mineralogist, **91**, 1378-1384 (2006)

Structure of the polycrystalline zeolite catalysts solved by enhanced charge flipping

Christian Baerlocher and Lynne McCusker
ETH Zürich, Switzerland

A research team from the Laboratory of Crystallography of ETH Zurich has succeeded in solving the structure of the zeolite IM-5, which was first synthesized about ten years ago. However its makeup is so complex that its structure could not be clarified until now. This was mainly because IM-5 is available only in powder form. All that researchers were able to infer from catalytic test reactions in 2000 was a rough picture of IM-5's pore system. The present studies show that IM-5 has a basic structure of 24 individual silicon atoms. A unit cell of the crystal consists of 864 atoms. However, because of various symmetries, "only" over 70 atomic positions needed to be determined. It should be stressed that up to now the upper limit for polycrystalline materials was 20 to 30 atoms. In the present case the structure is more than twice as big. This means the structure of IM-5 is as complex as that of the zeolite TNU-9. So far the latter has been the most complex structure that the same ETH Zurich research group was also able to solve.

One of IM-5's special features is its unusual pore and channel system. On the one hand this is two-dimensional, i.e. it has countless channels running in parallel, but on the other hand it has limited three-dimensionality as a result of cross-links between the parallel pores and dead end side-branches. Groups of three pore systems lying in a plane are interconnected. These nano-sized planes are separated by single walls. The team from the ETHZ and their colleagues from Stockholm University broke new ground to solve the structure. The structural determination was based on data from X-ray powder diffraction experiments collected at SNBL and at the Swiss Light Source, together with high resolution electron transmission microscopy images and a computer model ("Charge

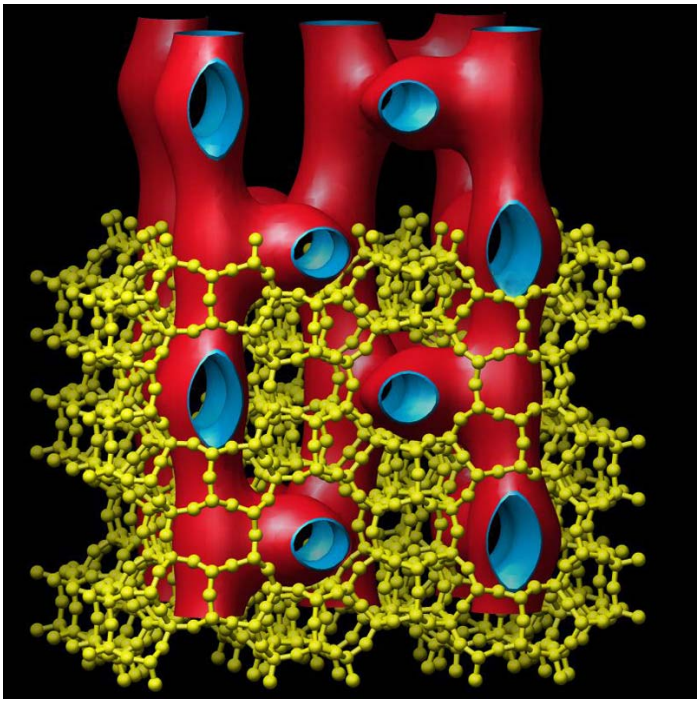

Fig. 1 *A model representation of the zeolite IM-5: the yellow skeleton outlines the position of the silicon-oxygen atoms and the red-blue tubes illustrate the unique pore system*

Flipping") which they adapted to the specific needs in determining the complex crystal structures of powders.

The use of the charge flipping algorithm for *ab initio* structure solution from single crystal data has rapidly become well-established, and is now incorporated into a number of different software packages. Amongst other examples, data was presented from SNBL on a zeolite ZSM-5 containing 38 atoms in the asymmetric unit.

In the case of the high-silica zeolite catalyst SSZ-74, it was indeed possible to obtain a high resolution TEM image (albeit only in one direction). This restriction meant that the phase information which could be extracted from the HRTEM image was very limited. Nevertheless, it was possible to use the image to construct a structure envelope for this zeolite, which could then be combined with the charge flipping procedure. After a series of cycles of phasing and inspection of the density maps, a fully connected atomic framework could be recognized. The original powder data collected at Brookhaven turned out to be of insufficient quality to proceed with a structure refinement, and therefore new data were collected at SNBL. The new powder data allowed not only 23 of the expected 24 Si atoms to be identified, but it was also possible to demonstrate conclusively that the missing Si atom was in fact an ordered vacancy. Such an ordered defect, with four framework oxygen atoms forming an approximate tetrahedron around a vacancy, has never been observed before in a high-silica zeolite.

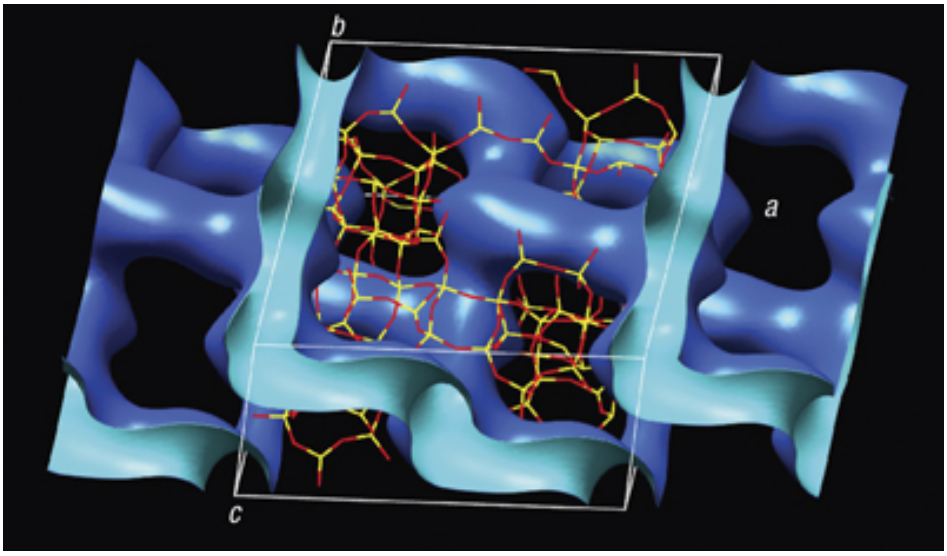

Fig. 2 *The framework structure and channel system of SSZ-74. Si:yellow, O:red. The periodic nodal surface depicts approximately the channel system within the framework structure.*

The key to the structure determination of this complex zeolite has proved to be the combination of powder diffraction and electron microscopy data within the charge-flipping algorithm. Not only could 89 atoms (23Si + 48O + 16C + 2N) in the asymmetric unit be located, but even the totally unexpected Si vacancy was revealed. This approach to structure determination is widely applicable, and therefore holds much promise for those polycrystalline materials which have hitherto resisted solution.

Publications:

Christian Baerlocher, Fabian Gramm, Lars Massüger, Lynne B. McCusker, Zhanbing He, Sven Hovmöller, and Xiaodong Zou *Science* **315** , 1113-1116 (2007)

Christian Baerlocher, Lynne B. McCusker and Lukas Palatinus *Z. Kristallographie* **222**, 47-53 (2007)

Christian Baerlocher, Dan Xie, Lynne B. McCusker, Song-jong Hwang, Ignatius Y. Chan, Kenneth Ong, Allen W. Burton and Stacey I. Zones *Nature Materials*, **7** 631-635 (2008)

Structural studies of novel materials for hydrogen storage

Bjørn C. Hauback and Magnus H. Sørby
Physics Department, Institute for Energy Technology (IFE), Norway

During the last decade there has been a significantly increased focus on hydrogen as the future energy carrier. The main reason is that a hydrogen economy may be an answer to the two major challenges facing the future global economy: climate changes and the security of energy supplies. The major components in the expected Hydrogen Economy involve production, storage and final use of hydrogen, e.g. in fuel cells. All parts in this chain are facing considerable technological challenges, in particular related to the key materials. Hydrogen storage is a crucial step for providing a ready supply of hydrogen fuel to an end user, such as in a car. Hydrogen storage remains an undisputed problem for hydrogen-fuelled vehicles, and it is considered by many to be the most technologically challenging aspect. It is also clear that the only acceptable sustainable long-term solution for vehicles is hydrogen storage in solid materials.

A major challenge is to find materials and hydrogen storage systems fulfilling international targets for hydrogen storage. Such research efforts require new materials and not simple, incremental improvements in current technologies. One of the main goals is related to the overall weight of the storage system, and thus the hydrogen storage materials should be based on light-weight elements in the Period Table. During the last years several new metal hydrides based on boron, aluminium, magnesium and nitrogen have been synthesized. Advanced characterization tools like synchrotron X-ray diffraction have to be used in order to for determination of:

- Crystal structure of the hydride and also intermediate phases that can be present during hydrogen absorption/desorption. For structural determination of hydrogen storage materials the combination of synchrotron powder X-rays (SR-PXD) and powder neutron diffraction (PND) is very important (details about hydrogen/deuterium positions from neutrons and heavier elements from X-rays)
- Hydrogen desorption and absorption reactions. The process for hydrogen absorption and desorption in many of the new light-weight hydrides can be very complex involving several steps and intermediate phases. *In-situ* SR-PXD experiments are important for detailed understanding of theses sorption processes.
- Effect of catalysts in novel complex hydrides. Catalysts are crucial for better kinetics in these compounds. However, the understanding of the effect of the catalysts in these compounds is still limited, and the use of SR-PXD in combination with for example TEM and spectroscopic techniques, contributes to a better understanding.

In the period 2005-2007 we have used both the A and B stations on BM01 at ESRF (SNBL) to investigate:

- Crystal structures for several new compounds (in combination with PND at IFE) including: $Mg(AlH_4)_2$, Na_2LiAlD_6, $Zr_2NiD_{4.5}$, α'-, β- and γ-AlD_3, $LiMg(AlD_4)_3$, $LiMgAlD_6$, $LiND_2$ and $Mg(ND_2)_2$.
- Detailed studies of desorption processes in different compounds based on Al ($Mg(AlH_4)_2$, $LiAlH_4$, α'-, β- and γ-AlD_3, $LiMg(AlD_4)_3$), N (Li-Mg-N-H systems), Mg (Mg-Co-H, Mg-Fe-H, Mg-Ti-Ni-H) and B ($Ca(BH_4)_2$, $Mg(BH_4)_2$).
- Details of effect of transition metal (TM) catalysts in $NaAlH_4$ including presence of TM-Al solid solutions and amorphous phases (in combination with high resolution TEM and PND).
- Substitution of fluorine for hydrogen in Na_3AlH_6 in order alter the stability.

In the following one example describing structure and decomposition of the different phases of AlH_3 and decomposition of the B-containing complex hydrides $Ca(BH_4)_2$ and $Mg(BH_4)_2$ will be presented.

Structural studies and decomposition of AlH_3

Aluminium hydride AlH_3 (alane) has both a high hydrogen content (10.1 wt%) and volumetric density (0.148 kg H_2/L) that can be released at moderate temperatures. However, the compound is not reversible at moderate conditions. AlH_3 has been found to take at least six different crystal structures depending on the synthesis route: α, α', β, γ, δ and ε. α-AlH_3 was the only structure known before this work. Based on SR-PXD experiments at SNBL (BM01B) in combination with PND the accurate structures of α'-, β- and γ-AlD_3 in addition to α-AlD_3 have been determined [1-3]. The structures of the different structures consisting AlD_6 octahedra are shown in Figure 1. For the α-, α'- and β modifications the octahedra are connected via corner-sharing in different ways, but for the γ-AlD_3 the structure consists of both corner- and edge-sharing AlD_6 octahedra.

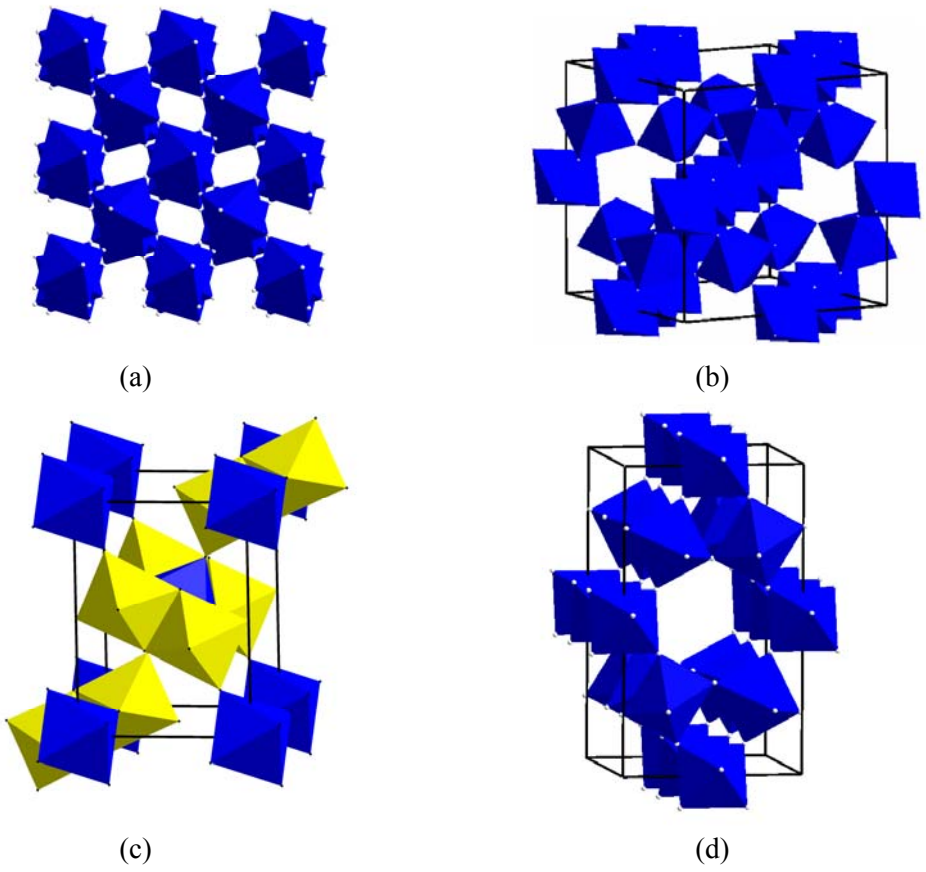

***Figure 1**. Structures of different modifications of AlD_3: (a) α-AlD_3; (b) α'-AlD_3; (c) β-AlD_3 and (d) γ-AlD_3.*

From old work it has been reported that the α polymorph is the most stable, but modelling work has shown that the β-state is more stable than the α-phase. To clarify these points, we have performed detailed studies of the decomposition of α'-, β- and γ-AlD_3 at BM01A [4-5]. The β-AlD_3 transforms into α-AlD_3 (starts at about 80 °C) prior to decomposition to Al and D_2. The transformation of γ-AlD_3 into α-AlD_3 starts at about 90 °C and the sample decomposes to Al and D_2 at a higher temperature. From about 110 °C γ-AlD_3 also decomposes directly into Al and D_2. Relative amounts of the different phases developed as a function of temperature during decomposition of β- and γ-AlD_3, respectively, are shown in Figure 2.

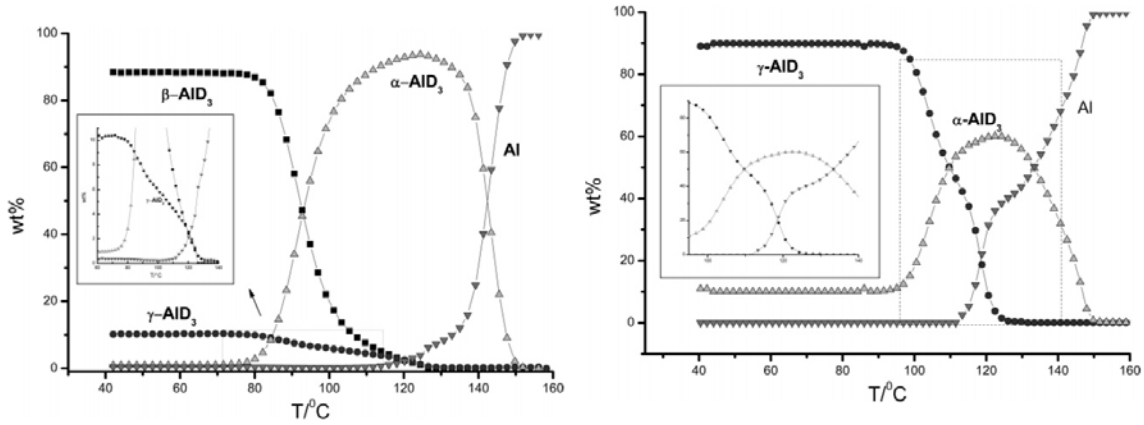

(a) (b)

***Figure 2**. In-situ SR-PXD studies of the decomposition of: (a) β-AlD_3 and (b) γ-AlD_3 as a function of temperature. Heating rate is 1 K/min and measurements are performed every 2nd minute. The relative amounts of the different compounds were determined by quantitative phase analysis using the Rietveld method based on the SR-PXD data.*

From similar analysis we have found that α'-AlD_3 transforms directly into Al and D_2 at around 80 °C [5]. At higher temperatures the transformation of α'-AlD_3 to α-AlD_3 was observed.

In-situ SR-PXD studies of phase transformation and thermal decomposition of $Mg(BH_4)_2$ and $Ca(BH_4)_2$

$Mg(BH_4)_2$ and $Ca(BH_4)_2$ with 14.9 and 11.6 wt% hydrogen, respectively, are among the most promising materials for mobile hydrogen storage, but the knowledge about their hydrogen desorption properties is limited. We have studied these materials by time-resolved *in-situ* SR-PXD at BM01A [6].

For $Mg(BH_4)_2$ system the phase transition from the α- to the β-modification is observed in the temperature range 450-460 K and the decomposition of the β-modification takes place between 520 and 580 K. After decomposition Mg, MgO, and, at higher temperatures, MgH_2 are identified as product phases.

The phase transitions and thermal decomposition of $Ca(BH_4)_2$ are very complex. We have found: (i) a continuous phase transition from the low temperature γ- to the high temperature β-$Ca(BH_4)_2$ and thereafter to "δ-$Ca(BH_4)_2$"; (ii) release of hydrogen in 2 steps (decomposition of β-

$Ca(BH_4)_2$ and "δ-$Ca(BH_4)_2$", respectively; (iii) CaH_2 present at 770 K. More work is needed to clarify the structural details for the different $Ca(BH_4)_2$ phases.

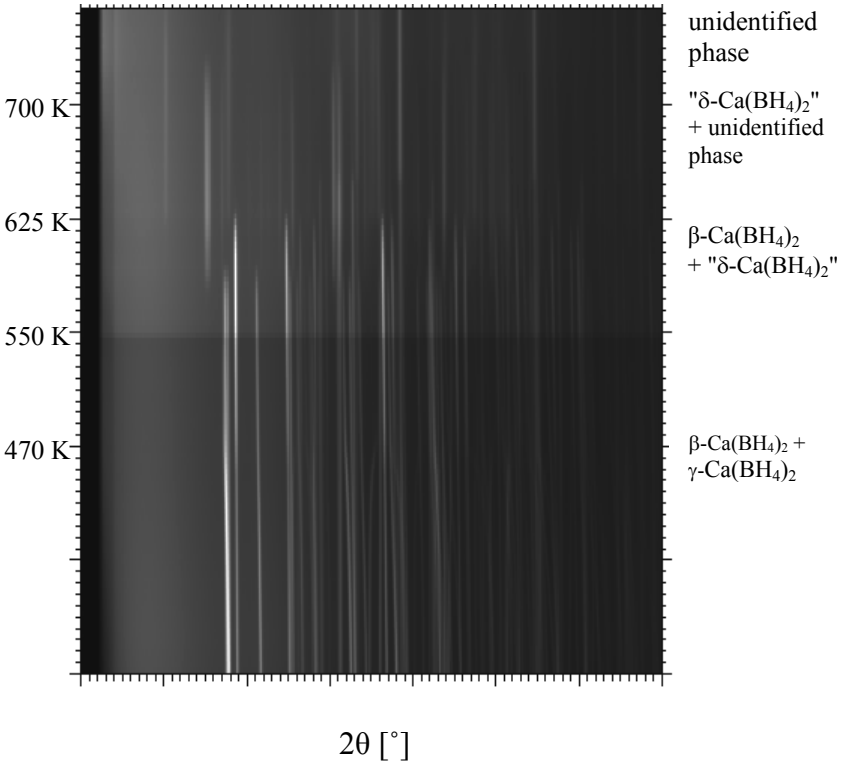

***Figure 3**. SR-PXD patters for $Ca(BH_4)_2$ as a function of temperature (310-770 K).*

Publications

1. H. W. Brinks, A. Istad-Lem, B. C. Hauback, Mechanochemical synthesis and crystal structure of α'AlD_3 and α-AlD_3. *J. Phys. Chem. B* **110** (2006) 25833-25837.
2. H. W. Brinks, W. Langley, C. M. Jensen, J. Graetz, J. J. Reilly, B. C. Hauback, Synthesis and crystal structure of β-AlD_3. *J. Alloys Compd.* **433** (2007) 180-183.
3. H. W. Brinks, C. Brown, C. M. Jensen, J. Graetz, J. J. Reilly, B. C. Hauback, The crystal structure of γ-AlD_3. *J. Alloys Compd.* **441** (2007) 364-367.
4. H. Grove, M. H. Sørby, H. W. Brinks, B. C. Hauback, In situ synchrotron powder X-ray diffraction studies of the thermal decomposition of β- and γ-AlD_3. *J. Phys. C* **111** (2007) 16693-16699.
5. S. Sartori, S. M. Opalka, O. M. Løvvik, M. N. Guzik, X. Tang, B. C. Hauback, Experimental studies of α-AlD_3 and α'-AlD_3 versus first-principles modelling of the alane isomorphs. *J. Mater. Chem.* **18** (2008) 2361-2370.
6. M. D. Riktor, M. H. Sørby, K. Chłopek, M. Fichtner, F. Buchter, A. Züttel, B. C. Hauback, *In situ* synchrotron diffraction studies of phase transitions and thermal decomposition of $Mg(BH_4)_2$ and $Ca(BH_4)_2$. *J. Mater. Chem.* **17** (2007) 4939-4942.

XAS Characterisation of Catalysts for Fuel Production

Magnus Rønning, Nina Hammer, Øyvind Borg, De Chen
Norwegian University of Science and Technology, NTNU
Department of Chemical Engineering,
N-7491 Trondheim, Norway

Identification of cobalt species during temperature programmed reduction of Fischer-Tropsch catalysts

Cobalt is considered to be the most favourable metal for the synthesis of long-chain hydrocarbons from natural gas-based synthesis gas because of its high activity, high selectivity to linear paraffins, high resistance towards deactivation, and low water-gas shift activity.

In order to maximise the exposure of cobalt to gaseous reactants, the metal is normally dispersed on a high surface area support. The choice of support is important for the final Fischer-Tropsch synthesis catalyst. In particular, the pore characteristics of the support have a significant effect on the Co_3O_4 crystallite size measured after impregnation and calcination. In some cases, the support interacts strongly with the active phase. Metal-support interactions may leave a fraction of the cobalt chemically inactive after reduction. In order to reduce the amount of non-reduced cobalt, a small amount of a second metal (Re, Pt) can be introduced into the catalyst system.

Temperature programmed reduction (TPR) is a valuable method for gathering information about the reduction process. The reduction properties of cobalt oxide deposited on different support materials have been extensively investigated. Unsupported, as well as supported Co_3O_4, are reduced to cobalt metal in two-steps:

$$Co_3O_4 + H_2 \rightarrow 3CoO + H_2O \quad (1)$$
$$3CoO + 3H_2 \rightarrow 3Co + 3H_2O \quad (2)$$

X-ray absorption spectroscopy (XAS) can give information about the nature and quantity of different cobalt species present during reduction. For supported cobalt, these species usually include Co_3O_4, CoO, and metallic cobalt. In addition, a part of the cobalt may interact with the support, making complete reduction difficult. XAS can conveniently be performed *in situ* with the possibility to follow the dynamics of the process.

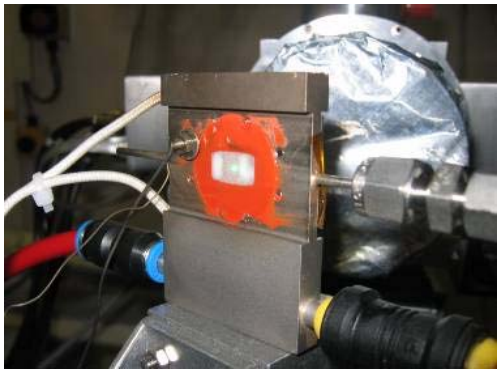

***Figure 1**. A versatile in situ catalysis cell that allows for combined measurements of XAS, XRD and Raman.*

Several *in situ* cells have been used for studying the catalyst materials. An example of a versatile cell is shown below. The cell allows for combining techniques such as XAS, XRD and Raman by selecting appropriate window materials (Kapton or glassy carbon for X-rays, suprasil or saphire for Raman).

The degree of reduction ranges from 63 to 85 percent using linear combination of XANES profiles, while EXAFS analysis yields values from 65 to 79 percent. The consistency between values obtained from XANES profiles and EXAFS analysis is good and

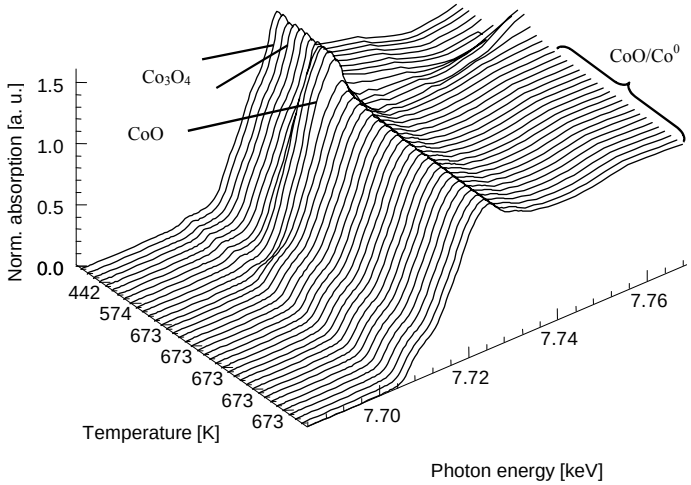

Figure 2. *XANES profiles at different reduction stages for CoRe/γ-Al_2O_3. Scans were taken continuously with a time gap of five minutes.*

within experimental errors. The extent of reduction obtained by the XAS techniques follows the order CoRe/SiO_2 > CoRe/TiO_2 > CoRe/α-Al_2O_3 > CoRe/γ-Al_2O_3.

XANES experiments at the Co K absorption edge were recorded during *in situ* reduction. According to a principal component analysis of the spectra, three primary components were needed to adequately reconstruct the spectra of all catalysts. Co_3O_4, CoO, and Co metal foil were chosen as model compounds.

An example of the change in XANES profiles during reduction of 12CoRe/γ-Al_2O_3 is shown in Figure 2. The pre-edge feature typical for Co in partially tetrahedral coordination, which is the case for bulk Co_3O_4, gradually decreases. This change is consistent with the transformation to octahedrally coordinated Co as in CoO. Finally, the profiles closely resemble that of metallic Co showing a less intense white line and a characteristic pre-edge shoulder.

Figure 3 display changes in Co_3O_4, CoO and Co metal fractions with temperature for the catalyst CoRe/γ-Al_2O_3. The shape of the component fraction plots for the other catalysts was similar to the catalyst presented here. The only significant differences for the various catalysts are the extent of reduction and the temperature in which the major transformation from Co_3O_4 to CoO occurs. For all catalysts the initial quantity of Co_3O_4 was completely transformed into other cobalt

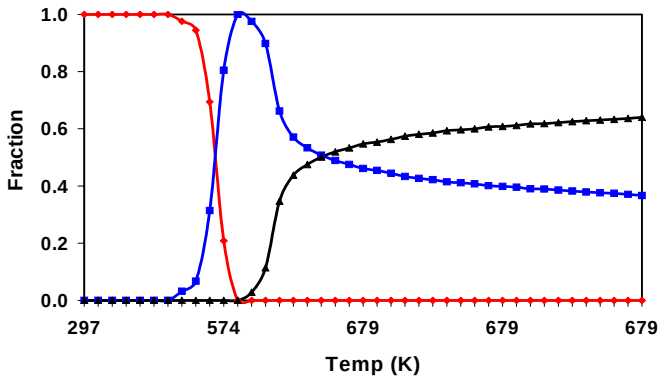

Figure 3. *Temperature programmed reduction of CoRe/γ-Al_2O_3 using the in situ XAS cell. Temperature ramping is indicated in the figure (Red = Co_3O_4, Blue = CoO, Black = cobalt metal)*

species before reaching the final reduction temperature of 673 K. Furthermore, CoO is the dominant intermediate during reduction for all supported cobalt catalysts included in this investigation.

The temperature for maximum CoO concentration coincides well with the temperature of the TPR peaks previously attributed to the reduction of Co_3O_4 to CoO. The XAS and TPR results are in agreement for the further reduction of cobalt, namely the reduction of CoO to cobalt metal. According to TPR, the reduction of CoO starts immediately after the reduction of Co_3O_4 is completed. The XAS results show a sharp drop in the fractional amount of CoO accompanied by an immediate rise in the cobalt metal content (Figure 3). The linear combination of XANES and the principal component analysis give very good fit to the experimental data.

In agreement with TPR and O_2 titration data, the degree of reduction was significantly higher for catalysts with high surface area than for the catalysts with low surface area. The degree of reduction was 70 % and 22 % after 3.5 h respectively. The degree of reduction did not change when the catalyst was exposed to synthesis gas. Thus, no oxidation of Co, which is a likely source for deactivation, occurred at the applied experimental conditions.

The results show that the XANES is capable of identifying the different cobalt species during the reduction. Linear combination of XANES profiles with those of selected reference compounds gives a relatively precise estimate of the extent of reduction of the cobalt particles.

Au-TiO_2 catalysts for the water-gas shift reaction stabilised by carbon nanofibres

The water-gas shift (WGS) reaction may provide a pathway to suppress the CO levels in the production of pure hydrogen for fuel-cell power systems. Gold nanoparticles in association with partially reducible oxides have been shown to exhibit high catalytic activity in the reaction. Carbon nanofibres (CNF) have been used in the present work to disperse and stabilise the TiO_2 support and hence the Au particles. The use of CNF as support material in heterogeneous catalysis has attracted growing interest due to their specific characteristics. The CNF are resistant to acid/base media and the precious metals can easily be recovered by burning off the support. The size and morphology of the CNF provide high surface areas while maintaining macroscopic pore sizes and hence good transport properties in the reactor, and reduced risk of micropore-induced diffusion limitations. The scope of the present work is to examine how the physical and chemical properties of the Au particles are influenced by the choice of support material and synthesis methods. The catalysts have been studied by various characterisation techniques and tested in the WGS reaction. The changes in the structure of Au and TiO_2 for different pre-treatments have been investigated by X-ray absorption spectroscopy. The Au catalysts have been prepared by deposition-precipitation and deposition of Au from colloid solutions on different supports. The supports used are TiO_2, CNF, and TiO_2 deposited on CNF. The results show that the properties obtained from the synthesis methods are highly dependent on the choice of support material.

XANES provides information about the oxidation states and site symmetries of the gold species. An *in situ* XAS study of the pre-treatment of the samples was performed. Linear combination of the edge profiles was performed using Au(0) (Au metal) and Au(I) (AuCl) as reference compounds to determine the distribution of valence states in the catalysts. No evidence of Au(III) could be detected in any of the samples before or during the different treatments. The changes in valence states for the Au catalysts are similar in oxygen and helium. Since the fraction of metallic Au is increasing with the same fraction in both gases it is likely that the changes observed are because of structural changes and rearrangements of the cluster-support induced by

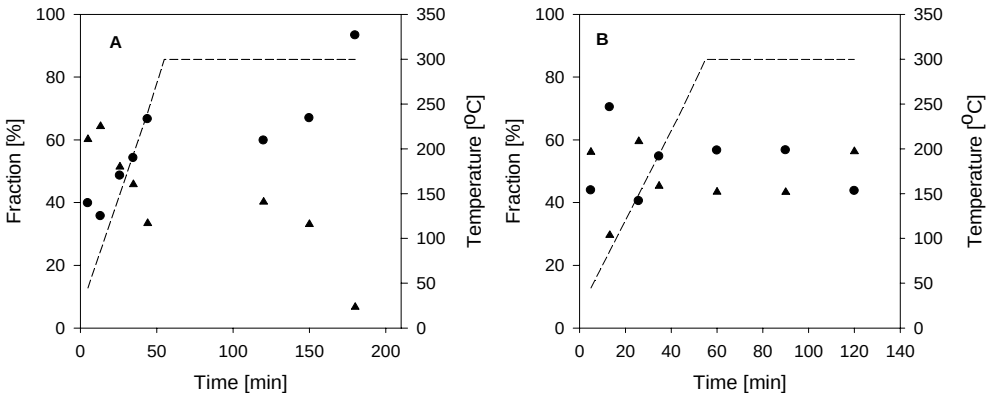

Figure 4. *Fractions of Au(0) (circle) and Au(I) (triangles) obtained from linear combination of XANES spectra during different pre-treatments of $AuTiO_2$CNF_Col, (A) treated in 5% O_2/He followed by (B) reduction in 5% H_2/He. The temperature is plotted as a dashed line.*

the thermal treatment. Since only Au(0) and Au(I) can be observed, oxidation of gold particles is not a likely explanation for the valence shift in the present samples. Others have reported EXAFS and XANES experiments and DFT calculations and are suggesting a model where a metallic gold cluster containing about 50 atoms is in intimate contact with the oxide support to the extent that up to 15 % of the gold atoms at the interface with the support may be located at cation vacancies. Such gold atoms would be expected to carry a small positive charge. This is in agreement with the positive charge that is observed in the XANES spectra being a result of gold-support interactions. However, it is clear that metallic gold is the main constituent in the samples from both synthesis methods.

The fraction of Au(I) is larger for $AuTiO_2$/CNF than for Au/CNF. This is because the average particle size is smaller for $AuTiO_2$/CNF, where a larger fraction of atoms is located at the metal-support interface where cationic gold is stabilised by the support. This indicates that titania has a stronger interaction with the Au particles than carbon. However, during heating in oxygen the fraction of metallic gold in $AuTiO_2$/CNF increases as well and after two hours the total fraction of Au(0) is larger than for Au/CNF. Purging the sample in helium followed by introduction of H_2/He immediately results in changes in the fraction of Au(I). The fraction of Au(I) increases to approximately 45 % and is relatively constant during the treatment, see Figure 4. The relatively large change in oxidation states for Au can be a combination of structural changes and adsorption of hydrogen on the surface. Note that the Au(I) fraction is merely an expression of the partial positive charge on the Au atoms ($Au^{\delta+}$) rather than of a formal oxidation state.

In situ XAS studies show that the WGS activity is higher when the fraction of $Au^{\delta+}$ is high, although the positive charge during WGS may arise from CO (or hydrogen) chemisorption on Au or by dynamic changes in the metal-support interaction. Since titania is a partially reducible oxide, hydrogen may create vacancies in the oxide structure that are able to promote the interaction with gold particles.

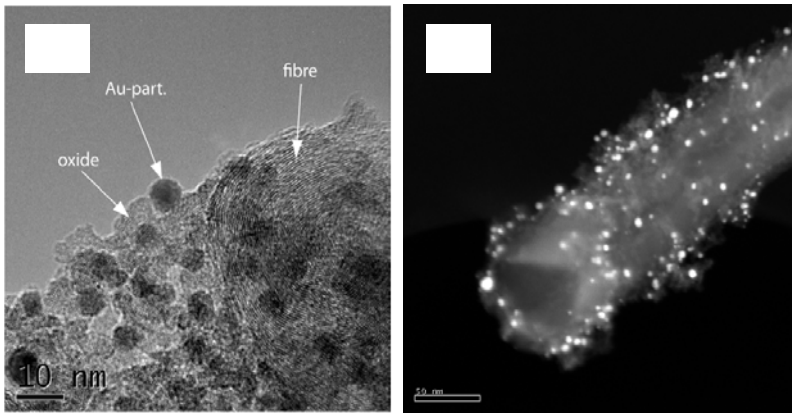

***Figure 5**. (A) TEM and (B) STEM images of the samples as-prepared showing Au particles selectively deposited on titania supported on CNF for $AuTiO_2CNF$.*

The Au-Au coordination number increases after thermal treatment in oxygen and helium. However, the increase in coordination number is less pronounced for samples containing CNF. Oxidation followed by reduction of $AuTiO_2$/CNF causes no further increase in coordination number and the Au-Au interatomic distance. This suggests that the oxygen treatment leads to stronger interaction between the gold particles and the TiO_2 and prevents further particle sintering.

The WGS activity significantly improves when titania is present in the catalytic material compared to deposition of Au directly on CNF. This shows that high catalytic activity in the water-gas shift reaction is obtained only when both Au and the oxide are present, indicating that the active sites are either on the Au-TiO_2 interface or that the reaction follows a bifunctional mechanism. The specific rate is 8 times higher for the catalyst prepared by deposition-precipitation which indicates that residue from the colloid preparation has a detrimental effect on the catalytic activity and that the two preparation methods require different pre-treatment procedures to obtain high activity.

Publications:

1. Ø. Borg, M. Rønning, S. Storsæter, W. van Beek, A. Holmen, Identification of cobalt species during temperature programmed reduction of Fischer-Tropsch catalysts, *Stud. Surf. Sci. Catal.* **163** (2006), 255
2. Ø. Borg, N Hammer, S. Eri, O.A. Lindvåg, R. Myrstad, E.A. Blekkan, M. Rønning, E. Rytter, A. Holmen, Fischer-Tropsch synthesis over un-promoted and Re-promoted γ-Al2O3 supported cobalt catalysts with different pore sizes, *Catal. Today* (2008) accepted
3. N. Hammer, I. Kvande, V. Gunnarsson, B. Tøtdal, X. Xu, D. Chen, M. Rønning, Au-TiO_2 Catalysts on Carbon Nanofibres Prepared by Deposition-Precipitation and from Colloid Solutions, *Catal. Today* **123** (2007) 245
4. N. Hammer, I. Kvande, D. Chen, W. van Beek, M. Rønning, Identification of valence shifts in Au during the water-gas shift reaction, *Topics in Catalysis,* **45** (2007) 25
5. N. Hammer, I. Kvande, D. Chen, M. Rønning: Au-TiO_2 catalysts stabilised by carbon nanofibres *Catal. Today* **122** (2007) 365
6. F. Huber, Z. Yu, S. Lögdberg, M. Rønning, D. Chen, H. Venvik, A. Holmen, Remarks on the passivation of reduced Cu-, Ni-, Fe-, Co-based catalysts, *Catal. Lett.* **110**(3,4) (2006) 211
7. M. Rønning, F. Huber, H. Meland, H. Venvik, D. Chen, A. Holmen, Relating catalyst structure and composition to the water-gas shift activity of Cu-Zn based mixed-oxide catalysts, *Catalysis Today,* **100** (2005) 249-254

Novel adsorption behavior of Carbon Dioxide in the isotypic nanoporous metal terephthalate MIL-53.

Philip L. Llewellyn[a], Sandrine Bourrelly[b], Christian Serre[b], Thomas Devic[b], and Gérard Férey[b]

([a]MADIREL, Université de Provence, Marseille, France, and [b]Institut Lavoisier, Université de Versailles, France)

One of the technological problems that face society today is the environmentally friendly and economically favourable separation and recovery of gases. Examples of current interest include the recovery of greenhouse gases (CO_2, CH_4) and the purification of hydrogen produced from biomass. Parts of these processes include an adsorption step in which microporous adsorbents such as activated carbon and zeolites are used. In such cases, it is the thermal regeneration step that is most costly in terms of energy.

Recent interest has focused on "Metal Organic Frameworks" (MOF) which are formed of metallic centres linked to each other through organic chains. Several of these organic-inorganic hybrid porous solids have the interesting feature, during adsorption, of being selectively flexible (breathing) as a function of the nature of the adsorptive fluid. A consequence of this particular property is the possibility to develop novel selective separation and storage processes with a favourable energetic cost with respect to already existing processes.

The structural topology of MIL-53(Cr) [1-3] corresponds to a 4^4 net (Fig.1). It consists of tilted chains of $Cr^{III}O_4(OH)_2$ octahedra sharing trans hydroxyl groups. These chains are linked via carboxylate groups of the terephthalate ions (1,4-benzene dicarboxylate or BTC) forming a 3-D framework.

The resulting pore system is one-dimensional of free diameter close to 0.85 nm. The chemical formula of the metal-benzenedicarboxylate is $Cr(OH)(O_2C–C_6H_4–CO_2)$. The sample was synthesised by the group in Versailles following a previously published protocol [3].

To understand the adsorption process we try to couple adsorption experiments up to 50 bars with in situ measurements such as calorimetry and XRD.

The direct calorimetric measurements obtained during adsorption give information on the energetic nature of adsorbents which can be of importance to characterize solids in terms of specific adsorption sites and defects. Moreover, such information is of great interest for defining the adsorbent performance in process design.

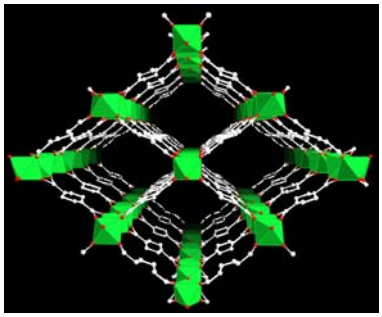

***Fig. 1** : Schematic diagram of the pore system of MIL53.*

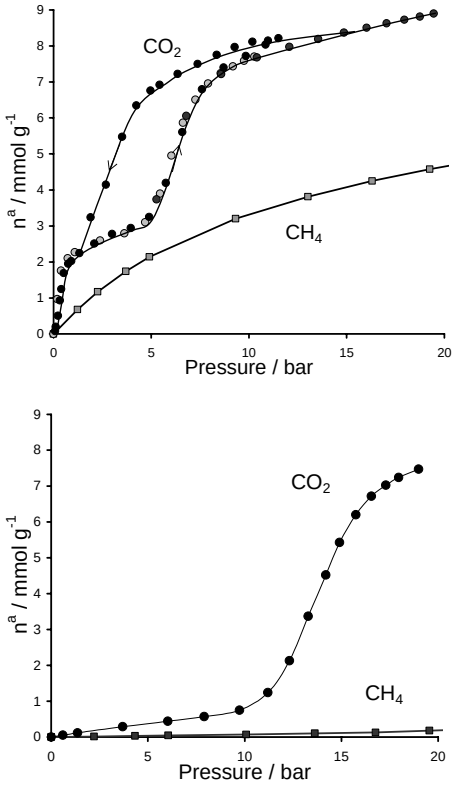

***Fig. 2** : CO_2 and CH_4 adsorption isotherms obtained at 303 K on the dehydrated (upper curves) and hydrated (lower curves) forms of MIL53(Cr).*

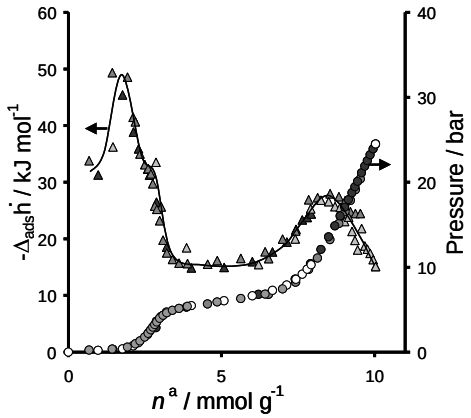

***Fig. 3** : Enthalpies and isotherm obtained for CO_2 adsorption at 303 K on dehydrated MIL53(Cr).*

The isotherms (Fig. 2) show the adsorption of CO_2 and CH_4 on MIL53(Cr) at 303K. The upper curves show results on samples outgassed until free of residual water. It can be seen that the behaviour of CH_4 is much like the adsorption on other nanoporous materials such as zeolites. However the adsorption of CO_2 shows a distinct step [5]. The latter proceeds in two stages after a very fast uptake at low pressure (~2-3 mmol.g^{-1}), the isotherm reaches first a plateau between 1 and 4 bars, followed by an adsorption of more than a double amount of CO_2 at higher pressures. Interestingly, desorption occurs with a hysteresis loop with the desorption branch returning to the adsorption one at *ca*. 2 bar.

The differential enthalpies of adsorption obtained with the dehydrated sample are shown in Figure 3. It can be seen that the initial adsorption occurs with an enthalpy of around -30 kJ mol^{-1}. The enthalpy then increases sharply. The second adsorption step is accompanied by a large decrease in the enthalpies and at the end of this second step, the enthalpies increase once again.

The differential enthalpies of adsorption obtained with the dehydrated sample are shown in Figure 3. It can be seen that the initial adsorption occurs with an enthalpy of around -30 kJ mol^{-1}. The enthalpy then increases sharply. The second adsorption step is accompanied by a large decrease in the enthalpies and at the end of this second step, the enthalpies increase once again.

The evolution of the adsorption enthalpies are quite surprising. Such variations could be due to an initial adsorption on localised sites followed by the filling of the remaining porosity. A second hypothesis is that the adsorption phenomena are due to a change in the structure of the porous phase. This hypothesis emanates from the fact that this structure undergoes a contraction on contact with residual water vapour [6].

To follow the structure of the solid phase, experiments were carried out on an adsorption system adapted for *in situ* X-ray diffraction experiments. The results obtained for the dehydrated system are shown in Fig. 4. The diffractograms show that the dehydrated sample is in the open form. The initial dose of carbon dioxide closes the structure. This closed structure remains to a pressure of around 6-7 bars at which point the opening of the structure is observed. This corresponds to the second step in the isotherm. On desorption, the open structure is maintained to a pressure of around 2 bars at which the structure closes once again. Interestingly, the pore contraction, which occurs in MIL-53 upon adsorption of CO_2 at 1 bar is slightly lower than that in the case of hydration: the unit cell shrinks to 1072 $Å^3$ in the case of the closed MIL53 (Cr) structure with CO_2 compared to ~1012 $Å^3$ for the hydrated structure. This would be consistent with the larger size of CO_2 compared to H_2O.

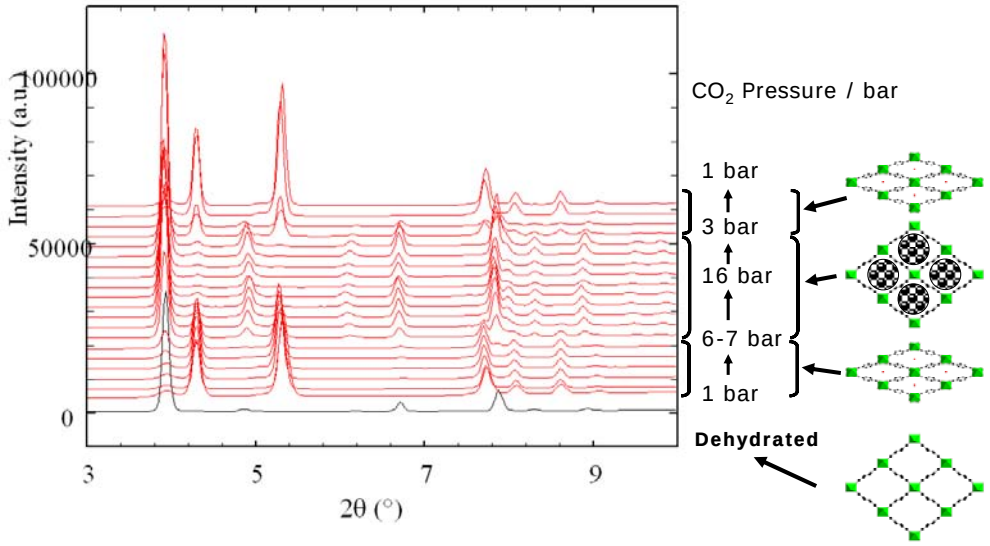

***Fig. 4**. X-ray diffraction spectra obtained on adsorption and desorption of CO_2 on the dehydrated MIL-53(Cr) sample.*

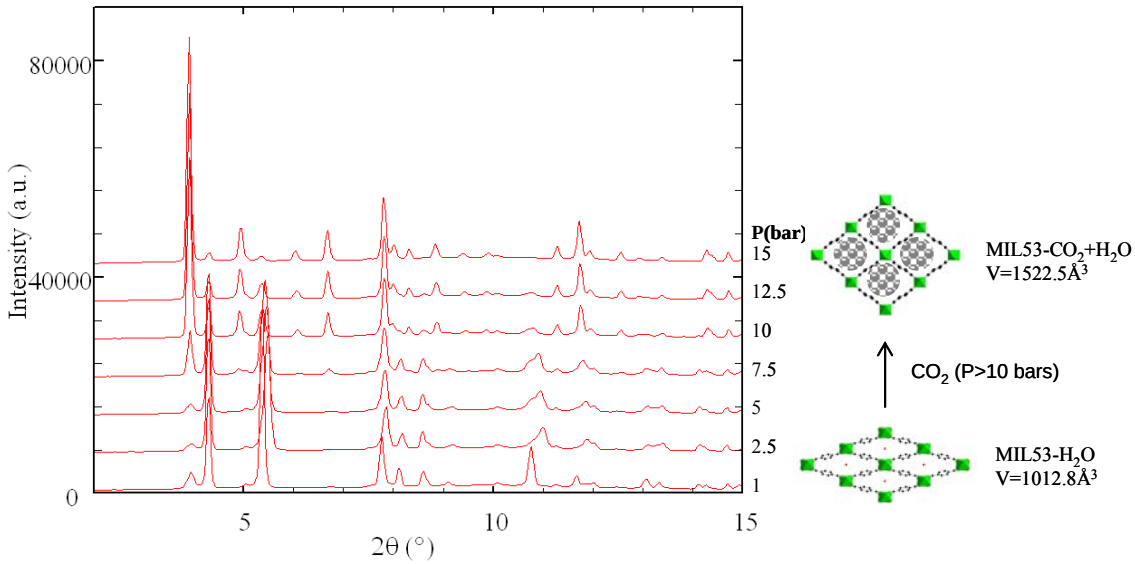

***Fig. 5**. X-ray diffractogram obtained on adsorption of CO_2 on the hydrated MIL-53 (Cr).*

The isotherms shown in Fig. 2 (lower curves) show the adsorption of CO_2 and CH_4 on MIL53(Cr) which has been left in the presence of humidity [7]. It has previously been shown that under such conditions the MIL53 is in a closed form [6] and thus virtually no CH_4 is adsorbed. However, there is an adsorption of CO_2 above 12 bars. The in situ X-ray diffraction (Figure 5) again allows an insight into the adsorption phenomena. As expected, the hydrated form of the MIL53(Cr) is contracted. The opening of the structure occurs in the region from 7.5 to 10 bars. With decreasing pressures (not shown), the desorption branch in the isotherm corresponds to a contraction of the MIL53 structure. Interestingly, the closed structure after desorption has the same cell volume as that observed during the initial adsorption of CO_2 on the dehydrated sample. Note also that the desorption branch on the hydrated sample does no rejoin the adsorprtion branch and that the final point corresponds to around 2 mmol g^{-1} which is a similar value to that observed with the dehydrated sample. These facts point to a replacement of the water in the hydrated sample by carbon dioxide.

Such results are of major significance for future applications in gas separation and storage. It can be appreciated that the important feature of the above results is that the apparent selectivity is drastically increased for the hydrated sample. That is to say that the relative amount of CO_2 adsorbed with respect to CH_4 is increased for the hydrated material. This is not the case for other carbon dioxide adsorbents such as zeolites where often the water blocks specific sites. It has previously been shown that the present sample is stable to higher humidity and thus a process where a significant amount of water is present may not harm the adsorption of carbon dioxide. Thus the need for a preadsorber in a PSA type process would not be required thus leading to simpler process design. Further work on the adsorption of carbon dioxide in the presence of increasing partial pressures of water is planned.

This work highlights the difference in adsorption behaviour between a polar and non-polar probe. To make a generalisation, it will be of importance to follow other molecules of varying polarity. Nevertheless, the above results are particularly interesting when one considers the recovery of carbon dioxide in mixed gas streams or the use of such materials in sensor type applications. As it would initially seem that the structural flexibility of these materials is related to the polar nature of the probe gas molecule, such results could pave the way for the use highly flexible MOFs for the separation of other mixtures of polar and non-polar gases. Initially, it will be of interest to study the feasibility to recover CO_2 in natural gas feeds in which the water content is significant.

[1] K. Barthelet, J. Marrot, D. Riou, G. Férey, *Angew. Chem. Int. Ed*., 41, (2002), 281-284.
[2] T. Loiseau, C. Mellot-Draznieks, H. Muguerra, G. Férey, M. Haouas, F. Taulelle, *C. R. Chimie,* 8(3-4), (2005), 765-772.
[3] C. Serre, F. Millange, C. Thouvenot, M. Noguës, G. Marsolier, D. Louër, G. Férey, *J. Am. Chem. Soc*., 124, (2002), 13519-13526.
[4] P. L. Llewellyn, G. Maurin, *C. R. Chimie,* 8, (2005), 283.
[5] S. Bourrelly, P. L. Llewellyn, C. Serre, F. Millange, T. Loiseau, G. Férey, *J. Am. Chem. Soc*., 127(39), (2005), 13519-13521.
[6] T. Loiseau, C. Serre, C. Huguenard, G. Fink, F. Taulelle, M. Henry, T. Bataille, G. Férey, *Chem. Eur. J.,* 10, (2004), 1373-1382.
[7] P. L. Llewellyn, S. Bourrelly, C. Serre, Y. Filinchuk, G. Férey, *Angew. Chem. Int. Ed*. 45(46), (2006), 7751-7754.

Synthesis and transformation of nanomaterials studied by *in situ* powder diffraction

Heidi Ø. Nielsen, Tao Gao, Rune E. Johnsen, Helmer Fjellvåg, and Poul Norby

Department of Chemistry and Center for Materials Science and Nanotechnology,

University of Oslo, P.O. Box 1033, Blindern, N-0315 Oslo, Norway

In order to obtain an improved understanding of the formation/synthesis and transformation of nanomaterials, we have undertaken a number of *in situ* studies using synchrotron X-ray powder diffraction. We are especially interested in size and morphology control in synthesis of nanocrystals and nanostructures.

In connection with establishment of a Centre for Resaerch Based Innovation in Norway (led by the University of Oslo) inGAP (Innovative Natural Gas Reactions and Processes), we have built up a system for studies of catalytic materials under operative conditions at SNBL. The system allows studies of materials under flow conditions with pressures up to 20 atm. to be performed while studying the exhaust gas composition using a mass spectrometer. Together with the *in situ* Raman spectrometer available at SNBL, we have a powerful and unique tool for studies of materials under a wide variety of chemical conditions. The gas system will be described in detail elsewhere.
Here we intend to give a few examples of *in situ* studies of synthesis and transformation of nanomaterials and nanostructures.

Hydrothermal synthesis of Co_3O_4 nanocubes[1].

Co_3O_4 is a promising material for use in e.g. gas sensors, pigments, catalysis, electrochemistry, magnetism, energy storage etc. We aim at synthesizing Co_3O_4 nanocubes for use in different applications in nanodevices. The nanocrystals may for example be of interest for use in core-shell materials. For this purpose, the nanoparticles should be free standing, monodisperse, have a well defined morphology and small size distribution[1,2].

A hydrothermal synthesis route for preparation of well-facetted Co_3O_4 nanocrystals has been developed in the research group [3]. These syntheses typically yield nanocrystals from 10 – 90 nm, and the crystals tend to agglomerate. An alternative hydrothermal approach utilizing micro waves for heating has been successfully explored[1], which gives a smaller size distribution (10 – 20 nm). A reflux method developed by Xu *et al*.[4] using a surfactant, Tween-85, also yields well-facetted Co_3O_4 crystals, with a very narrow size distribution.

The hydrothermal formation of Co_3O_4 nanocubes was studied using *in situ* synchrotron X-ray powder diffraction in order to obtain information on the formation mechanism of the nanocrystals. Our emphasis has been on investigating the intermediate phases and crystallite size as a function of time or temperature. We have also briefly started to explore the reaction kinetics, revealing crystallization mechanisms.

In a typical synthesis, 0.00125 mmol of $Co(NO_3)_2 \cdot 6H_2O$ (98 %, Merck) and 0.0176 mmol $NaNO_3$ (>99.0%, J.T. Baker) was dissolved in 12.5 mL ion exchanged water. 0.0025 mmol of tetra ethyl ammonium hydroxide, (TENOH, $N(CH_2CH_3)_4OH$, 97 %, 20 wt-%, Aldrich), was added slowly while stirring. In one experiment, 0.00034 mmol

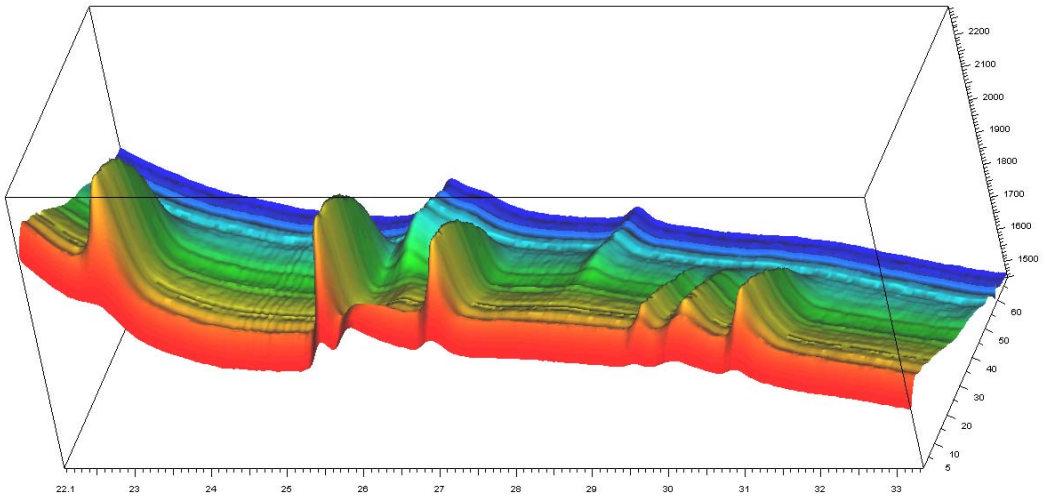

Figure 1. *3-Dimensional representation of in situ powder diffraction data. The x-axis shows the diffraction angle, the z-axis the intensity and the y-axis denotes the different data sets, as they are recorded with increasing temperature.*

H_2O_2 (30 wt-%, Norsk Medisindepot) was added to investigate the effect on oxidation of Co^{2+} to Co^{3+} necessary to make the spinel Co_3O_4.

A quartz capillary tube with d=0.7 mm was filled with reactants and mounted on a goniometer head with a Swagelok T-piece. This allows for a N_2 pressure to be applied, and thereby hydrothermal conditions are maintained, when the applied pressure is higher than the vapour pressure of the reaction mixture at the reaction temperature. A pressure of ~10 bar was used. A hot air blower was used to heat a part of the capillary from room temperature to 200 ºC using heating rates of 2, 5 and 10 ºC/minute.

Time-resolved *in situ* experiments (time resolution 107 seconds) were performed using a MAR345 area detector at the Swiss-Norwegian Beam Line BM01A at ESRF.
Figure 1 shows an example of the *in situ* powder diffraction data. The first data set (in front) was collected at room temperature, and the temperature was increased (2ºC/min) to 200ºC. This temperature was held until the amount of products was stabilized.

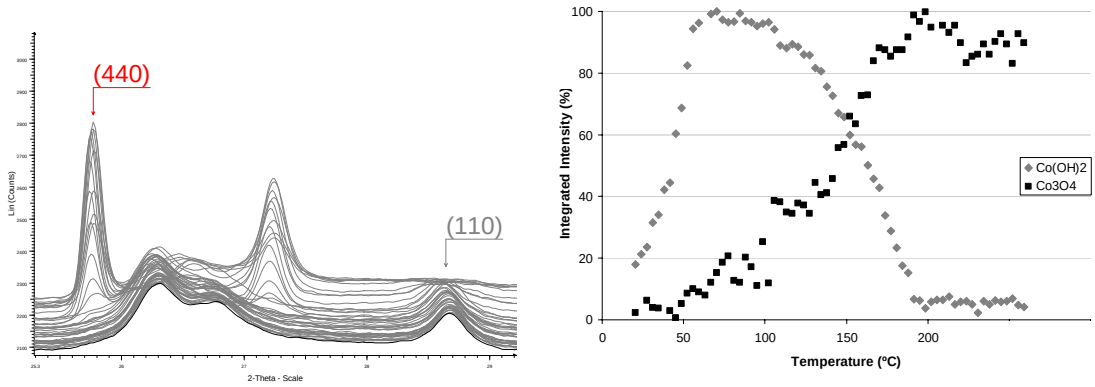

Figure 2*. a) The figure shows the (440) peak for Co_3O_4 and the (110) peak for $Co(OH)_2$ in a small area in the sample with a heating rate of 2 °C/min. b) Relative amounts of Co_3O_4 and $Co(OH)_2$ from the integrated intensity of the two peaks.*

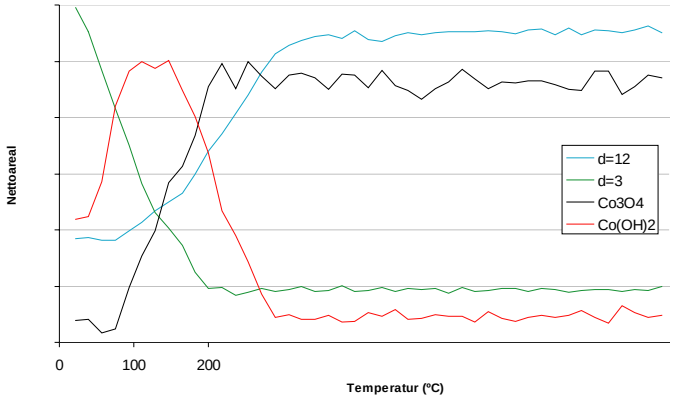

Figure 3. *Relative amounts of different phases correlated to Co_3O_4 and $Co(OH)_2$ in the sample with hating rate 10 °C/min.*

Some $Co(OH)_2$ is already present at the beginning of the synthesis, and the amount increases with temperature. The formation of Co_3O_4 begins at a higher temperature when the amount of $Co(OH)_2$ almost is at the maximum, see Figure 2. This may indicate that the reaction involves other phases. The existence of additional phases is indicated by the appearance and disappearance of broad features in the powder diffraction patterns. The phases involved could be one or more disordered layered structure. The formation of Co_3O_4 is complete approximately at the same time as a peak at d≈3 Å disappears. The amount of $Co(OH)_2$ reaches zero at the same time as the peak at d≈12 reaches its maximum. The theory of a layered structure can be confirmed by a small peak at d≈1,5 which could very well be the (110)-peak in a hydrotalcite-like phase for example $Co_x^{3+}Co_{1-x}^{2+}(OH)_{2-x}(NO_3)_x \bullet nH_2O$.

The existence of additional phases is indicated by the appearance and disappearance of broad features in the powder diffraction patterns. The phases involved could be one or more disordered layered structure. The formation of Co_3O_4 is complete approximately at the same time as a peak at d≈3 Å disappears. The amount of $Co(OH)_2$ reaches zero at the same time as the peak at d≈12 reaches its maximum. The theory of a layered structure can be confirmed by a small peak at d≈1,5 which could very well be the (110)-peak in a hydrotalcite-like phase for example $Co_x^{3+}Co_{1-x}^{2+}(OH)_{2-x}(NO_3)_x \bullet nH_2O$. However, further studies are necessary to address this.

[1] Nielsen, H.Ø, Master Thesis, Department of Chemistry, Faculty of Mathematics and Natural Sciences, University of Oslo, Norway, **2006**.
[2]Heidi Østbye Nielsen, Ola Nilsen, Helmer Fjellvåg and Poul Norby "Synthesis of Co_3O_4 nanocubes; an *in situ* synchrotron powder diffraction study" In preparation.
[3] Yang, J.; Quaresma, S.; Mei, S.; Ferreira, J. M. F.; Norby, P.; *Key Eng. Mater.* **2005**, *280-283*, 713-716.
[4] Xu, R.; Zeng, H. C.; *Langmuir* **2004**, *20*, 9780-9790.

Figure 4. *Schematic drawing of the tetragonal crystal structure of β-MnO_2 viewed along [001].*

In situ studies of hydrothermal synthesis of β-MnO_2 nanorods[5] and thermal transformation of cryptomelane nanofibers[6,7].

Hydrothermal synthesis of β-MnO_2 nanorods was followed by means of in situ *synchrotron X-ray diffraction of a redox reactions in a mixed $(NH_4)_2S_2O_8$ and $MnSO_4$ solution. The diffraction data, combined with SEM and Raman studies, show that γ-MnO_2 is formed first during the hydrothermal synthesis and subsequently transforms into β-MnO_2 with increasing temperature. The growth of the γ-MnO_2 crystallites follows a nucleation-dissolution-anisotropic growth mechanism. The Raman spectrum of the as-synthesized β-MnO_2 nanorods feature four bands at 759 (B_{2g}), 664 (A_{1g}), 576 (Ramsdellite impurity), and 537 (E_g) cm^{-1}, in agreement with Mn-O lattice vibrations expected for a rutile-type MnO_6 octahedral matrix.*

The *in situ* hydrothermal synthesis was performed using a micro-reaction cell. Equal volumes of $(NH_4)_2S_2O_8$ (0.1 M) and $MnSO_4$ (0.1 M) aqueous solutions were mixed under stirring at room temperature. A small amount of the obtained transparent solution was injected into a quartz glass capillary (diameter 0.7 mm) which was mounted in a

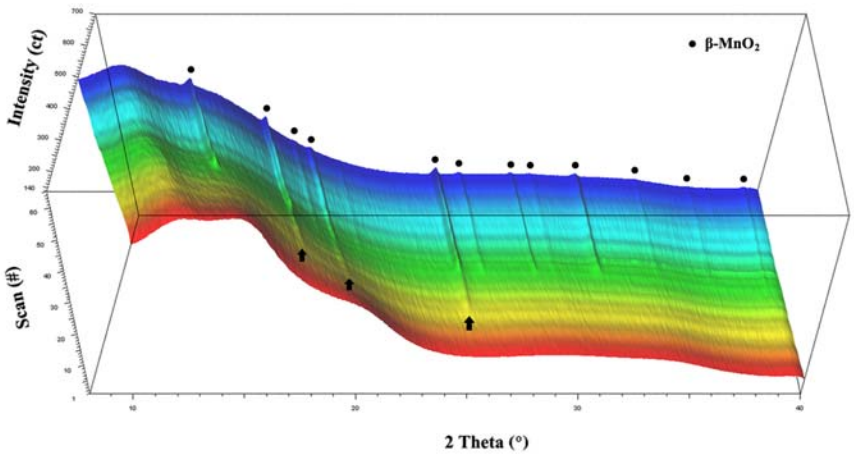

Fig. 5 *In situ synchrotron XRD patterns during hydrothermal synthesis of β-MnO_2 nanorods. Reflections from the β-MnO_2 phase are marked with dots. The presence of an intermediate phase is illustrated by arrows. The broad bump between 10 and 20° in 2θ is due to scattering from the quartz glass capillary and solvent.*

Swagelok fitting. An internal pressure (N_2) was used in order to maintain hydrothermal conditions and the reaction cell was heated up to 160°C at a rate of 2°C/min.

In situ synchrotron X-ray powder diffraction data were collected at the Swiss-Norwegian Beam Line BM01A, at ESRF ($1 \leq 2\theta \leq 40°$, $\lambda = 0.071096$ nm) using a MAR345 detector.

Figure 5 shows a 3-dimensional representation of the time-resolved synchrotron XRD patterns collected during hydrothermal synthesis. Upon gradual increase of the reaction temperature to about 90°C (after 25 scans), an intermediate phase was observed which could be identified as γ-MnO_2. As the reaction temperature increases further to 135°C (after 38 scans), tetragonal β-MnO_2 starts to form.

The reactions were followed also *ex situ* using conventional hydrothermal synthesis. Figure 6 shows SEM images and powder diffraction patterns of the final and intermediate phases.

Other manganese oxide nanomaterials were produced, e.g. cryptomelane nanofibers, K_xMnO_2. This material was prepared by hydrothermal from aqueous solutions of $MnSO_4$ (0.1 M) and $KMnO_4$ (0.1 M). The suspension was heated in a teflon-lined stainless steel autoclave at 140°C for 24 h without shaking or stirring[6].

The thermal transformation of cryptomelane nanofibers was followed by heating in a controlled atmosphere (air or N_2 flow) from 20 to 900°C. Powder diffraction patterns were collected using the MAR345 imaging plate detector. Upon heating, a disproportionation reaction takes place resulting in formation of a potassium rich cryptomelane phase together with bixbyite, Mn_2O_3. By Rietveld refinement of the collected powder diffraction data the structure evolution of the two phases was determined. Figure 8 shows the development in the unit cell parameters and the population

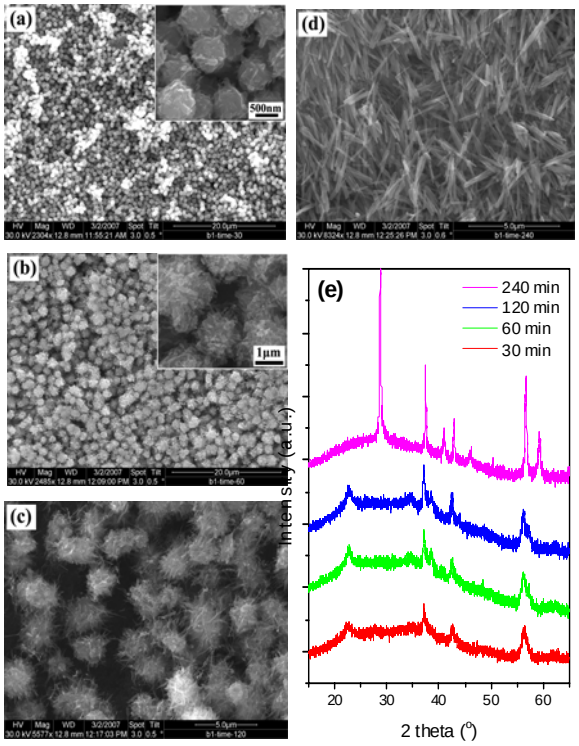

Figure 6. *SEM images (a-d) and corresponding XRD patterns (e) of MnO_2 materials prepared by hydrothermal treatment of a mixed solution of $(NH_4)_2S_2O_8$ and $MnSO_4$ at 140°C for 30 min (a), 60 min (b), 120 min (c), and 240 min (d). Insets to (a) and (b) show enlarged pictures. The X-ray wavelength is 0.15406 nm. The XRD patterns are shifted vertically for clarity.*

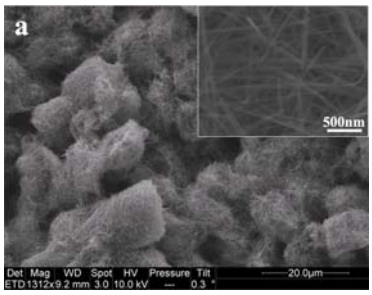

Figure 7. *SEM images of cryptomelane nanofibers[6].*

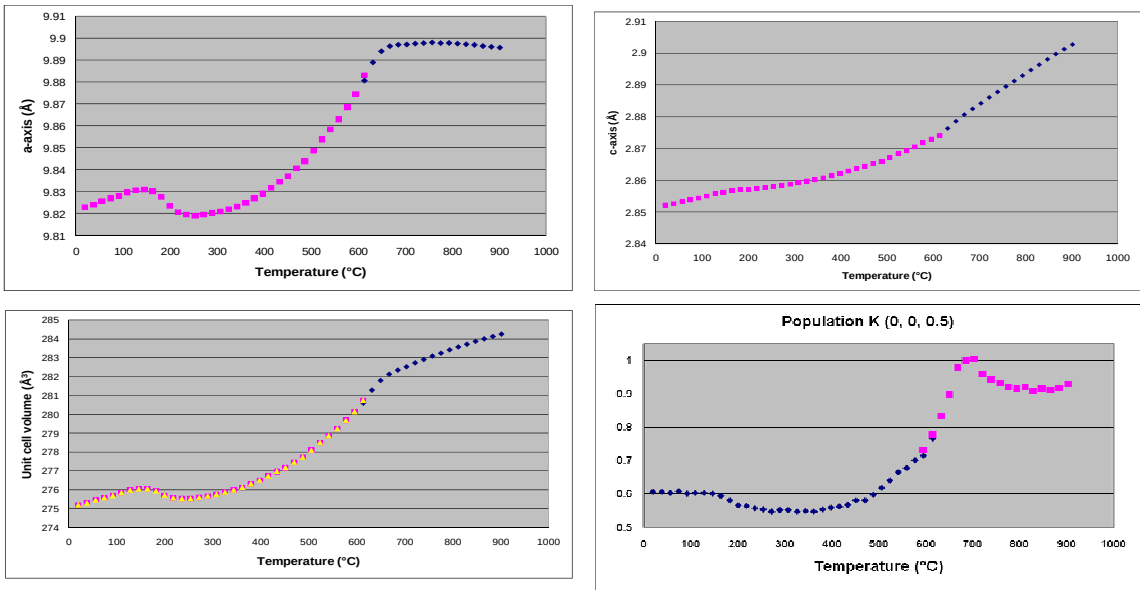

***Figure 8**. Development in unit cell parameters and potassium content in cryptomelane nanofibers during heating from room temperature to 900C in air.*

of the potassium site in cryptomelane as a function of temperature.

[5] Tao Gao, Poul Norby, and Helmer Fjellvåg "*In situ* studies of hydrothermal synthesis of β-MnO_2 nanorods" In preparation.
[6] Tao Gao, Marianne Glerup, Frank Krumeich, Reinhard Nesper, Helmer Fjellvåg, and Poul Norby "Microstructures and Spectroscopic Properties of Cryptomelane-type Manganese Dioxide Nanofibers" *J. Phys. Chem.* ***C*** **2008**, *112,* 13134–13140
[7] Tao Gao, Poul Norby, and Helmer Fjellvåg "*In situ* studies of thermal transformations of cryptomelane nanofibers" To be published

V.2 In-house research

Antiisostructural phases and anomalous thermoelasticity in In-based alloys

V. Dmitriev, D. Chernyshov, and Ya. Filinchuk
Swiss-Norwegian Beam Lines at ESRF, BP220, 38043 Grenoble, France

Anomalous elastic properties of a IIIA group metal indium, and its unusual for metallic elements crystal structure give rise to intense, both experimental and theoretical, studies. Elemental indium has at ambient conditions a body centered tetragonal structure [$(c/a)_{fct}$ >1] with one atom in a primitive unit cell (Z_p=1). A contraction (negative expansion) occurs in In along a four-fold axis and an expansion in a basal plane with increasing temperature. One could have expected that the tetragonal distortion is removed by application of external pressure. However, high-pressure studies of In revealed the stability of the fct structure [1,2]. Moreover, it lowers the symmetry from tetragonal to orthorhombic at about 45 GPa [3]. Alloying In with IIA group metal Cd (x_{Cd}>5 at.%) and IVA group metal Pb (x_{Pb}>30 at.%) allows not only to remove a tetragonal distortion of the crystal lattice and stabilize a face-centered cubic (fcc) structure [4,5], but it switches the sign of distortion and stabilizes another tetragonal structure (bct') with $(c/a)_{fct}$ <1.

The rich and reliable experimental information accumulated for In-based alloys stimulated, in last decade, numerous theoretical works. However, no mechanism was suggested explaining negative thermal expansion, no approach was elaborated allowing to understand atypical behaviour of tetragonal distortion in the compressed metal.

There is an unexplored aspect of the phase transitions occurring in In-based alloys - they are proper ferroelastic transformations. It allows, therefore, by applying rather simple phenomenological formalism, to uncover the generic features of phase stability and crystal lattice transformations. Such approach is symmetry based and, therefore, model free. Its important advantage consists as well in easy incorporation of different external variables, like pressure, concentration or temperature, so that, for instance, the latter is not restricted to T=0 K.

In situ high-temperature and high-pressure data were obtained at the Swiss-Norwegian Beam Lines (BM1A) of the European Synchrotron Radiation Facility (ESRF, Grenoble, France). X-ray diffraction patterns were collected in angle-dispersive geometry using an image plate detector (MAR345).

It is convenient to classify a phase transition as ferroelastic if it involves a change in crystal system, accompanied by a change in strain owing to the difference in unit cell shape. The experimentally measured strain $\varepsilon_1=(c_t/a_t-1)$ carrying parent cubic lattice to tetragonal one is one of two symmetry equivalent strains

$$\varepsilon_1 = \tfrac{1}{\sqrt{6}}(e_1 + e_2 - 2e_3)\,, \quad \varepsilon_2 = \tfrac{1}{\sqrt{2}}(-e_1 + e_2), \tag{1}$$

The symmetrical combinations of the diagonal components e_i (i=1÷3) of the strain tensor can be, therefore, considered as order-parameter (OP) components for a cubic-to-tetragonal proper ferroelastic transformation. The corresponding non-equilibrium thermodynamic potential is a functional of two polynomials invariant by cubic symmetry group of the parent phase:

$$I_1 = \varepsilon_1^2 + \varepsilon_2^2 = \eta^2\,, \qquad I_2 = \varepsilon_1^3 - 3\varepsilon_1\varepsilon_2^2 = \eta^3 Cos3\varphi\,; \tag{2}$$

The corresponding variational free energy (Landau potential) is

$$F(P,T,\varepsilon_1,\varepsilon_2) \equiv \Phi(P,T,\eta,\varphi) = \Phi_0(P,T) + a_1 I_1 + a_2 I_2 + a_{11} I_1^2 + a_{12} I_1 I_2 + a_{111} I_1^3 + a_{22} I_2^2\,. \tag{3}$$

The equations of state $\partial\Phi/\partial\eta=0$, $\partial\Phi/\partial\varphi=0$ result from the minimization of Φ with respect to the variables η and φ (or F to ε_1 and ε_2), and yield four possible equilibrium structures:

0. $\eta=0$ $\{\varepsilon_1=\varepsilon_2=0\}$: *Fm3m* (Z_P=1);

I. $\eta\neq0$, $Cos\varphi=1$ $\{\varepsilon_1=\varepsilon\,,\ \varepsilon_2=0;\ e_1=e_2>e_3\}$: *I4/mmm* (Z_P=1, c/a<1);

II. $\eta\neq0$, $Cos\varphi=-1$ $\{\varepsilon_1=-\varepsilon,\ \varepsilon_2=0;\ e_1=e_2<e_3\}$: *I4/mmm* (Z_P=1, c/a>1);

III. $(a_2+a_{12}I_2+2a_{22}I_2)=0$

$\{\varepsilon_1\neq0,\ \varepsilon_2\neq0,\ \varepsilon_1\neq\varepsilon_2\}$: *Fmmm* (Z_P=1). (4)

The equations of state determine, in addition to the cubic parent phase 0, two low symmetry phases, I and II, with identical tetragonal symmetry. They are associated with opposite values of the equilibrium order parameter components, i.e. phases I and II are *antiisostrural* [6]. The orthorhombic symmetry of phase III is the maximal common subgroup of the symmetry groups of phases I and II.

The space groups of the I and II phases are the same but the sign of the order-parameter components changes from one phase to another [Fig. 1(b)]. In terms of the spontaneous strain tensor components one has on one phase $e_3>e_2=e_1$, whereas in the other phase $e_3<e_2=e_1$ [see Eqs. (4)]. Accordingly, in the case of cubic-to-tetragonal transformation two antiisostructural phases are associated with the opposite signs of the tetragonal distortion (c/a-1). Figure 1(b) shows the shape of $\eta(\tilde{a})$ along thermodynamic paths defined by straight lines $\tilde{a}=\alpha_0a_1+\beta_0a_2$ in the (a_1,a_2) plane, which correspond to various sequences of the phases indicated in Fig. 1(a).

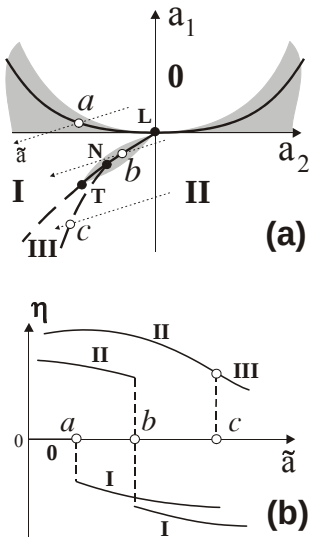

Fig. 1. *(a) Phase diagrams corresponding to the thermodynamic potential defined by Eq. (3). Dotted lines denoted a-c are thermodynamic paths, which correspond to different sequences of phases. (b) Order parameter variation for the various paths shown in (a).*

The overall phenomenological Landau approach can be tested against available structure data determined at room temperature as a function of pressure, across the In-Pb alloys. The pure indium metal crystallizes in a body-centered tetragonal structure (*I4/mmm*, Z_P=1) [5], which corresponds to a slightly distorted face-centered cubic (fcc) structure with $(c/a)_{fct}$=1.076 [phase II in (6)]. High-pressure x-ray diffraction experiments revealed that the c/a ratio increases with pressure, reaching a maximum around 24 GPa, and then uncommonly decreases with further compression [1]. At 45 GPa Indium transforms to a face-centered orthorhombic (fco) phase *Fmmm* (Z_P=1), which is obtained by a simple orthorhombic distortion of the low-pressure tetragonal phase [3]. One notices that this sequence corresponds to the path *c* in Fig. 1(a). The $In_{.90}Pb_{.10}$ alloy, at ambient conditions, has the same In-type fct structure with c/a>1 (phase II). Under pressure, it undergoes a phase transition to another tetragonal structure, with a discontinuous jump of the axial ratio from c/a>1 (phase II) to c/a<1 (phase I) [7], i.e. it follows the path *b* in Fig. 1(a).

The Pb-enriched alloys $In_{.85}Pb_{.15}$ and $In_{.78}Pb_{.22}$ crystallize in the latter fct' structure (phase I) and show no phase transition up to, at least, 40 GPa [8]. Alloys $In_{1-x}Pb_x$ with 30>*x*>60 at.% have a cubic structure [parent phase 0 in (4)] and, under pressure, transform from fcc (phase 0) to fct' structure with c/a<1 (phase I, path *a*) [9].

Therefore, all above features of the phase evolution in In-Pb alloys are evidently encountered in the framework of the phenomenological model with the Landau potential (3).

Figure 2 shows the phase diagram identical to Fig. 1(a) but complemented with third dimension that is order parameter η. One finds that plane sections of the theoretical diagram [Fig. 1(b) and Fig. 2] perfectly reproduce order parameter, η=(c/a-1), evolution as a function of pressure, experimentally obtained by different authors [1-3,7-8]. The correct mapping of the

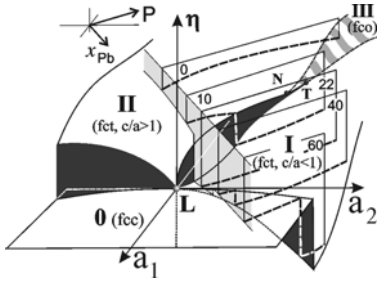

***Fig. 2**. Equilibrium phase diagram corresponding to the thermodynamic potential (3), in the (a_1,a_2,η) space. Greyish plane is an ambient isobaric plane. Vertical planes are (η,P) isothermal sections corresponding to $In_{1-x}Pb_x$ with different Pb content. Dashed lines in the planes show order parameter η=(c/a-1) as a function of pressure. The numbers indicate the atomic percentage of lead.*

structural phases and η=(c/a-1) as a function of pressure implies that the symmetry-based theory with nonequilibrium potential (3) gives a unifying picture of phase stability and pressure induced elastic behaviour for $In_{1-x}Pb_x$ alloys. This conclusion encourages us to study pressure- and temperature-induced elastic strains in other In-based alloys, namely $In_{1-x}Sn_x$ and $In_{1-x}Cd_x$, in order to validate the phenomenological model.

An important question, which this study addresses, regards the origin of a remarkable thermoelastic anisotropy in the pure In metal and In-based alloys. Its thermal expansion coefficient α_{11} perpendicular to the tetragonal axis is positive, but the coefficient α_{33} parallel to the axis is negative and decreases with increasing temperature. However, accurate measurements on pure In samples and its alloys with Pb, Sn, and Cd allow us to conclude that above property is characteristic of a tetragonal structure with c/a>1, i.e. of the phase II, but not phase I with c/a<1 (Fig. 3). The sign of α_{33} correlates, therefore, with the sign of ferroelastic OP.

Simultaneous heating fct/fct' two-phase mixture in identical conditions provides us with an unambiguous evidence that pressure and concentration play only secondary role in the effect. We have managed to manufacture such a mixture for one of In-Pb alloys at ambient conditions. Following Fig. 2, an alloy with near critical concentration x_{Pb}=10 at.%, at ambient conditions is very close to the fct-fct' transition line, so that the difference in energy between stable II and metastable I should be very small and the corresponding energy barrier should be very tiny. We found that phase content of $In_{.90}Pb_{.10}$ samples depends on the preparation procedure. Original alloy lumps are single-phase, only phase II is present. Although a small chip cut with a blade remains single-phase, rasping the lump transforms a part of the sample powder to phase I. Shear stresses, induced by rasping off, promote, therefore, a transition between fct and fct' structures even at ambient conditions. The fct' (I) structure is retained in the sample up to T=135°C (melting point for the alloy is T=150°C), and then irreversibly transforms to fct (II).

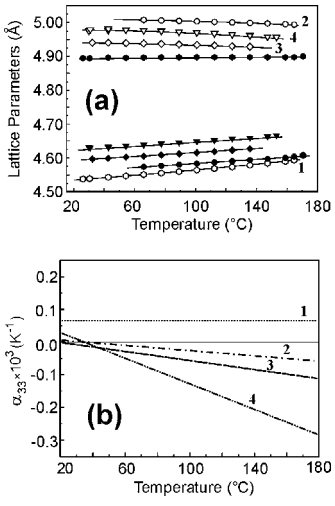

***Fig. 3.** (a) Thermal expansion of In-based alloys. Circles correspond to $In_{.92}Sn_{.08}$, triangles $In_{.90}Pb_{.10}$, diamonds In, hexagons $In_{.78}Pb_{.22}$. Open spots correspond to the lattice parameter c, closed a.*
(b) Temperature variation of the principal expansion coefficient α_{33} for $In_{.78}Pb_{.22}$ (1), $In_{.92}Sn_{.08}$ (2), In (3), and $In_{.90}Pb_{.10}$ (4)

Heated now in identical conditions, fct (phase II) and fct' (phase I) structures exhibit, nevertheless, different thermoelastic behaviour. In the stable fct structure a contraction occurs along a four-fold axis, with increasing temperature, while the metastable fct' one shows dilatation in the same direction (Fig. 4).
A total strain induced in a distorted structure by temperature variation consists of two parts:

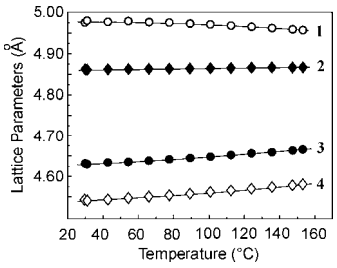

Fig. 4. *Temperature variation of the lattice parameters of $In_{.90}Pb_{.10}$ in phases I and II, at ambient pressure: 1 - c_{II}, 2 - a_I, 3 - c_I, 4 - a_{II}.*

$\varepsilon_T=\varepsilon_{th}+\varepsilon_{OP}$, where ε_{th} corresponds to an ordinary thermal expansion (non-symmetry breaking), and ε_{OP} is a spontaneous strain induced by a ferroelastic phase transition (symmetry breaking). Thermal expansion of a tetragonal structure is entirely characterised by two principal linear expansion coefficients $\alpha_1=\alpha_{11}=\alpha_{22}= (\partial\varepsilon_1/\partial T)=(\partial a/\partial T)/a$, and $\alpha_3=\alpha_{33}= (\partial\varepsilon_3/\partial T) =(\partial c/\partial T)/c$. If a tetragonal structure can be considered as a distorted cubic one, and this is the case for the In alloys, the latter coefficient takes the form $\alpha_3^t = \alpha_1^c + \alpha_{cr}$, where α_1^c is the corresponding coefficient for the cubic structure, and $\alpha_{cr} = \frac{1}{c}\frac{\partial(\Delta c)}{\partial T} \cong \frac{\partial \eta}{\partial T}$ is a "critical" (symmetry breaking) contribution of an order parameter reduced symmetry from cubic to tetragonal. Order parameter values for phases I and II should be found as solutions of the equations of state. Our analysis of experimental data on the In-based alloys concludes that the consideration can be restricted, without loosing of generality, to the vicinity of the Landau point (see Figs. 1 and 2) where fourth-degree terms dominate over six-degree one. It allows, in turn, to restrict the Landau expansion (3) to the forth degree terms. A simplified quadratic equation yields two solutions:

$$\eta_{I,II} = \frac{\mp 3a_2 \pm (9a_2^2 + 32a_1a_{11})^{1/2}}{8a_{11}}, \qquad (5)$$

one corresponding to phase I (upper signs in the numerator), the other to phase II (lower signs).

Remember, that the other our conclusion fixed up the direction of the T-axis parallel to a_1 making all other phenomenological coefficients temperature-independent. Thus, it yields

$$\alpha_{cr}^{I,II} \cong \left(\frac{\partial \eta}{\partial T}\right)_{P,x} = \pm 2\alpha_1\left[9a_2^2 + 32\alpha_1(T-T_C)a_{11}\right]^{-1/2}. \qquad (6)$$

One finds an additive to the equilibrium cubic expansion coefficient to be positive in phase I (upper sign), but negative in phase II (lower sign). The latter decreases when temperature raises approaching T_C: $\alpha_{cr} \propto -(T-T_C)^{-1/2}$. Thus, α_3 may become negative, and it should decrease. Figure 2 clearly shows how the order parameter $\eta=(c_t/a_t-1)$ decreases in phase II with temperature increasing, i.e. lattice parameter c_t decreases approaching a_t. This negative contribution, becoming dominant, results in the uniaxial contraction (negative expansion) of the tetragonal lattice.

The unified phenomenological theory worked out for In-based alloys maps, therefore, all the structural phases observed experimentally so far, and correctly describes transitions between them. The model discloses the origin of the anomalous elastic anisotropy as being related to the spontaneous strain induced by a proper ferroelastic transition.

Alloying In with IIA and IVA group metals provides an extraordinary example of proper ferroelastic compounds. To the best of our knowledge, this is the first case when variation of external thermodynamical parameters (T, P, *x*) reveals a complete variety of stable phases and phase transitions between them, predicted by a theory with multicomponent order parameter. It is specially applied to direct transitions between antiisostructural phases.

References

[1] K. Takemura, *Phys. Rev. B* **44**, 545 (1991); **[2]** O. Schulte and W. B. Holzapfel, *Phys. Rev. B* **48**, 767 (1993); **[3]** K. Takemura and H. Fujihisa, *Phys. Rev. B* **48**, 8465 (1993); **[4]** *A Handbook of Lattice Spacings and Structures of Metals and Alloys*, ed. W. B. Pearson (Pergamon, Oxford, 1964), vv. 1-2; **[5]** P. Villars and L. D. Calvert, *Pearson's Handbook of Crystallographic Data for Intermetallic Phases* (American

Society for Metals, Metals Park, Ohio, 1985); **[6]** P. Toledano and V. Dmitriev, *Reconstructive Phase Transitions in Crystals and Quasicrystals* (World Scientific, Singapore, 1996); **[7]** V. F. Degtyareva et al. *J. Phys.: Condens. Matter* **15**, 1635 (2003); **[8]** V. F. Degtyareva et al. *High Pressure Research* **24**, 551 (2004); **[9]** O. Degtyareva et al. *J. Phys.: Condens. Matter* **13**, 7295 (2001).

Publication

Dmitriev V.P., Chernyshov D., Filinchuk Y.E., Degtyareva V.F. Anti-isostructural phases and anomalous thermoelasticity in In-based alloys: Synchrotron x-ray diffraction experiments and unified phenomenological model. *Phys. Rev. B*, 2007, **75**, 024111.

X-Ray induced radiation damage in taurine: a combined X-ray diffraction and Raman study

J. A. Beukes[a], F. Mo[a] and W. van Beek[b]
[(a)] NTNU, Trondheim, Norway; [(b)] SNBL at ESRF

Taurine (2-aminoethanesulfonic acid) is one of the nonessential amino acids. Its origin can be dietary sources or it can be synthesized in the adult human body from methionine via cysteine. Some mammals lack the ability to produce it in sufficient amounts. Taurine is not a constituent of proteins. It forms taurocholic acid with cholesterol, the sodium salt of this acid is the major ingredient of the bile of carnivorous animals. It is present in meat, fish and poultry, in relatively high concentrations in all electrically excitable tissues such as the brain, sensory organs and the heart, and in certain endocrine glands. In mammalian heart tissue taurine is by far the most abundant free amino acid, comprising in excess of 50% of the total free amino acid pool. Some of the physiological functions of taurine are established, such as being an essential constituent to newborns of most mammal species, however, the cellular mechanisms of taurine are still mostly a matter of speculation.

Radiation damage is an important and very well recognized problem, in particular in macromolecular crystallography, but the understanding of its nature is still incomplete. In this work, the impact of X-radiation on the small sulphur-containing amino acid taurine has been monitored by combined time-resolved Raman and X-ray powder diffraction studies at 296 K, succeeded by time-resolved single crystal diffraction studies at 120 K and 296 K.

The most significant changes with exposure in the Raman spectra are shifts and broadening of some of the lines.

The three major effects that are observed from Raman spectroscopy of the irradiated powder sample of taurine give indications of the mechanism involved. Firstly, the broadening of bands could indicate that the forces acting in the molecules are not constant within the assembly of taurine molecules, but attain a diverging spectrum with exposure.

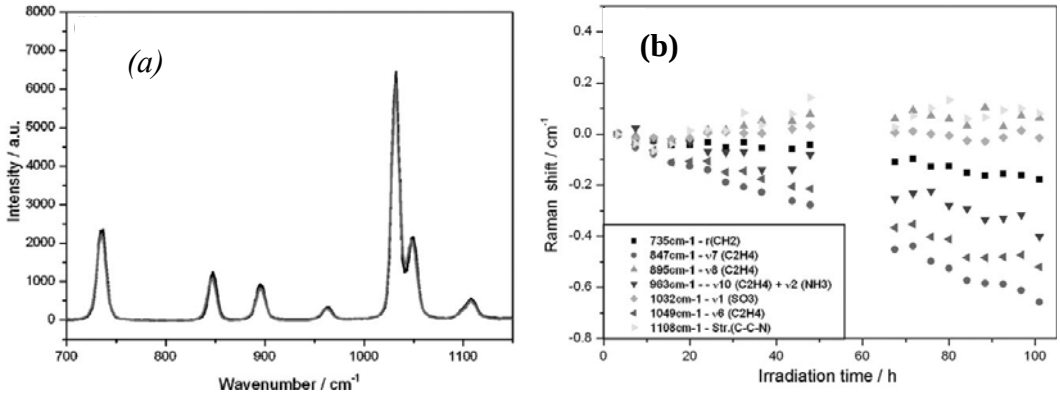

Fig. 1 *(a) Selected 700–1150 cm^{-1} region of the spectrum. (b) Frequency shifts of the bands in the 700–1150 cm^{-1} region. Most of the shifts are towards smaller wavenumbers and are approximately linear with irradiation time indicating changes in the electronic potentials and/or formation of new chemical species.*

This fact suggests that X-rays induce local molecular changes at scattered sites in the crystal. The broadened Raman bands are associated with different parts of the molecule, implying that the induced inhomogeneity of forces is distributed over the entire molecule. Secondly, the Raman intensities change, and the intensities are directly related to the polarizability of the molecular species in the sample. Evidently, changes in chemical composition would create spectral changes. However, new lines are not observed, but the intensity changes of certain lines are fairly large. If new products were formed in sufficiently large quantities then both new bands and bands in partial overlap with the native taurine spectrum would be expected. The lack of new observable bands indicates that there is no significant formation of compounds with new chemical groups. Thirdly, the intramolecular forces are affected by the intermolecular electrostatic environment. The normal coordinates calculated by *ab initio* methods for non-zwitterionic taurine provide a qualitative picture of the magnitudes of atomic displacement along different crystallographic directions. The red-shift identify a weakening of the parent force constants, and it is interesting that the largest effect is observed in the ‘‘backbone’’ vibrations which have the principal motion of non-hydrogen atoms along the c axis. A blue-shift indicates a narrowing of the electronic potentials, and is observed for the fundamental vibrations with main movements in the *ab*-plane. These axes contract slightly with increasing exposure, the contraction is much smaller than the expansion along the c axis.

The diffraction experiments reveal systematic changes in the unit-cell parameters, the most pronounced being a linear expansion of the *c* axis, broadening of the powder diffraction lines, a linear increase in the ADPs, for which the largest values are those of the terminal O atoms, and an accumulation of negative charge in the SO3 group. The residual density in the three planes C(1)−S−O(*i*) is shown in Figs. 2 (a)-(b), at the beginning and at the end of the 296 K experiment. The S atom resides in a negative region of electron density, *i.e.* has a positive charge due to transfer of electron density into each of the adjoining bonds. The total charge and the partitioning of charge over the atoms can be calculated by different methods. Hibbs *et al.* found that the positive charge on the S atom in taurine exceeds +2 electrons, but the negative charge on the O atoms makes the

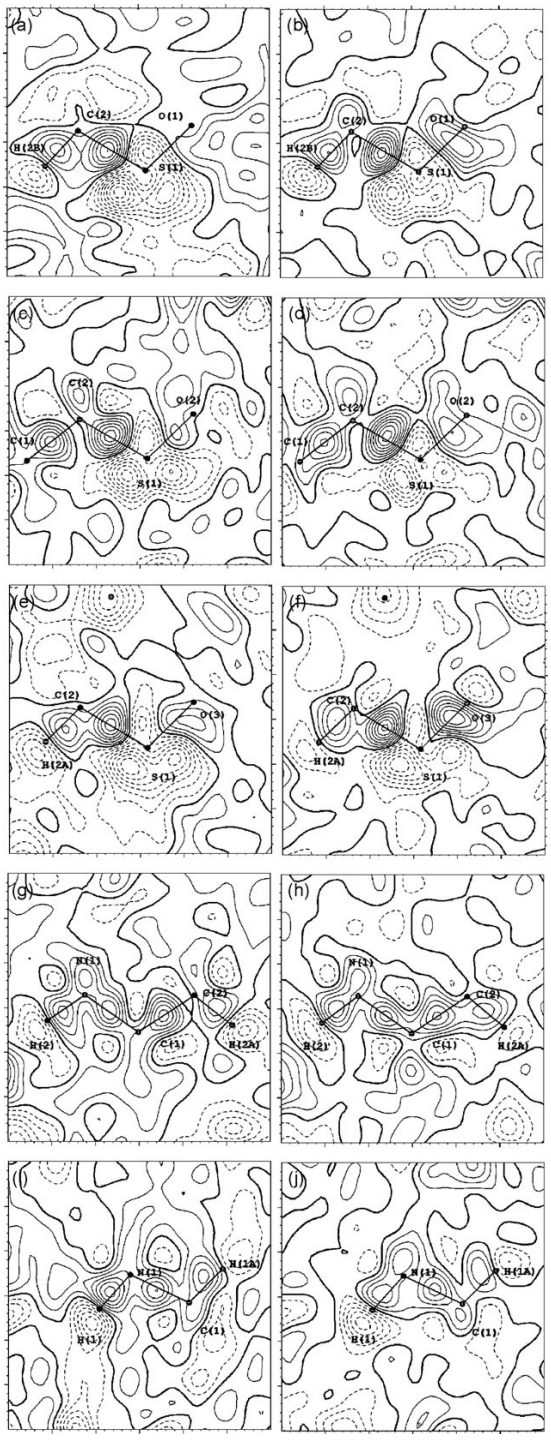

Fig. 2 *Fourier difference maps, Dr(X - XHO), in some selected planes from the study at 296 K. Left: maps calculated from the first data set, 0.5–4.3 h exposure. Right: maps calculated from the last data set, 56.6–60.3 h exposure. Negative contours are shown as hatched lines, heavy line is the zero contour. Equidistance: 0.05 e A* $^{-3}$

SO_3 group negatively charged, q_{total} being ~ − 0.97. Here we will make a qualitative assessment of changes in the charge from the details in the maps. A common effect of radiation in the three density sections in Fig. 2 appears to be: a depletion of positive charge near the S site, an enhancement of negative charge in the C−S and the three S−O bonds, and an increased charge in the lone-pair region near the O atoms. In total these changes imply an increased negative charge on the SO_3 group.

All these observations may be attributed to a primary formation of radicals, predominantly involving the SO_3 end of the molecule, occurring as scattered events throughout the crystal, presumably with the highest frequency on the surface of entrance. Secondary reactions will create structures that are different from the taurine molecule, thereby introducing an enhanced local decay of crystalline order, *i.e.* enhanced static disorder, and a build-up of local strain. A study of the cell parameters and of the hydrogen bonding at the two different temperatures provides evidence for linking the accumulation of foreign species in the crystal to the linear increase in ADPs as well as in the *c* axis. It has been suggested that the irreversible increase in *d* spacings or in unit-cell volume of organic and protein crystals could be used as a metric of radiation-induced damage. However, a detailed understanding of the processes involved is lacking. In our study of a small sulphur-containing molecule we have obtained results pointing to the radiation-induced creation of radicals and a secondary formation of foreign molecular fragments or species in the crystal as the most probable mechanism for the observed changes in various physical parameters. This may well be a general mechanism also for larger structures.

Publication:

J. A. Beukes, F. Mo and W. van Beek
X-Ray induced radiation damage in taurine: a combined X-ray diffraction and Raman study
Phys. Chem. Chem. Phys., 2007, **9**, 4709 - 4720

Structural transformations of light metal borohydrides

Y. Filinchuk, D. Chernyshov, and V. Dmitriev
Swiss-Norwegian Beam Lines at ESRF, BP220, 38043 Grenoble, France

Light metal hydrides are considered as perspective energy carriers for future mobile applications. Hydrogen can be produced from borohydrides of alkaline metals by varing thermodynamic parameters such as temperature and pressure or in the reaction with water. In order to understand the stability and find ways to influence it we studied structure and transformations of $NaBH_4$ and $LiBH_4$ at various temperatures and pressures using single-crystal and powder diffraction techniques.

The ambient pressure fcc α-phase of $NaBH_4$ transforms at ~6 GPa into a closely related tetragonal β-phase, and above 8 GPa into a new orthorhombic γ-phase [1]. We collected synchrotron powder diffraction data for $NaBH_4$ in a diamond-anvil cell up to 11.2 GPa. For a successful structure solution, it was absolutely essential to model the sample texture, including it as a variable in a global optimization. Strong texture indicates an oriented growth of crystallites, specific for the β- to γ-$NaBH_4$ transition. The structure (Figure 1) was solved *ab initio* from diffraction data, using program FOX, with most crystallites having their *a*-axes approximately aligned with the compression direction, and then refined by the Rietveld method. Elimination of the correction for the preferred orientation leads to an increase in R_B from 7.9% to 45%. That means that not only the structure solution, but also the refinement would fail if we did not take the texture into account. Elimination of hydrogen atoms increases R_B from 7.9% to 17%, thus showing that their contribution to X-ray diffraction intensities is sufficient for localization of H-atoms, even from high-pressure synchrotron data.

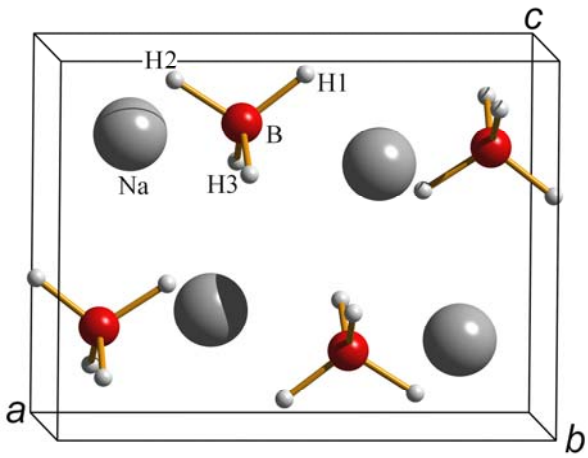

Fig. 1. *Crystal structure of γ-$NaBH_4$ at 11.2 GPa, determined ab-initio from diamond-anvil cell synchrotron powder diffraction data.*

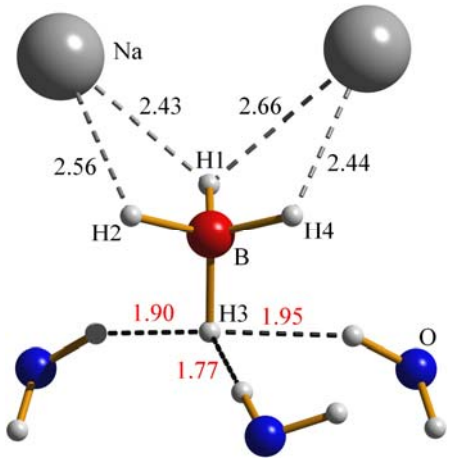

Fig. 2. *Dihydrogen bonds in $NaBH_4 \cdot 2H_2O$, determined from synchrotron diffraction on single crystals.*

The structure of $NaBH_4 \cdot 2H_2O$ was solved from single crystal diffraction data. It contains sodium cations, which are octahedrally coordinated

by four water molecules and two borohydride anions. The BH_4^- anion has a nearly ideal tetrahedral geometry and is bridged with two Na^+ ions via the tetrahedral edges. The structure does not contain classical hydrogen bonds, but reveals strong dihydrogen O-$H^{\delta+}$…$^{\delta-}$H-B bonds of 1.77-1.95 Å (Figure 2). The H…H distances are much shorter than twice the van der Waals radius of a hydrogen atom (2.4 Å). IR and Raman spectra of $NaBH_4 \cdot 2H_2O$ are consistent with the presence of the dihydrogen bonds for the three O-H groups, and the absence of the dihydrogen bonding for the forth one. An increased accuracy of X-ray diffraction applied to low-Z hydride systems was achieved by introducing a 0.10 Å empirical correction for the B-H distances, which brings H atom positions determined from X-ray diffraction in borohydrides to a direct comparison with those derived from neutron diffraction.

Two $LiBH_4$ polymorphs are known at ambient pressure, with a transition at ~380 K. Substantial theoretical and experimental efforts have been made to characterize their crystal structure. Certain discrepancies remained, however:

- in the low-temperature (LT) phase, all theoretical studies showed nearly ideal tetrahedral geometry of the BH_4 unit, while experiments described it as considerably distorted;
- the high-temperature (HT) phase, reported from synchrotron powder diffraction data to be hexagonal [2], was found unstable by theory; a monoclinic structure has been suggested from *ab initio* calculations [3].

In order to resolve these discrepancies, we studied both $LiBH_4$ phases by synchrotron diffraction on single crystals. We showed that in the LT polymorph the BH_4 group has a geometry of a regular tetrahedron. The space group $P6_3mc$ has been determined unambiguously for the HT phase. Anisotropic displacement ellipsoids, refined also for hydrogen atoms, reveal a libration-like smearing of the BH_4 group, which is well approximated by a TLS model. The revealed disorder suggests that the unaccounted entropy is the reason why *ab initio* calculations have failed to evaluate correctly the stability of the $P6_3mc$ structure.

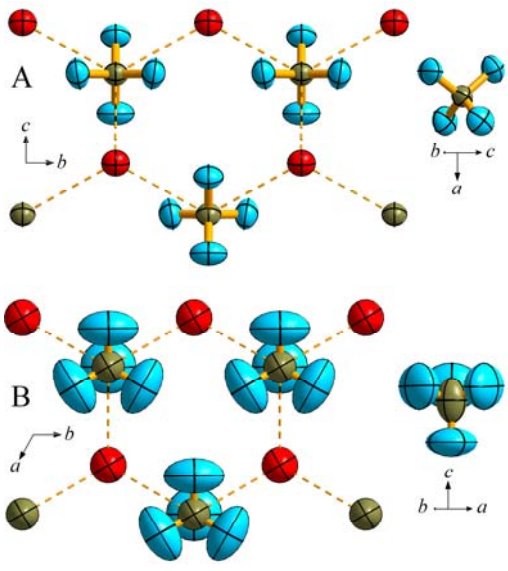

***Fig. 3**. Six-membered Li-BH_4 rings (left) and BH_4 units (right) in $LiBH_4$ structures. 40% probability ellipsoids are shown. (a) The low-temperature phase at 225 K. (b) The high-temperature phase at 535 K.*

Synchrotron diffraction of $LiBH_4$ single crystals (Fig. 3) already provides structural results as accurate as those from neutron powder diffraction study of triply (!) isotopically substituted $^7Li^{11}BD_4$ [4]. However, we evaluated even a more accessible technique, synchrotron powder diffraction, for its ability to provide accurate information on the positions of

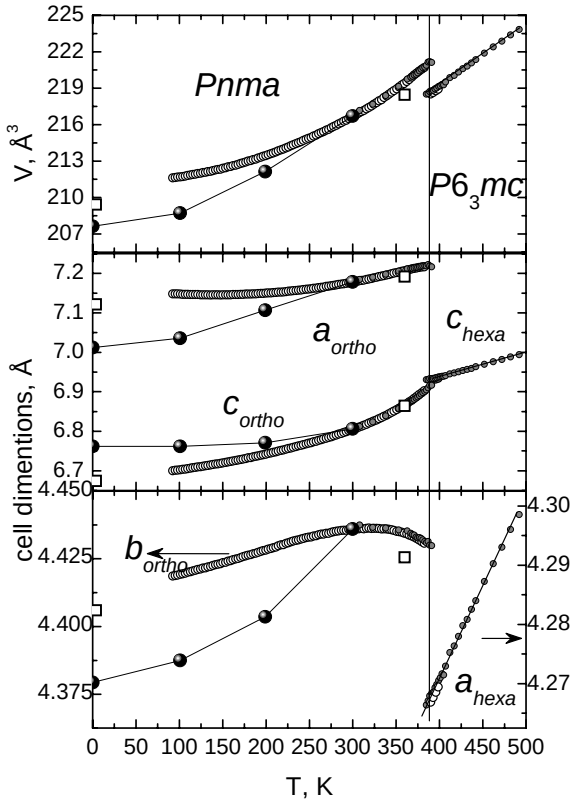

***Fig. 4**. Unit cell parameters of $LiBH_4$ as a function of temperature. Big dark circles connected by lines represent results of ab-initio calculations [5] scaled to our experimental values at 300 K, open squares represent neutron powder diffraction data [4].*

hydrogen atoms. Refinement of the LT structure from the integrated 2D diffraction images (MAR345 detector) resulted in a non-distorted BH_4 geometry. We concluded that the previous powder diffraction studies done with 1D detectors suffer from a poor powder average. The HT phase remains hexagonal from the polymorphic transition at 381K up to decomposition at ~560K. Refinement of the TLS tensor showed that the libration-like disorder of the BH_4 group is nearly isotropic, in agreement with the single crystal experiment.

In-situ powder diffraction revealed a highly anisotropic thermal expansion of LT $LiBH_4$ (Fig. 4). The cell dimension *b* continuously contracts on heating from 300 K to the transition temperature. The cell parameter *a* deviates from linear dependence below 200 K, shows a minimum at ~150 K and then increases on cooling. Such thermal expansion reflects an anharmonicity of the potential of the crystal binding. A decrease of the unit cell volume upon the LT-to-HT transition phase is remarkable (Figure 4). Thus, the disorder of the borohydride groups and strong lattice anharmonicity were revealed from diffraction data measured at various temperatures. These phenomena, being ignored, lead to a failure of theoretical predictions of structural stability of light borohydrides.

Our studies of $LiBH_4$ in diamond anvil cells showed that its high-pressure phase has a structures different from the one predicted by theory. The structure of a phase observed between 1.2 and 10 GPa has been determined *ab initio* from high-quality powder diffraction data. The new *Ama*2 structure of $LiBH_4$ reveals a novel coordination of the

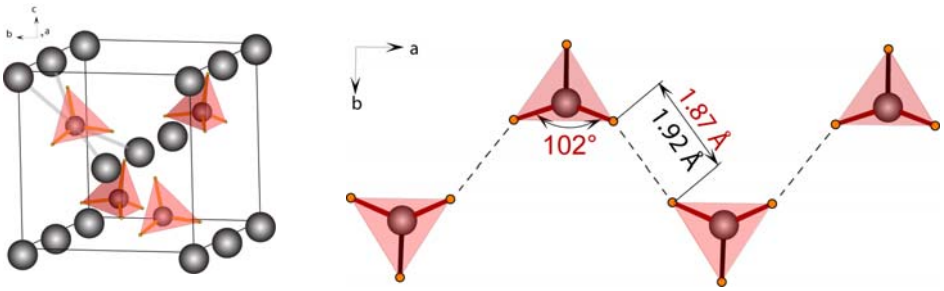

***Fig. 5**. Square-planar coordination coordination of the BH_4 anion in high-pressure phase of $LiBH_4$ (left). Short H…H contacts (experiment at 2.4 GPa: 1.92 Å; DFT: 1.87 Å) linking the BH_4 groups into chains (above).*

BH_4 anion by Li atoms (Fig. 5, left), and exceptionally short B-H...H-B distaces of 1.9 Å at 2.4 GPa. The DFT-optimized structure indicates the deformation of the BH_4 unit (Figure 5), which is likely to decrease an activation barrier for hydrogen desorption. The internal pressure in the structure may be tuned by a partial chemical substitution. The resulting $LiBH_4$-based substance with *Ama*2 structure may show more favourable hydrogen storage properties than pure $LiBH_4$ and may turn out to be useful for hydrogen storage applications. We suggest the dense structure found in our high-pressure experiments to be targeted for obtaining improved hydrogen storage materials. We have also found a second phase transition into the previously predicted cubic phase of $LiBH_4$, which occurs at higher pressures, above the reach of all previous experiments.

An *in situ* combined high-temperature high-pressure synchrotron diffraction allowed to map a phase diagram of $LiBH_4$ to 10 GPa and 500K (Fig.6). Mechanisms of phase transitions were analyzed using a phenomenological model. It suggests an existence of cation-anion layers in all four known $LiBH_4$ phases. This conclusion is not trivial from purely geometrical point of view, but it can find a rational crystal-chemical explanation. The relative complexity of $LiBH_4$ structures and of the P-T phase diagram can be linked with the directional interaction of the tetrahedral BH_4 groups with spherical metal atoms. We hypothesize that the directional BH_4...M interaction in metal borohydrides leads to a formation of anion-centered complexes, determining structures of individual phases and mechanisms of their polymorphic transformations.

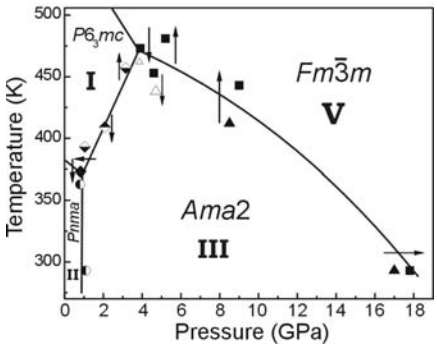

***Fig. 6**. P-T diagram of $LiBH_4$ based on the diffraction data.*

References

[1] R. S. Kumar, A. L. Cornelius, *Appl. Phys. Lett*. **87**, 261916 (2005). [2] J.-P. Soulié, G. Renaudin, R. Černý, K. Yvon, *J. Alloys Compd*. **346**, 200 (2002). [3] Z. Łodziana, T. Vegge, *Phys. Rev. Lett*. **93**, 145501 (2004). [4] M. R. Hartman, J. J. Rush, T. J. Udovic, R. C. Bowman Jr, S.-J. Hwang, *J. Solid State Chem*. **180**, 1298 (2007). [5] T. J. Frankcombe, G. J. Kroes, *Phys. Rev. B*, **73**, 174302 (2006).

Publications

Filinchuk Y., Talyzin A.V., Chernyshov D., Dmitriev V. High pressure phase of $NaBH_4$: crystal structure from synchrotron powder diffraction data. *Phys. Rev. B*, 2007, **76**, 092104.

Filinchuk Y., Hagemann H. Structure and properties of $NaBH_4 \cdot 2H_2O$ and $NaBH_4$. *Eur. J. Inorg. Chem*., 2008, 3127-3133.

Filinchuk Y., Chernyshov D., Nevidomskyy A., Dmitriev V. High-pressure polymorphism as a step towards destabilization of $LiBH_4$. *Angew. Chem. Int. Ed*., 2008, **47**, 529-532.

Filinchuk Y., Chernyshov D., Cerný R. The lightest borohydride probed by synchrotron X-ray diffraction: experiment calls for a new theoretical revision. *J. Phys. Chem. C*, 2008, **112**, 10579-10584.

Dmitriev V., Filinchuk Y., Chernyshov D., Talyzin A.V., Dzwilevski A., Andersson O., Sundqvist B., Kurnosov A. Pressure-temperature phase diagram of $LiBH_4$: synchrotron XRD experiments and theoretical analysis. *Phys. Rev. B*, 2008, **77**, 174112.

In situ time-resolved XRD study of the interaction of thiophene with Ni nanoparticles supported on SiO_2 or ZnO

I. Bezverkhyy,[a] O.V. Safonova,[b] P. Afanasiev,[c] J.-P. Bellat[a]

[a] *Institut Carnot de Bourgogne, Dijon (France)*
[b] *SNBL at ESRF (France)*
[c] *Institut de Recherches sur la Catalyse, Villeurbanne (France)*

1. Introduction

Thiophene is a typical aromatic sulfur-containing molecule, which is present in the middle boiling petroleum feedstocks. Its interaction with Ni nanoparticles is interesting from two points of view. On the one hand, thiophene is a strong poison for Ni nanoparticles deposited on the inert supports (SiO_2, Al_2O_3), which are widely used as catalysts in chemical industry [1]. Understanding of the poisoning mechanism is therefore important for increasing the stability of these catalysts. On the other hand, Ni nanoparticles can be also applied to remove sulfur-containing molecules from fuels. For example Ni nanoparticles supported on ZnO are used in so-called "reactive adsorption process" [2]. The nanoparticles are supposed to desulfurise the organic molecules and produce H_2S, which reacts with ZnO and can thus be removed from fuel. However, there is no direct information available on the state of the Ni during this process. This fact is related to the problems of instability in air of the intermediate phases and final products formed during the sulfidation. To exclude these problems we decided to use an *in situ* time-resolved XRD at synchrotron radiation source. This technique allowed us to follow on the minute time scale the modification of the crystal structure of Ni nanoparticles supported on SiO_2 and ZnO during interaction with thiophene.

2. Experimental

Ni/SiO_2 (18 wt. % Ni) samples were prepared by incipient wetness impregnation using $Ni(NO_3)_2{\cdot}6H_2O$ and Davisil Silica Gel (S_{BET}=282 m^2/g, V_p=1.15 cm^3/g). After drying the powders were directly reduced in hydrogen at 450°C for 10h in order to produce Ni nanoparticles. The size of the nanoparticles calculated from the width of (111) peak of Ni using the Sherrer equation was about 6 nm. Before reaction with thiophene all the samples were reduced again *in situ* in H_2 flow (360°C, 1h) to be sure that the nanoparticles were metallic.
Ni/ZnO (12 wt. % Ni) samples were prepared by a coprecipitation of $Ni(NO_3)_2{\cdot}6H_2O$ and $Zn(NO_3)_2{\cdot}6H_2O$ in Na_2CO_3 solution that was followed by an annealing of the precipitate in air at 400°C. After these procedures the samples were in the oxidized form (i.e. NiO/ZnO). Two different pretreatments were used in our *in situ* experiments. In the former the initial sample was heated up to the reaction temperature (360°C) in N_2 and then exposed to thiophene/H_2 flow. In the latter before the reaction with thiophene the sample was reduced in H_2 at 360°C for 3h in order to obtain Ni^0/ZnO.

The experiment was done at BM01B using the high-resolution powder diffractometer. All the measurements were performed at the wavelength of 0.5 Å. The

sample powder was placed inside the capillary plug flow reactor (1mm quartz capillary with 20 micron walls) and connected to the gas flow and the exhaust. The experiment was done at the atmospheric pressure. Gas blower oven was used to control the sample temperature inside the capillary. The samples were pre-heated up to the reaction temperature (280-360°C) in the flow of H_2 or N_2 (5 ml/min) and then H_2 saturated with thiophene vapor (40 mbar for Ni/SiO_2 and 20 mbar for Ni/ZnO) was introduced in the reactor. The time per one XRD spectrum varied from 5 to 20 minutes depending on the angular range and the data quality requirements.

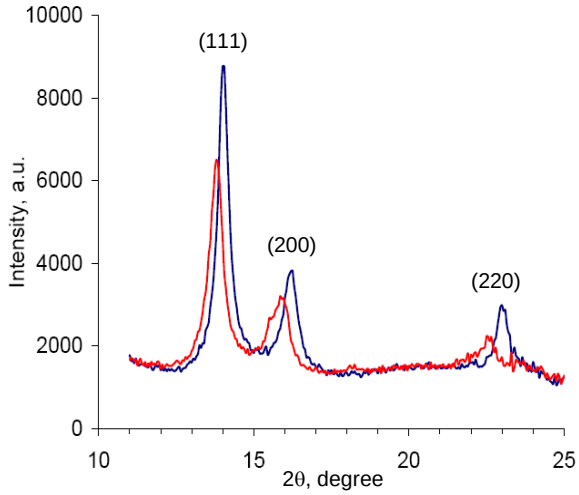

Figure 1 *XRD patterns of reduced Ni/SiO_2 before (blue) and after the contact with thiophene/H_2 mixture at 360°C.*

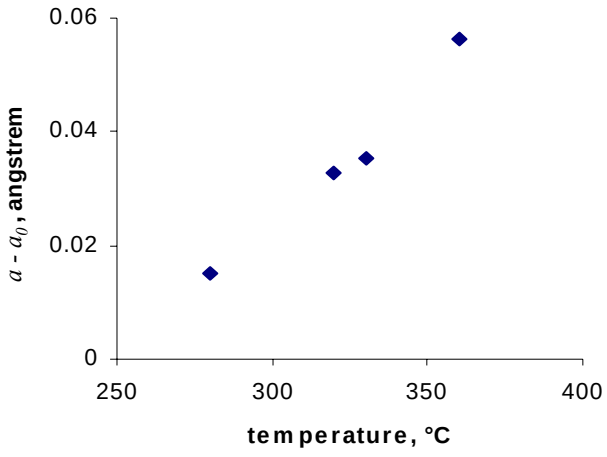

Figure 2 *Increase of Ni cell parameter in Ni/SiO_2 after interaction with thiophene/H_2 mixture at different temperatures.*

3. Results and discussion

3.1. Interaction of Ni/SiO_2 with thiophene

For better understanding the reaction mechanism and kinetics we performed the experiments at four different temperatures: 280, 320, 330, and 360°C.

Initial stage

A rather unexpected effect was observed in the initial stage (after *ca*. 25 min) of contact between thiophene and supported Ni particles (Fig.1), which is reproducible at different temperatures. Along with the appearance of Ni sulfide (a shoulder at $2\theta = 15.5°$) the peaks of Ni phase (cubic) shift towards lower 2θ values indicating an increase of the cell parameter of Ni cell. In other words a *surface interaction* with sulfur-containing molecule leads to a noticeable change of the *bulk* structure of metal nanoparticles. Such an influence of the surface reactivity on the bulk structure can be attributed to a small size of Ni clusters (6 nm). The magnitude of the change of the cell parameter increases with the interaction temperature and reaches 0.06 Å (a = 3.61 Å) at 360°C (Fig.2). The reason why the Ni structure dilates

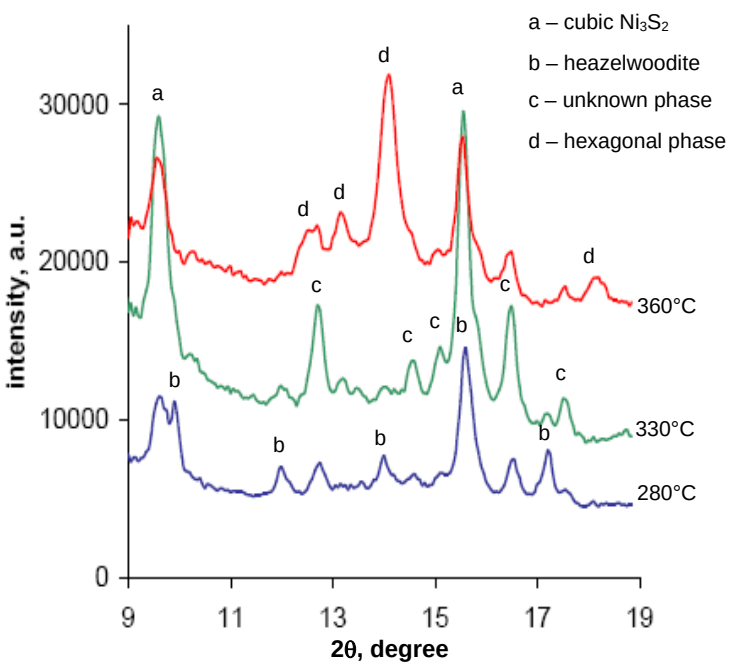

Figure 3 *XRD patterns of the stable phases obtained after interaction between Ni/SiO_2 and thiophene/H_2 mixture (40 mbar of thiophene) at different temperatures.*

is not clear so far. It is known that decomposition of thiophene on Ni surface leads to the formation of a Ni sulfide layer but also to the appearance of coke-like carbon species [3]. We expect that surface coverage of Ni nanoparticles with Ni sulfide or coke can be the possible reasons for the Ni structure dilatation. However, in the future experiment we are planning to do similar studies using H_2S instead of thiophene. In this case coke should not be formed and we will be able to see whether Ni sulfide formation alone can explain the dilatation of the structure of Ni nanoparticles. To better understand the mechanism it would be also interesting to study the effect of the Ni nanoparticle size on this process.

Final stage

After the initial stage the bulk Ni sulfidation proceeds further and finally (after 1-3h, depending on conditions) gives a complex mixture of products whose composition depends strongly on the interaction temperature (Fig.3). At the lowest temperature (280°C) Ni is completely sulfided and mainly the mixture of cubic Ni_3S_2 (JCPDF 00-027-0341) and heazelwoodite (JCPDF 00-044-1418) is formed. At 330°C much less heazelwoodite is formed. In all patterns we also observed several additional peaks, which cannot be attributed to any known Ni sulfide. The unknown phases can be particular modifications of a non-stoichiometric $Ni_{3+x}S_2$ existing only at high temperatures.

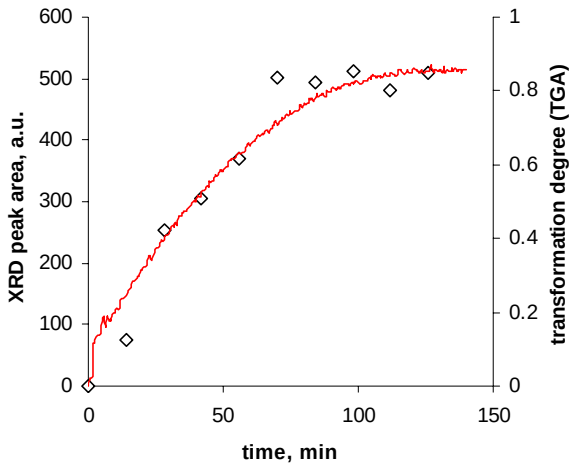

Figure 4 *Evolution of sulfidation degree of Ni/SiO_2 in thiophene/H_2 mixture at 330°C and 40 mbar measured by TGA (line) and in situ synchrotron XRD (points).*

It is also interesting that the kinetic profile of the sulfidation calculated from the integral intensity of sulfide peak at 2θ = 9.65° corresponds well to the

sulfidation profile measured by TGA in the laboratory experiment (Fig.4). It means that kinetics of this solid-gas interaction is not much influenced by the configuration of the experimental setup.

At the highest temperature (360°C) the sulfidation is only partial. This fact was previously observed in our TGA study [4]. The incomplete Ni transformation is surprising, because in the open system (under gas flow) a solid transformation, once started, must go to completion. It should be like this because the thermodynamic activity of the solid in the expression for the equilibrium constant does not depend on solid amount. The use of an *in situ* XRD in the present experiment has brought important new information allowing to understand this phenomenon. This information concerns the state of the remaining Ni, which stays non-sulfided. As it follows from XRD pattern (Fig.3), at the final stage cubic Ni completely disappears and new hexagonal phase forms (a = 2.65 Å, c = 4.36 Å). The nature of this phase has not been clearly established yet. Some authors consider that it is hexagonal modification of metallic Ni, while others attribute it to Ni_3C [5]. But whatever is the exact composition of this phase, it is important that Ni, which is not sulfided at the highest temperature (360°C), does not remain in its initial cubic structure but *transforms* into a different one. In this case the thermodynamic activity of solid also changes and a new equilibrium can be established. In other words, at 360°C in used atmosphere the formation of stable (thermodynamically or kinetically) hexagonal phase (hexagonal Ni or Ni_3C) prevents the sample from complete sulfidation.

3.2. Interaction of Ni/ZnO with thiophene

We observed in our previous work dealing with Ni/ZnO sulfidation that preliminary reduction of the sample in H_2 flow slows down the reaction with thiophene [6]. It was supposed that the reason of this effect is a partial reduction of ZnO and formation of NiZn alloy. This assumption was nicely confirmed by the present *in situ* XRD study. We observed that Ni^0 forms rapidly from NiO during heating the sample in H_2 to 360°C (Fig.5). However, on further annealing the pattern changes: after 1h at 360°C the NiO peak at 2θ = 13.83° shifts to 2θ = 13.73°, (200) peak of Ni^0 (2θ = 15.9°) disappears and new one rises at 2θ = 14.6° (NiZn). All these changes are characteristic of formation of NiZn alloy (JCPDF 01-072-2666).

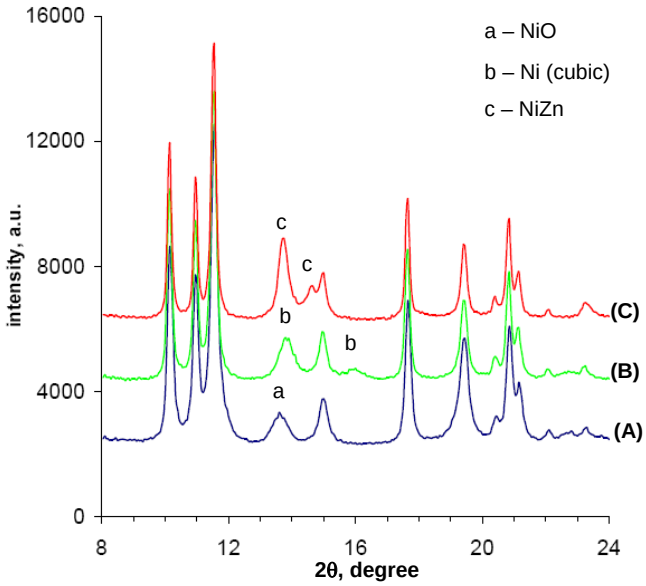

Figure 5 *XRD patterns of initial NiO/ZnO sample (A) after its heating in H_2 to 360°C (B) and after annealing in H_2 at 360°C for 1h (C). All unmarked peaks are those of ZnO*

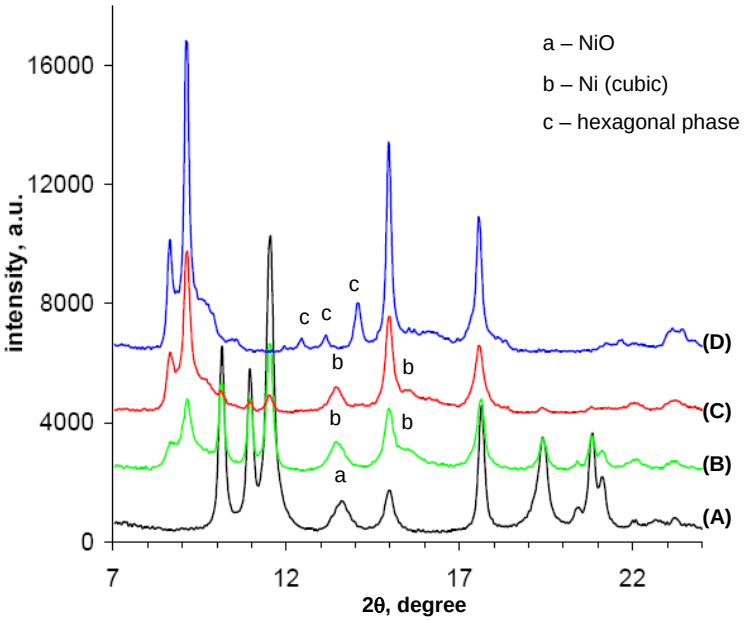

Figure 6 *XRD patterns of the initial NiO/ZnO sample (A) and after its reaction with thiophene/H_2 mixture at 360°C for 24 min (B), 84 min (C) and 148 min (D). All unmarked peaks are those of ZnO and/or ZnS.*

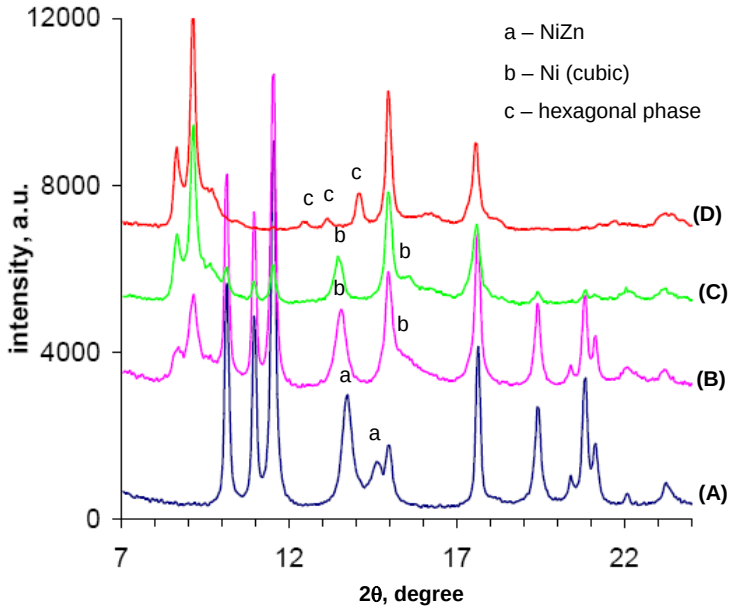

Figure 7 *XRD patterns of the NiO/ZnO sample after reduction in H_2 flow at 360°C for 3h (A) and its further reaction with thiophene/H_2 mixture at 360°C for 24 min (B), 208 min (C) and 300 min (D). All unmarked peaks are those of ZnO and/or ZnS.*

The direct reaction between unreduced NiO/ZnO sample and thiophene/H_2 mixture leads to a rapid formation of Ni^0 as well (Fig.6). However, in this case the lattice parameter of formed cubic Ni (3.70 Å, calculated from the position of (111) peak) is much bigger than the one of standard cubic Ni (a = 3.55 Å). The same process we observed before for Ni/SiO_2. Obviously, the dilatation of Ni structure is due to the presence of thiophene decomposition products on the surface of formed Ni nanoparticles (*ca.* 6 nm, as estimated from the width of (111) peak). After this initial change the state of Ni remains intact during sulfidation of ZnO, showing that the active form of Ni during reactive adsorption is surface-sulfided Ni particles. Disappearance of the peaks of ZnO in XRD patterns coincides with the change of Ni state and the same hexagonal phase, which was observed for partially sulfidized Ni/SiO_2, is formed (hexagonal Ni or Ni_3C, a = 2.66 Å, c = 4.37 Å). It is interesting that the hexagonal phase forms only in the presence of free sulfur species. Indeed, as long as ZnO is present in the sample it absorbs all H_2S produced from thiophene, so that H_2S is absent in the gas phase [6]. The fact that the hexagonal phase appears

only when ZnO is completely sulfided, means that free H_2S is needed for the formation of this phase. This observation indicates that the phase in question is rather surface-sulfided pure Ni than Ni_3C, as it seems doubtful that formation of Ni_3C would need the presence of H_2S.
Reaction between reduced Ni/ZnO (containing NiZn alloy) and thiophene proceeds in a similar way as for the unreduced NiO/ZnO sample (Fig.7). At the beginning the alloy particles decompose producing Ni^0 particles. Their cell parameter (a = 3.68 Å) indicates that the structure is dilated similarly to other cases. Then, Ni particles remain intact during the whole ZnO sulfidation and only change to the hexagonal phase when ZnO is completely transformed.

Conclusions

Application of *in situ* synchrotron XRD gave a lot of new information concerning state of Ni nanoparticles supported on SiO_2 or ZnO during their interaction with thiophene in hydrogen atmosphere.

1. For the first time it was observed that *surface* reaction between 6 nm metal nanoparticles (Ni/SiO_2) and thiophene may result in a substantial increase of the *bulk* cell parameter of the metal (from 3.55 to 3.61 Å at 360°C).
2. Another unexpected result is related to the fact that in partially sulfidized Ni/SiO_2 samples at 360°C the remaining Ni forms another hexagonal structure, whose exact nature needs further investigated.
3. For Ni/ZnO it is shown that during sulfidation of ZnO metallic Ni (cubic dilated phase), which forms at the initial stage of the reaction, remains intact until ZnO-ZnS transformation has finished.
4. All these results illustrate the great potential of *in situ* time-resolved XRD at synchrotron sources for catalysis and chemical engineering.

References

1. C.H. Bartholomew, P.K. Agrawal, J.R. Katzer, Advances in Catalysis 31 (1982) 135.
2. K. Tawara, T. Nishimura, H. Iwanami, T. Nishimoto, T. Hasuike, Ind. Eng. Chem. Res. 40 (2001) 2367-2370.
3. F. Zaera, E.B. Kollin, J.L. Gland, Langmuir 3 (1987) 555-557.
4. I. Bezverkhyy, A. Ryzhikov, G. Gadacz, J.P. Bellat, Catalysis Today 130 (2008) 199-205.
5. V. Rodriguez-Gonzalez, E. Marceau, P. Beaunier, M. Che, C. Train J. Solid State Chem. 180 (2007) 22.
6. A. Ryzhikov, I. Bezverkhyy, J.P. Bellat Applied Catalysis B: Environmental (2008), *in press* doi:10.1016/j.apcatb.2008.06.009

Spin Crossover under the Magnifying Glass: Order and Disorder in Experiment and Theory

Dmitry Chernyshov,[a] Karl W. Törnroos,[b] and Hans-Beat Bürgi[c]

[a] SNBL at the ESRF, (France); [b] Department of Chemistry, University of Bergen, (Norway); [c] Universität Bern (Switzerland)

Spin crossover (SC) is the property of molecular complexes, to change their spin state under controlled external stimuli. It affects associated physical properties like color, magnetism, density, dielectric response, etc. Much of the continuing activity in SC research concentrates on octahedral complexes with 3d metals. Preparation of the first thin films and nano-dots of SC complexes have been reported recently. Much of this research is motivated by potential applications for display, memory and switching devices [1-5]. From the point of view of fundamental research, SC in solids is an example of a cooperative response of a complex system; recently it has been suggested that SC may represent a new universality class for phase transformations [6].

Most SC compounds known today have complex crystal architectures assembled from spin-active complexes, spin-inactive counterions and solvent molecules. The structural complexity of these molecular solids renders the study, modeling and understanding of SC difficult as some of the spin-inactive components may undergo temperature-induced re-arrangements in parallel with the SC process.

Here we give a short review of our experimental and theoretical SC studies based on data collected at SNBL. We focus on ordering processes uncovered and quantified in the course of these studies and on their relation to SC.

Needless to say that symmetry is an important aspect of solid state processes. Correspondingly, an assumption-free, symmetry-based phase transition theory (Landau theory) gives access to most generic features of a phase transformation. In most molecular complexes a change of the spin state is associated with a totally symmetric deformation. The corresponding order parameter (OP) is a scalar and the space group remains unchanged at any value of the OP; such a process is called an isostructural phase transition. A generic phase diagram for an isostructural SC process based on experimental data is given in Ref. [7]. Interestingly, this phase diagram contains a single point where a 2^{nd} order transition is possible. Due to co-existence of hetero-phase and critical fluctuations one expects peculiar correlation properties in such a singular 2^{nd} order point. Recently numerical Ising-like models have revealed critical behavior around such a 2^{nd} order SC transition. Modeling has has also shown that this transition belongs to the mean-field class but has very special correlation properties.

We have extended the Landau-model to include ordering of high- and low-spin states [7] in order to account for our earlier observation on the solvate $[Fe^{II}(2\text{-pic})_3]Cl_2$ EtOH [8]. The resulting generic phase diagram contains a line along which 2^{nd} order

transitions are possible. As mentioned in the preceding paragraph for a singular point, one also expects interesting correlation phenomena along the 2nd order transition line, due to a competition between heterophase (HS-HS and LS-LS) and critical HS-LS-ordering fluctuations. For this part of the phase diagram, a line not a point in the p-T space, it should be possible to search for new critical behavior, not only theoretically but also experimentally.

Symmetry-based Landau theory does rationalize observed trends in the pressure and temperature evolution of SC compounds. Being phenomenological, it cannot account for microscopic aspects of the observed processes. Microscopic models based on Ising Hamiltonians are too simplistic to account for the structural complexity of real, molecular SC compounds. As we have shown, six different alcohol solvates of $[Fe^{II}(2\text{-pic})_3]Cl_2$, all with very similar structure at 200 K, exhibit drastically different spin crossover scenarios [9]. These experiments indicate that minor modification of packing forces arising from different solvent molecules, affect SC the potential energy surface and the vibrational behaviour as much as a modification of the ligand field. We interpret this observation to mean that the free energy surface of this structure type exhibits relatively flat ranges with several minima, whose location and depth may differ slightly depending on the alcohol. The experimental finding that several minima of free energy coexist within a few kJ/mole of the global minimum, is reminiscent of analogous computational results obtained during blind tests of structure prediction methods.

To illustrate the solvent effect, Fig. 1 shows transition curves for three solvates of $[Fe^{II}(2\text{-pic})_3]Cl_2$. The plateau in the transition curve of the EtOH solvate observed around a 50/50 ratio of HS and LS states corresponds to the above mentioned HS-LS ordering and can be parameterized by Landau theory or by an Ising-like model considering only spin-active sublattices. For the 2-Propanol solvate the plateau is found at a high concentration of HS states; this is a new type of SC scenario. From multi-temperature diffraction experiments combined with calorimetric and magnetization measurements we have shown that the plateau corresponds to a new ordered arrangement of HS and LS

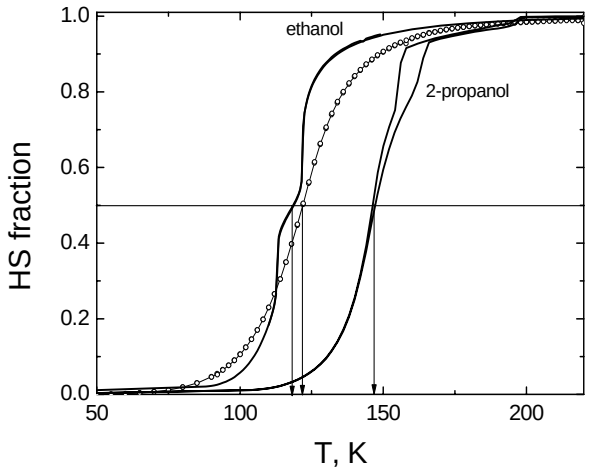

Fig. 1. *The fraction of HS states as a function of temperature (transition curves) for the ethanol, 2-propanol and the ethanol-propanol mixed solvates, all from SQUID data. Arrows show the corresponding transition temperatures.*

states. This new scenario can be modeled by combining free energy terms for spin crossover (from an Ising-like model) and for an ordering process (from Landau theory), see Fig.2. Another interesting point emerging from this study is a correlation between the spin state of spin-active molecules, the disorder of the spin isomers, and the disorder of the solvent molecules. Full details of this study can be found in Ref. [10]. A strong indication for a correlation of spin state and order-disorder aspects (rather than for a fortuitous coincidence) is seen in Fig. 1: introducing chemical disorder, as in the mixed Etoh-PropOH solvate, completely suppresses the ordering processes in the spin-active sub-lattice.

In order to account for this correlation in the behaviour of spin-active and spin-inactive components of a crystal structure we have recently developed a modified multi-sublattice Ising-like model [11]. The new model considers co-existing and coupled lattice processes, here spin conversion of Fe(II) complexes together with ordering of solvent molecules. The model explains available experimental data including the temperature-dependence of magnetization data, the structural changes associated with spin crossover of magnetically active and silent components of the crystal lattice as well as the correlation between the two.

We conclude with a remark on experimentation. Results from X-ray crystal structure analyses at many closely spaced temperatures and over a substantial temperature range were an important driving force for this work. It is only through such experiments (or others providing similarly detailed information) that the nature and degree of structural changes in magnetically 'silent', spin-inactive parts of the crystal lattice could be observed and their importance on SC processes appreciated.

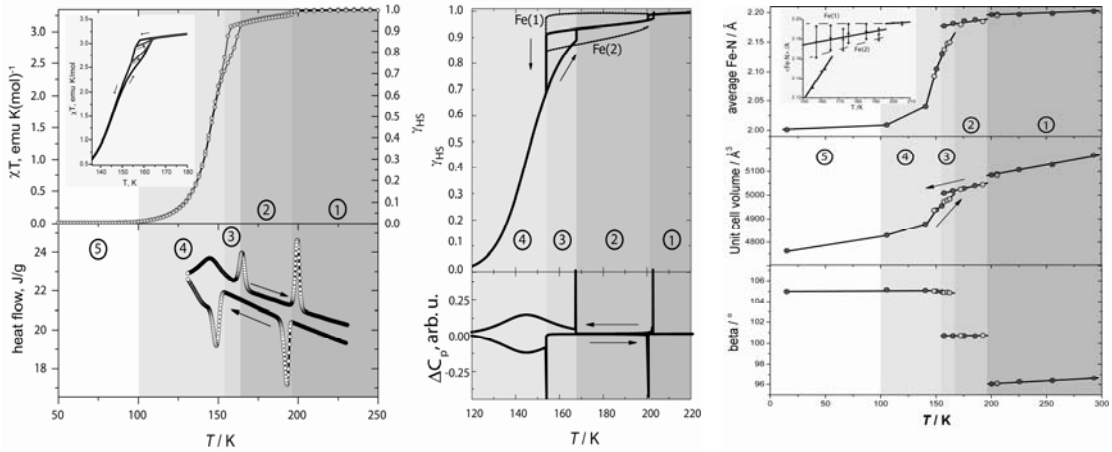

Fig. 2. *Macroscopic and microscopic properties of $[Fe^{II}(2\text{-pic})_3]Cl_2 \cdot$2-propanol as a function of temperature.*

LEFT PANEL. (Top): The numbered grey zones indicate the following macroscopic regimes: ① High-temperature phase, purely HS, ② Intermediate HS phase , ③ Hysteresis zone, ④ Low-temperature phase, HS/LS zone ⑤ Low-temperature phase, purely LS. (Bottom): DSC trace

MIDDLE PANEL. (Top): HS fraction from a phenomenological model (see Ref. 12). The temperature dependence of the average HS fraction is shown as a bold solid line, the HS fractions of the two different iron sites within zone ② as thin dashed lines. (Bottom): specific heat from the model.

RIGHT PANEL: Structural properties of $[Fe(2\text{-pic})_3]Cl_2 \cdot$2-propanol as a function of temperature.

References:

[1] P. Gütlich, Y. Garcia, H. Spiering in *Magnetism: Molecules to Materials IV* (Eds.: J. S. Miller, M. Drillon), Wiley-VCH, Weinheim, **2002**, 271
[2] O. Kahn, C. J. Martinez, *Science* **1998**, *279*, 44
[3] A. Bousseksou, G. C. Molnar, *C. R. Chimie* **2003**, *6*, 1175
[4] S. Gobo, G. Molnar, J. A. Real, A. Bousseksou, *Angew. Chem. Int. Ed.*, **2006**, 45, 5786
[5]G. Molnár , S. Cobo , J. A. Real , F. Carcenac , E. Daran , C. Vieu , A. Bousseksou, *Advanced Mat.*, **2007**, 19 2163
[6] S. Miyashita, Y. Konishi, M. Nishino, H. Tokoro, and P. A. Rikvold, *Phys. Rev. B* **77**, 014105 (2008)
[7] D. Chernyshov, H.-B. Bürgi, M. Hostettler, and K.W. Törnroos, *Phys. Rev. B* **70**, 094116 (2004).
[8] D. Chernyshov, M. Hostettler, K.W. Törnroos, and H.-B. Bürgi, *Angew. Chem.* **115**, 3955 (2003); *Angew. Chem., Int. Ed.* **42**, 3825 (2003).
[9] M. Hostettler, K.W. Törnroos, D. Chernyshov, B. Vangdal, and H.-B. Bürgi, *Angew. Chem.* **116**, 4689 (2004); *Angew. Chem., Int. Ed.* **43**, 4589 (2004).
[10] K.W. Törnroos, M. Hostettler, D. Chernyshov, B. Vangdal, and H.-B. Bürgi*, Chem.-Eur. J.* **12**, 6207 (2006).
[11] D. Chernyshov, N. Kinduhov, K. W. Törnroos, Marc Hostettler, B. Vangdal, and H.-B. Bürgi, *Phys. Rev. B* **76**, 014406 (2007)

VI. SNBL – FACTS and FIGURES

VI.1 Beam time allocation and user groups

The two Swiss-Norwegian Beam Lines, BM1A and BM1B, provide around 800 shifts per annum to its users. This allows the user groups to carry out on average about 85 projects every year. The Agreement between ESRF and SNX attributes 1/3 of this time to the international use, while 2/3 of the beam time should be allocated to Swiss and Norwegian users. It is worth noting that both collaborating countries are contributing members of ESRF, and researchers from Switzerland and Norway have a legal right to submit their proposals to ESRF, requesting nevertheless beam time at BM1A and BM1B lines.

Although the demand for beam time on the SNBL fluctuates from year to year, the beam lines remain very attractive for users. Figures VI.1 and VI.2 show the statistics for requested and allocated shifts over 2005-2008 years. In international part the mean overbooking ratio for these years reach 2.5. It drops down to 2.0 for Swiss and Norwegian users indicating a bit easier their access to the facility.

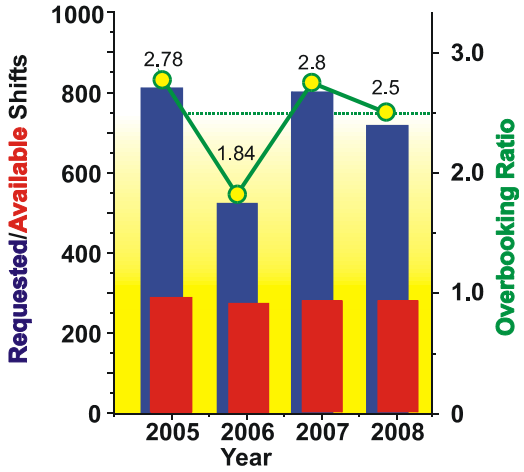

Fig. VI.1 *Requested and allocated at SNBL beam time for ESRF users*

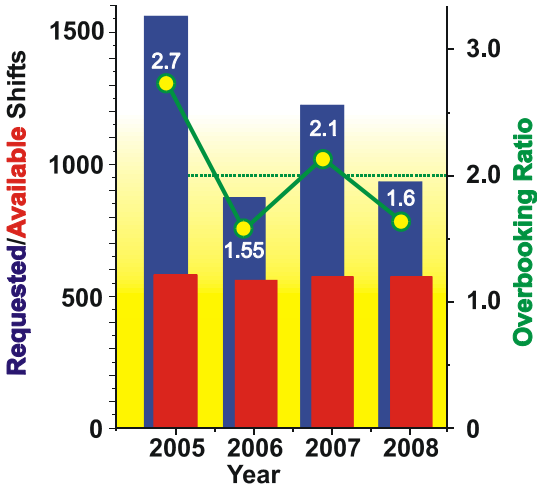

Fig. VI.2 *Requested and allocated at SNBL beam time for Swiss and Norwegian users*

The distribution of the allocated shifts by countries (Fig. VI.3) demonstrates just mentioned fact that Swiss and Norwegian groups constitute an important part of international users at SNBL. In contrast to the ESRF statistics, where Swiss groups are dominating, Norwegian users are more active in using SN-attributed beam time (Fig. VI.4).

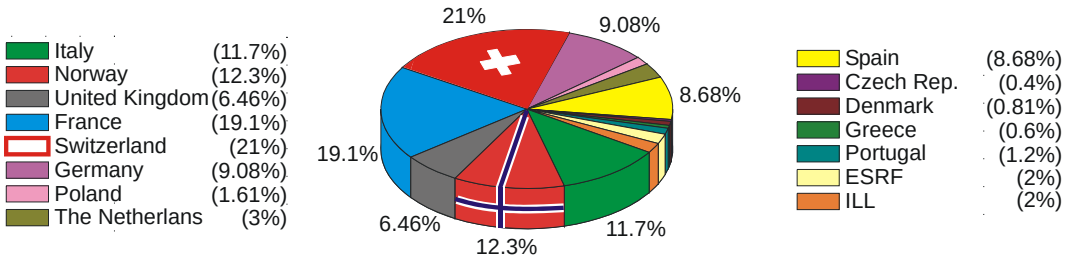

Fig. VI.3 *Distribution of the ESRF attributed beam time at SNBL by countries*

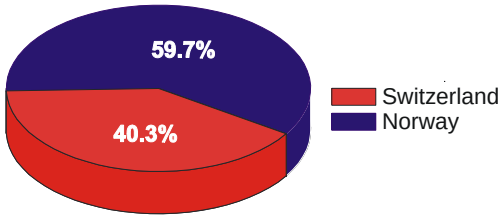

Fig. VI.4 *The use of SN beam time by Swiss and Norwegian groups*

Summarising number of shifts received at SNBL by two communities through both ESRF and SNBL allocation procedures one comes to the proportion **44%-CH** and **56%-N** – a rough equilibrium important for a bi-national facility.

The research groups from both partner countries, showed considerable interest and seriously contributed to the SNBL activity, belong to leading Swiss and Norwegian universities and research institutes. Figures VI.5 and VI.6 list Swiss and Norwegian institutes present at SNBL and show their activity in using the corresponding beam time.

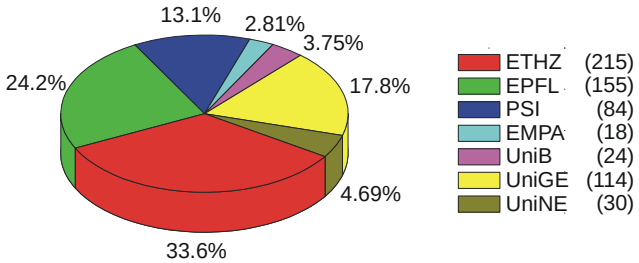

Fig. VI.5 *Distribution of the beam time by Swiss institutes in 2005-2007 (abbr. see in Appendix C)*

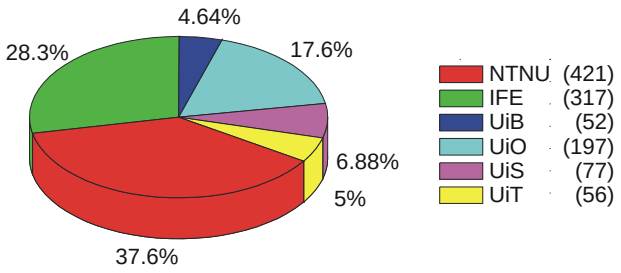

Fig. VI.6 Distribution of the beam time by Norwegian institutes in 2005-2007*(abbr. see in Appendix C)*

The variety of Review Committees selecting projects for SNBL (Figs. VI.7 and VI.8) reflects the concept formed after discussions by the beamline management with the SN user community; it had strong links to their research strategy, and aimed to providing the most appropriate assistance to their projects, both those already running and others still in planning. The SN beam lines are seen as multifunctional, dedicated to complex *in situ* experiments requiring combinations of diffraction and spectroscopic techniques. The approach seems to be well received also beyond the SN users community.

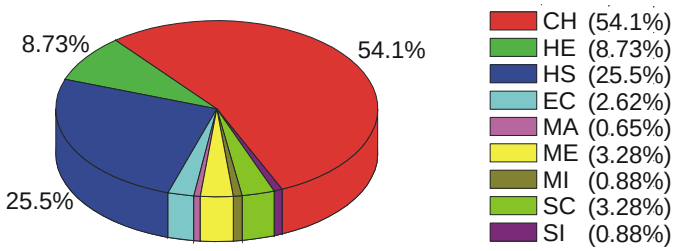

Fig. VI.7 *Distribution of beam time allocated to international users at SNBL by Review Committees in 2005-2007 years*

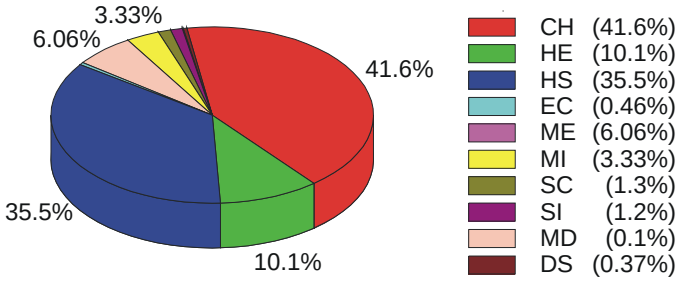

Fig. VI.8 *Distribution of shifts by Review Committees for SN users in 2005-2007 years*

Finally, Fig. VI.9 demonstrates a stable and well equilibrated interest of users to all techniques developed at SNBL. Remarkable is increasing and extending requests of combined set up, especially including combinations of traditional for SNBL X-ray based techniques with Raman spectroscopy. In 2007 already all SNBL instruments were connected by fibre optics to the Raman spectrometer, and the new opportunity was reflected by significant amount of projects requiring corresponding simultaneous measuring.

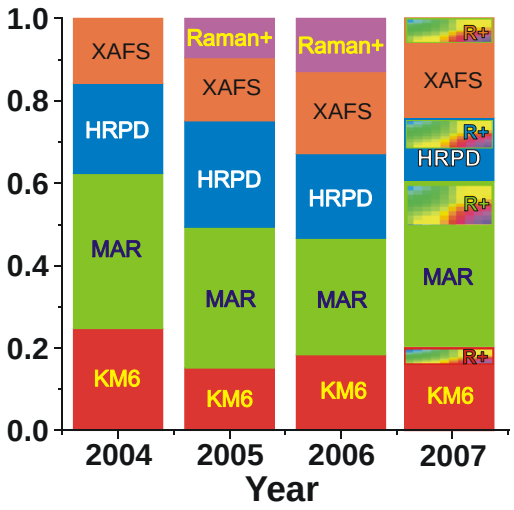

Fig. VI.9 *Distribution of requested beam time by different techniques. In 2007 parts requesting combined, with Raman, measurements are shown for each instrument.*

VI.2 Publication Output

The SNBL users exploited the high throughput of the beamlines with an increase in the publication rate. So far more than 750 papers from SNBL were published in peer-reviewed journals. The number of papers which appeared in the period 2005-2007 using data collected on SNBL reached an unprecedented level of 112 in publications 2007, and it shows a stable trend to keep the same level in 2008 (see Appendix A). Taking into account the typical number ~85 of projects carried out at the beamlines one finds the efficiency of the SNBL users in using beam time quite impressive. Figure VI.10 compares the number of papers published by the users, both international and SN, to the precise numbers of projects for years 2005-2007.

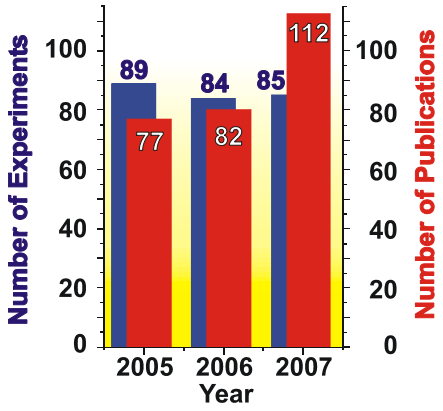

Fig. VI.10 *Publication rate of SNBL compared to the number of projects carried out every year*

The graph of Fig. VI.11, showing the distribution of publications in 2005-2007, demonstrates, in fact, strong focus of the beam lines to structural chemistry and material science applications.

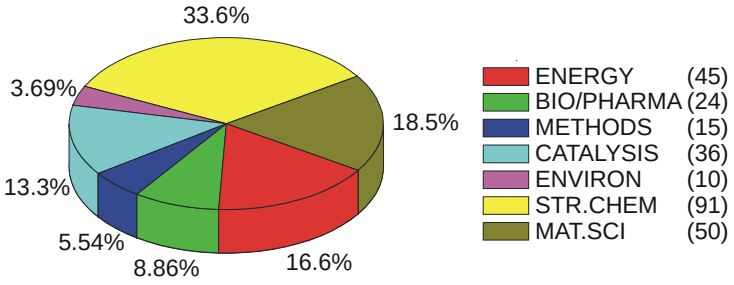

Fig. VI.11 *Distribution of publications based on the data obtained at SNBL in 2005-2007 by subject*

Last but not least, SNBL serves as an important facility for PhD students from Swiss and Norwegian universities. In 2005-2007 fifteen theses were carried out and defended using data obtained at SNBL (see the list in Appendix B).

VII. CONCLUSIONS

- We have just concluded a major refurbishment of SNBL. This represents a substantial investment in the project by our funding agencies, and puts us in an excellent position to exploit the facility for many years to come.

- We have benefited from generous technical support from our colleagues at the SLS, who have provided us with the latest generation of electronic strip detector for rapid, time-resolved experiments in powder diffraction. This development, together with the availability of secondary focussing for single crystal measurements, will extend both the quantity and quality of experiments which can be performed at SNBL.

- An active and efficient user community has been formed around SNBL. It has strong research programs in several fields, including energy storage materials, the chemistry of catalysis and the characterization of new materials using a combination of in-situ techniques.

- The presence of several groups of researchers from various institutes in Switzerland and Norway carrying out long-term programs at SNBL ensures that our facility will continue to benefit from the input from our user community and that the beamtime will be in high demand.

- The solid financial basis ensured by the national governmental agencies, as well as the important additional contributions made by the user's institutes, allow SNBL not only to maintain the existing level of the activity on the beam lines but also continue to upgrade and develop our instrumentation.

- The staff of SNBL show their motivation, expertise, and efficiency both in providing a high-level service to users, and in developing their own research and instrumentation programs.

VIII. ACKNOWLEDGEMENTS

On behalf of the SNBL team we would like to gratefully acknowledge all of the people who have supported us in our work and who have contributed significantly to the success of our common project named SNBL:

- Former and current SNX Council members, including: R.Abela (SLS/PSI), D.Nicholson (NTNU), G.Chapuis (EPFL), J.D.Grunwaldt (ETHZ), K.Knudsen (IFE), H.Larsen (UiS), and J.van Bokhoven (ETHZ).

- Former and current SNX advisors: J.P.Ruder and M.Steinaher (SER), N.Maras and A.M.Hundere (NSR).

- ESRF contact engineer for CRGs: A.Kaprolat and his *charmante équipe*.

- ESRF technical support (E.Dettona) and computer support (E.Papillon).

The proactive role of our users in forming the strategy for the development of SNBL has been invaluable. Moreover their contributions both financially and intellectually have played a crucial role in the ongoing development of the project.

APPENDIX A

List of Publications
2005

2005-1. **Albertsen, J.Z., Grong, Ø., Mathiesen, R.H., Schmid, B.** *Metallurgical investigation of metal dusting corrosion in plant-exposed nickel-based alloy 602CA*
Corrosion Eng. Science & Technology, **40**, 3, 239-243, 2005

2005-2. **Beale, A. M., Sankar, G., Nicholson, D. G., VanBeek, W.** *In situ study of the crystallisation of nanosized zinc and cobalt aluminate spinel catalysts from ionexchanged zeolite precursors*
Physica Scripta, **T115**, 678-680, 2005

2005-3. **Blanchard, D., Brinks, H.W., Hauback, B.C., Norby, P., Muller, J.** *Isothermal decomposition of $LiAlD_4$ with and without additives*
J. Alloys and Compounds, **404-406,** 743-747, 2005

2005-4. **Boldyreva, E., Ivashevskaya, S., Sowa, H., Ahsbahs, H., Weber, H.-P.** *Effect of hydrostatic pressure on the γ - polymorph of glycine. 1. A polymorphic transition into a new δ-form*
Z. Kristallogr., **220**, 50-57, 2005

2005-5. **Boldyreva, E., Kolesnik, E., Drebushchak, T., Ahsbahs, H., Beukes, J. A., Weber, H.-P.** *A comparative study of the anisotropy of lattice strain induced in the crystals of L-serine by cooling down to 100 K or by increasing pressure up to 4.4 GPa*
Z. Kristallogr., **220**, 58-65, 2005

2005-6. **Bricogne, G., Capelli, S.C., Evans, G., Mitschler, A., Pattison, P., Roversi, P., Schiltz, M.** *X-ray absorption, refraction and resonant scattering tensors in selenated protein crystals: implications for data collection strategies in macromolecular crystallography*
J. Appl. Cryst., **38**, 168-182, 2005

2005-7. **Brinks, H.W., Fossdal, A., Fonneløp, J.E., Hauback, B.C.** *Crystal structure and stability of $LiAlD_4$ with TiF_3 additive*
J. Alloys and Compounds, **397**, 1-2, 291-295, 2005

2005-8. **Brinks, H.W., Hauback, B.C., Jensen, C.M., Zidanc, R.** *Synthesis and crystal structure of Na_2LiAlD_6*
J. Alloys and Compounds, **392**, 1-2 , 27-30, 2005

2005-9. **Brinks, H.W., Hauback, B.C., Srinivasan, S. S., Jensen, C. M.** *Synchrotron X-ray studies of $Al_{1-y}Ti_y$ formation and Re-hydriding inhibition in Ti-enhanced $NaAlH_4$*
J. Phys. Chem. B, **109**, 33, 15780 -15785, 2005

2005-10. **Bürgi, H. B., Hauser, J.** *Supramolecular architecture in a disordered perhydrotriphenylene inclusion compound from diffuse X-ray diffraction data*
Crystal Growth & Design, **5**, 6, 2073 -2083, 2005

2005-11. **Bus, E., Miller, J. T., Van Bokhoven, J. A.** *Hydrogen chemisorption on Al_2O_3-supported gold catalysts*
J. Phys. Chem. B, **109**, 30, 14581 -14587, 2005

2005-12. **Cerný, R., Favre-Nicolin, V.** *FOX: A friendly tool to solve nonmolecular structures from powder diffraction*
Powder Diffraction, **20**, 4, 359-365, 2005

2005-13. **Cruciani, G., Matteucci, F., Dondi, M., Baldi, G., Barzanti, A.** *Structural variations of Cr-doped (Y,REE)AlO_3 perovskites*
Z. Kristallographie, **220**, 11, 930-937, 2005

2005-14. **Dubarry, M., Gaubicher, J., Guyomard, D., Durupthy, O., Steunou, N., Livage, J., Dupré, N., Grey, C.P.** *Sol gel synthesis of $Li_{1+\alpha}V_3O_8$. 1. From pecursors to xerogel*
Chem. Mater., **17**, 9, 2276 - 2283, 2005

2005-15. **Dubrovinskaia, N., Dubrovinsky, L., Kantor, I., Crichton, W. A., Dmitriev, V., Prakapenka, V., Shen, G., Vitos, L.,Ahuja, R. , Johansson, B., Abrikosov, I. A.** *Beating the miscibility barrier between Iron group elements and magnesium by high-pressure alloying*
Phys. Rev. Lett., **95**, 245502, 2005

2005-16. **Filinchuk, Y. E., Yvon, K.** *Boron-Induced hydrogen localization in the novel metal hydride $LaNi_3BH_x$ (x = 2.5-3.0)*
Inorg. Chem., **44**, 12, 4398 -4406, 2005
2005-17. **Filinchuk, Y. E., Yvon, K.** *Deuterium-induced copper pairing in $Zr_2CuD_{\sim 5}$*
Inorg. Chem., **44**, 23, 8191 - 8193, 2005
2005-18. **Fossdal, A., Brinks, H.W., Fichtner, M., Hauback, B.C.** *Determination of the crystal structure of $Mg(AlH_4)_2$ by combined x-ray and neutron diffraction*
J. Alloys and Compounds, **387**, 1-2, 47-51, 2005
2005-19. **Fossdal, A., Brinks, H.W., Fichtner, M., Hauback, B.C.** *Thermal decomposition of $Mg(AlH_4)_2$ studied by in situ synchrotron X-ray diffraction*
J.Alloys & Compounds, **404-406**, 752-756, 2005
2005-20. **Fossdal, A., Brinks, H.W., Fonneløp, J.E., Hauback, B.C.** *Pressure–composition isotherms and thermodynamic properties of TiF_3-enhanced Na_2LiAlH_6*
J. Alloys and Compounds, **397**, 1-2 , 135-139, 2005
2005-21. **Grunwaldt, J.-D., Kiener, C., Schüth, F., Baiker, A.** *X-ray absorption spectroscopy on CuZnO catalysts selected by high throughput experimentation techniques*
Physica Scripta, **T115**, 819-821, 2005
2005-22. **Grzechnik, A., Dmitriev, V., Weber H.-P.** *Dilithium zirconium hexafluoride Li_2ZrF_6 at high pressures: A new monoclinic phase*
J. Phys.& Chem. of Solids, **66**, 10, 1769-1774, 2005
2005-23. **Grzechnik, A., Friese, K., Dmitriev, V., Weber H.-P., Gesland J.-Y., Crichton, W.** *Pressure-induced tricritical phase transition from the scheelite structure to the fergusonite structure in $LiLuF_4$*
J.Phys.: Condens. Matter, **17**, 763-770, 2005
2005-24. **Iosub, V., Joubert, J.-M., Latroche, M., Cerný, R., Percheron-Guégan, A.** *Hydrogen cycling induced diffraction peak broadening in C14 and C15 Laves phases*
J. Solid State Chem., **178**, 6, 1799-1806 2005
2005-25. **Johnsen, L., Dalhus, B., Leiros, I., Nissen-Meyer, J.** *1.6 Å crystal structure of EntA-Im: A bacterial immunity protein conferring immunity to the antimicrobial activity of the pediocin-like bacteriocin enterocin A*
J. Biol. Chem., **280**, 19, 19045-19050, 2005
2005-26. **Jordá, J.L., Prokic, S., McCusker, L. B., Baerlocher, C., Chun Feng Xue, Dong, J.** *Synthesis and structure analysis of the potassium calcium silicate CAS-1. Application of a texture approach to structure solution using data collected in transmission mode*
Comptes Rendus Chimie, **8**, 3-4, 331-339, 2005
2005-27. **Joubert, J.-M., Cerny, R., Latroche, M., Percheron-Gueguan, A., Yvon, K.** *Compressibility and thermal expansion of $LaNi_5$ and its substitutional derivatives ($LaNi_{5-x}M_x$; M=Mn, Al,Co)*
Intermetallics, **13**, 227-231, 2005
2005-28. **Kallen, J., Sedrani, R., Zenke, G., Wagner, J.** *Structure of human cyclophilin A in complex with the novel immunosuppressant sanglifehrin A at 1.6 Å resolution*
J. Biol. Chemistry, **280**, 23, 21965-21971, 2005
2005-29. **Karau, F. W., Schnick, W.** *High-pressure synthesis and X-ray powder structure determination of the nitridophosphate BaP_2N_4*
J. Solid State Chemistry, **178**, 1, 135-141, 2005
2005-30. **Kobas, M., Weber, Th., Steurer, W.** *Structural disorder in the decagonal Al–Co–Ni. I. Patterson analysis of diffuse x-ray scattering data*
Phys. Rev., **B 71**, 224205, 2005
2005-31. **Kohlmann, H., Renaudin, G., Yvon, K., Wannek, C., Harbrecht, B.** *Hydrogen-induced atomic rearrangement in $MgPd_3$*
J. Solid State Chemistry, **178**, 4, 1292-1300, 2005
2005-32. **Kohlmann, H., Yvon, K., Wang, Y.** *Synthesis, crystal structure and magnetism of the mixed metal hydrides $Eu_{1-x}Sr_xMg_2H_6$ (0 <= x <= 0.6)*
J. Alloys and Compounds, **393**, 1-2, 11-15, 2005
2005-33. **Kolberg, M., Logan, D.T., Bleifuss, G., Pötsch, S., Sjöberg, B.-M. Gräslund, A., and al**. *A new tyrosyl radical on Phe^{208} as ligand to the diiron center in escherichia coli ribonucleotide reductase, mutant R2-Y122H*
J. Biol. Chemistry, **280**, 12, 11233-11246, 2005

2005-34. **Kuelpmann, A., Osman, M.A., Kocher, L., Suter, U.W.** *Influence of platelet aspect ratio and orientation on the storage and loss moduli of HDPE-mica composites*
Polymer, **46**, 2, 523-530, 2005

2005-35. **Maehlen, J.P., Stange, M., Yartys, V.A., Delaplane, R.G.** *Hydrogen assisted order–disorder transformations in Cu–Sn sublattices of the (La,Ce)CuSn–D_2 systems*
J. Alloys and Compounds, **404-406** , 112-117, 2005

2005-36. **Martucci, A., Alberti, A., Cruciani, G., Frache, A., Marchese, L., Pastore, H.O.** *Temperature-induced transformations in CoAPO-34 molecular sieve: a combined in situ X-ray diffraction and FTIR study*
J. Phys. Chem. B, **109**, 28, 13483 -13492, 2005

2005-37. **Mathisen, K., Nicholson, D. G., Fitch, A. N., Stockenhuber, M.** *Selective catalytic reduction of NOx over microporous CuAPO-5: structural characterisation by XAS and XRD*
J. Mater. Chem., **15**, 204-217, 2005

2005-38. **Mathisen, K., Nicholson, D. G., Stockenhuber, M.** *The influence of silicon on the catalytic properties of CuSAPO-5 towards the selective reduction of NO_x in the presence of propene*
Microp. & Mesop. Materials, **84**, 1-3 , 261-274, 2005

2005-39. **Miletich, R., Hejny, C., Krauss, G., Ullrich, A.** *Diffraction techniques: Shedding light on structural changes at extreme conditions in Mineral Behaviour at Extereme Conditions* EMU Notes in Mineralogy (Eotovos Univ. Press, Budapest), **7**, 281, 2005

2005-40. **Nachtegaal, M., Scheidegger, A. M., Dähn, R., Chateigner, D., Furrer, G.** *Immobilization of Ni by Al-modified montmorillonite: A novel uptake mechanism*
Geochimica et Cosmochimica Acta, **69**, 17, 4211-4225, 2005

2005-41. **Nazaraly, M., Wallez, G., Chanéac, C., Tronc, E., Ribot, F., Quarton, M., Jolivet, J. -P.** *The first structure of a cerium(IV) phosphate: ab initio rietveld analysis of $Ce^{IV}(PO_4)(HPO_4)_{0.5}(H_2O)_{0.5}$*
Angewandte Chemie Int. Ed., **44**, 35, 5691 - 5694, 2005

2005-42. **Nicosia, D., Prins, R.** *The effect of glycol on phosphate-doped $CoMo/Al_2O_3$ hydrotreating catalysts* J. Catalysis, **229**, 2, 424-438, 2005

2005-43. **Oudenhuijzen, M. K., Van Bokhoven, J. A., Miller, J. T., Ramaker, D. E., Koningsberger, D. C.** *Three-site model for hydrogen adsorption on supported platinum particles: influence of support Ionicity and particle size on the hydrogen coverage*
J. Am. Chem. Soc., **127**, 5, 1530 -1540, 2005

2005-44. **Paillaud, J.-L., Marichal, C., Roux, M., Baerlocher, Ch., Chézeau, J. M.** *Tripling of the Unit Cell Volume of the Non-centrosymmetric AlPO4-SOD after Dehydration: A Structural Study of a Reversible Process*
J. Phys. Chem. B, **109**, 24, 11893 -11899, 2005

2005-45. **Paul-Boncour, V., Guillot, M., André, G., Bourée, F., Wiesingerd, G., Percheron-Guégan, A.** *Origin of the first order magnetostructural transition in YFe2D4.2*
J. Alloys& Compounds, **404-406**, 355-359, 2005

2005-46. **Ramin, M., Grunwaldt, J.-D., Baiker, A.** *Behavior of homogeneous and immobilized zinc-based catalysts in cycloaddition of CO_2 to propylene oxide*
J. Catalysis, 234, 2, 256-267, 2005

2005-47. **Renaud, J., Bischoff, S. F., Buhl, T., Floersheim, P., Fournier, B., Geiser, M., Halleux, C. and al.** *Selective estrogen receptor modulators with conformationally restricted side chains. Synthesis and structure-activity relationship of Er-alpha-selective tetrahydroisoquinoline ligands*
J. Med. Chem., **48**, 364-379, 2005

2005-48. **Rohr, M., Grunwaldt, J.-D., Baiker, A.** *A simple route to highly active ruthenium catalysts for formylation reactions with hydrogen and carbon dioxide*
J. Mol. Catalysis A: Chemical, **226**, 2, 253-257,2005

2005-49. **Rohr, M., Grunwaldt, J.-D., Baiker, A.** *Formylation with supercritical carbon dioxide over Ru/Al_2O_3 modified by phosphines: heterogeneous or homogeneous catalysis?*
J. Catalysis, **229**, 144-153, 2005

2005-50. **Rohr, M., Günther, M., Jutz, F., Grunwaldt, J.-D., Emerich, H., Van Beek, W., Baiker, A.** *Evaluation of strategies for the immobilization of bidentate ruthenium–phosphine complexes used for the reductive amination of carbon dioxide*

Applied Catalysis A: General, **296**, 2 , 238-250, 2005

2005-51. **Rønning, M., Huber, F., Meland, H., Venvik, H., De Chen, Holmen, A.** *Relating catalyst structure and composition to the water–gas shift activity of Cu–Zn-based mixed-oxide catalysts*
Catalysis Today, **100**, 3-4, 249-254, 2005

2005-52. **Rumyantseva, M.N., Kovalenko, V.V., Gaskov, A.M., Pagnier, T., Machon, D., Arbiol, J., Morante, J.R.** *Nanocomposites SnO2/Fe2O3: Wet chemical synthesis and nanostructure characterization*
Sensors and Actuators B: Chem., **109**, 1, 64-74, 2005

2005-53. **Sato, M., Denys, R.V., Riabov, A.B., Yartys, V.A.** *Influence of Al- and Cu-doping on the thermodynamic properties of the LaNiIn–H system*
J. Alloys & Compounds, **400**,1-2, 184-187, 2005

2005-54. **Sato, M., Stange, M., Maehlen, J. P., Yartys, V. A.** *Crystal structure of $LaNi_5Sn$* J. Alloys and Compounds, **397**, 1-2, 165-168, 2005

2005-55. **Simoncic, P., Armbruster, Th.** *Cationic methylene blue incorporated into zeolite mordenite-Na: a single crystal X-ray study*
Microp. & Mesop. Materials, **81**, 1-3, 87-95, 2005

2005-56. **Snell, E.H., Helliwell, J.R.** *Macromolecular crystallization in microgravity*
Rep. Prog. Phys. **68**, 799-853, 2005

2005-57. **Sørby, M.H., Fjellvåg, H., Hauback, B.C.** *In situ powder synchrotron and neutron diffraction study of Zr_2Ni deuterides*
J. Alloys and Compounds, **394**, 1-2 , 107-115, 2005

2005-58. **Srinivasan, S.S., Jensen, C. M.** *Dehydrogenation kinetics and long term cycling behavior of Titanium doped $NaAlH_4$*
Mater. Res. Soc. Symp. Proc., 837, 2005

2005-59. **Stange, M., Maehlen, J.P., Yartys, V.A., Norby, P., Van Beek, W., Emerich, H.** *In situ SR-XRD studies of hydrogen absorption–desorption in $LaNi_{4.7}Sn_{0.3}$*
J. Alloys and Compounds, **404-406**, 604-608, 2005

2005-60. **Stange, M., Paul-Boncour, V., Latroche, M., Percheron-Guégan, A., Isnard, O., Yartys, V.A.** *Ce-valence state and hydrogen-induced volume effects in Ce-based intermetallic compounds and their hydrides*
J. Alloys and Compounds, **404-406**, 144-149, 2005

2005-61. **Staub, U., Shi, M., Schulze-Briese, C., Patterson, B. D., Fauth, F., Dooryhee, E. & al.** *Temperature dependence of the crystal structure and charge ordering in Yb_4As_3*
Phys. Rev. B, **71**, 075115, 2005

2005-62. **Steurer, W.** *Structural phase transitions from and to the quasicrystalline state*
Acta Cryst., **A61**, 28-38, 2005

2005-63. **Swamy, V., Dubrovinsky, L., Dubrovinskaia, N., Langenhorst, F., Simionovici, A., Drakopoulos, M., Dmitriev, V., Weber, H. -P.** *Size effects on the structure and phase transition behavior of baddeleyite TiO_2*
Solid State Comm., **134**, 8, 541-546, 2005

2005-64. **Szytula, A., Isnard, O., Yartys, V.A., Riabov, A.B.** *Crystal and magnetic structure of $HoNiSnD_{0.67}$*
J. Alloys & Compounds, **404-406**, 200-203, 2005

2005-65. **Talyzin, A. V., Langenhorst, F. , Dubrovinskaia, N. , Dub, S., Dubrovinsky, L. S.** *Structural characterization of the hard fullerite phase obtained at 13 GPa and 830 K*
Phys. Rev. **B 71**, 115424, 2005

2005-66. **Thorkildsen, G. , Larsen, H. B., Weckert, E., Mo, F., Mathiesen, R. H.** *Three-beam resonant X-ray diffraction in germanium - Laue transmission cases*
Acta Cryst., **A61**, 460-470, 2005

2005-67. **Törnroos, K.W., Chernyshov, D., Hostettler, M., Bürgi, H.-B.** *Co-crystallized cis and trans isomers of dichlorobis(2-picolylamine)iron(II)*
Acta Cryst., **C61**, 450-452, 2005

2005-68. **Tuel, A., Jorda, J.-L., Gramlich, V., Baerlocher, Ch.** *Synthesis and characterization of two aluminophosphates templated by N-methyl-1,3-diaminopropane*
J. of Solid State Chem., **178**, 782-791, 2005

2005-69. **Voegelin, A., Pfister, S., Scheinost, A. C., Marcus, M. A., Kretzschmar, R.** *Changes in zinc speciation in field soil after contamination with zinc oxide*
Environ. Sci. Technol., **39**, 17, 6616 -6623, 2005

2005-70. **Vrålstad, T., Øye, G., Rønning, M., Glomm, W. R., Stöcker, M., Sjöblom, J.** *Interfacial chemistry of cobalt(II) during sol–gel synthesis of cobalt-containing mesoporous materials*
Microp. & Mesop. Mat., **80**, 291-300, 2005

2005-71. **Vukojevic,S., Trapp, O., Grunwaldt, J.-D., Kiener, Ch., Schüth, F.** *Quasi-Homogeneous methanol synthesis over highly active copper nanoparticles*
Angewante Chem. Int. Ed., **44**, 48 , 7978 - 7981, 2005

2005-72. **Wattanasin, S., Kallen, J., Myers, S., Guo, Q., Sabio, M., Ehrhardt, C., Albert, R., Hommel, U., Weckbecker, G., Welzenbach, K., Weitz-Schmidt, G.** *1,4-Diazepane-2,5-diones as novel inhibitors of LFA-1*
Bioorg.& Med. Chem. Letters, **15**, 4, 1217-1220, 2005

2005-73. **Weiher, N., Bus, E., Gorzolnik, B., Möller, M., Prins, R., Van Bokhoven, J. A.** *An in situ and operando X-ray absorption spectroscopy setup for measuring sub-monolayer model and powder catalysts*
J. Synchrotron Rad., **12**, 675-679, 2005

2005-74. **Wiesinger, G ., Paul-Boncour, V ., Filipek, S. M., Reichl, Ch., Marchuk, I.,Percheron-Guégan, A.** *Structural and magnetic properties of RFe_2D_x deuterides (R = Zr, Y and x=3.5) studied by means of neutron diffraction and ^{57}Fe Mössbauer spectroscopy*
J. Phys.: Condens. Matter, **17**, 893-908, 2005

2005-75. **Wijnhoven, J. E.G.J**. *Seeded growth of monodisperse gibbsite platelets to adjustable sizes*
J. Colloid& Interface Science, **292**, 2 , 403-409, 2005

2005-76. **Zbinden, K. G., Banner, D. W., Ackermann, J., D'Arcy, A., Kirchhofer, D., Ji, Y.-H., Tschopp, T. B., Wallbaum, S., Weber, L.** *Design of selective phenylglycine amide tissue factor/factor VIIa inhibitors*
Bioorganic & Medicinal Chem. Letters, **15**, 3, 817-822, 2005

2005-77. **Zbinden, K. G., Obst-Sander, U., Hilpert, K., Kühne, H., Banner, D. W., Böhm, H.-J., Stahl, M., Ackermann, J., Alig, L., Weber, L., Wessel, H. P., Riederer, M. A., Tschopp, Th. B., Lavé, Th.** *Selective and orally bioavailable phenylglycine tissue factor/factor VIIa inhibitors*
Bioorganic & Medicinal Chem. Letters,**15**, 23, 5344-5352, 2005

2006

2006-1. **Altermark, B., Smalås, A.O., Willassen, N.P., Helland, R.** *The structure of Vibrio cholerae extracellular endonuclease I reveals the presence of a buried chloride ion*
Acta Cryst., **D62**, 1387-1391, 2006

2006-2. **Avdoshenko, S., Goryunkov, A., Ioffe, I., Ignat'eva, D., Sidorov, L., Pattison, Ph., Kemnitz, E., Troyanov, S.** *Preparation, crystallographic characterization and theoretical study of $C_{70}(CF_3)_{16}$ and $C_{70}(CF_3)_{18}$*
Chem. Commun., 2463 - 2465, 2006

2006-3. **Birkedal, H., Andersen, A.M.K., Arakcheeva, A., Chapuis, G., Norby, P., Pattison, P.** *The room-temperature superstructure of ZrP_2O_7 is orthorhombic: there are no unusual 180° P-O-P Bond Angles*
Inorg. Chem., **45**, 11, 4346 - 4351, 2006

2006-4. **Birkedal Nielsen, R.K., Kongshaug, K.O., Fjellvåg, H.** *Syntheses, crystal structures and thermal properties of 3D coordination polymers assembled from 1,4,5,8-naphthalenetetracarboxylic acid*
Solid State Sciences, **8**, 10, 1237-1242, 2006

2006-5. **Birkedal, H., Pattison, P.** *Bis[4-(salicylideneamino) phenyl] methane*
Acta Cryst. C Crystal Structure Comm., **62**, 3, 139-141, 2006

2006-6. **Boldyreva, E., Ahsbahs, H., Chernyshev, V., Ivashevskaya, S., Oganov, A.** *Effect of hydrostatic pressure on the crystal structure of sodium oxalate: X-ray diffraction study and ab initio simulations*
Z. Kristallogr., **221**, 3, 186-197, 2006

2006-7. **Boldyreva, E., Dmitriev, V., Hancock, B.** *Effect of pressure up to 5.5 GPa on dry powder samples of chlorpropamide Form-A*
International J.Pharmaceutics, **327**, 51-57, 2006

2006-8. **Boldyreva, E.V., Sowa, H., Seryotkin, Yu.V., Drebushchak, T.N., Ahsbahs, H., Chernyshev, V., Dmitriev, V.** *Pressure-induced phase transitions in crystalline L-serine studied by single-crystal and high-resolution powder x-ray diffraction*
Chemical Physics Letters, **429**, 4-6, 474-478, 2006

2006-9. **Bonhoure, I., Baur, I., Wieland, E., Johnson, C. A., Scheidegger, A. M.** *Uptake of Se(IV/VI) oxyanions by hardened cement paste and cement minerals: An X-ray absorption spectroscopy study*
Cement and Concrete Research, **36**, 1, 91-98, 2006

2006-10. **Boulineau, A., Joubert, J.-M., Cerný, R**. *Structural characterization of the Ta-rich part of the Ta–Al system* J. Solid State Chem., **179**, 11, 3385-3393, 2006

2006-11. **Brinks, H.W., Istad-Lem, A., Hauback, B.C.** *Mechanochemical synthesis and crystal structure of α'-AlD_3 and α-AlD_3*
J. Phys. Chem. B, **110**, 51, 25833 -25837, 2006

2006-12. **Brinks, H.W., Sulic, M., Jensen, C. M., Hauback, B. C.** T*iCl_3-enhanced $NaAlH_4$: impact of excess Al and development of the $Al_{1-y}Ti_y$ phase during cycling*
J. Phys. Chem., **110**, 6, 2740 -2745, 2006

2006-13. **Canton, P., Fichtner, M., Frommen, M., Léon, A.** *Synchrotron X-Ray Studies of Ti-Doped $NaAlH_4$*
J. Phys. Chem., **110**, 7, 3051 -3054, 2006

2006-14. **Cerný, R., Renaudin, G., Tokaychuk, Y., Favre-Nicolin, V.** *Complex intermetallic compounds in the Mg-Ir system solved by powder diffraction*
Z. Kristallog. Suppl., **23**, 411-416, 2006

2006-15. **Chotard, J.-N., Filinchuk, Y., Revaz, B., Yvon, K.** *Isolated $[Ni_2H_7]^{7-}$ and $[Ni_4H_{12}]^{12-}$ Ions in $La_2MgNi_2H_8$*
Angew.Chem.Int., **45**, 46, 7770-7773, 2006

2006-16. **Christensen, M., Lock, N., Overgaard, J., Iversen, Bo B**. *Crystal structures of thermoelectric n- and p-type $Ba_8Ga_{16}Ge_{30}$ studied by single crystal, multitemperature, neutron diffraction, conventional X-ray diffraction and resonant synchrotron X-ray diffraction*
J. Am. Chem. Soc., **128**, 15657-15665, 2006

2006-17. **Dalconi, M. C., Cruciani, G., Alberti, A., Ciambelli, P.** *Over-loaded Cu-ZSM-5 upon heating treatment: A time resolved X-ray diffraction study*
Microp.& Mesop. Materials, **94**, 1-3 , 139-147, 2006

2006-18. **Damay, F., Carretero-Genevrier, A., Cousson, A., Van Beek, W., Rodriguez-Carvajal, J., Fillaux, F.** *Synchrotron and neutron diffraction study of 4-methylpyridine-N-oxide at low temperature*
Acta Cryst. **B62**, Structural Science, 627-633, 2006

2006-19. **Dähn, R., Jullien, M., Scheidegger, A.M., Poinssot, Ch., Baeyens, B., Bradbury, M.H.** *Identification of neoformed Ni-phyllosilicates upon Ni uptake in montmorillonite: a transmission electron microscopy and extended X-Ray absorption fine structure study*
Clays and Clay Minerals, **54**, 2, 209 - 219, 2006

2006-20. **De Armas, H.N., Peeters, O.M., Blaton, N., De Ridder, D. J. A., Schenk, H.** *X-ray powder diffraction data and crystal data of polymorphic form 2 of carnidazole*
Powder Diffraction, **21**, 1, 56-58, 2006

2006-21. **De Armas, H.N., Peeters, O.M., Blaton, N., Van den Mooter, G., De Ridder, D.J.A., Schenk, H.** *Crystal structure of carnidazole form II from synchrotron X-ray powder diffraction: Structural comparison with form I, the hydrated form and the low energy conformations in vacuo*
J. Pharmaceutical Sci., **95**,10, 2123 - 2136, 2006

2006-22. **Dietzel, P. D. C., Panella, B., Hirscher, M., Blom, R., Fjellvåg, H.** *Hydrogen adsorption in a nickel based coordination polymer with open metal sites in the cylindrical cavities of the desolvated framework*
Chemical Communications, 959 - 961, 2006

2006-23. **Dmitriev, V.P., Dubrovinsky, L., Le Bihan, T., Kuznetsov, A., Weber, H.-P., Poniatovsky, E.G.** *Collapsed hexagonal ω phase in a compressed TiZr alloy: Angle-dispersive synchrotron-radiation x-ray diffraction study*
Phys. Rev. B, **73**, 094114-094120, 2006

2006-24. **Dorozhkin, E.I., Ignat'eva, D.V., Tamm, N.B., Vasilyuk, N.V., Goryunkov, A.A., Avdoshenko, S.M., Ioffe, I.N., Sidorov, L.N., Pattison, Ph. at al.** *Structure of 1,4,10,19,25,41-C70(CF3)6, isomer with unique arrangement of addends*
J. Fluorine Chem., **127**, 10, 1344-1348, 2006

2006-25. **Dubarry, M., Gaubicher, J., Guyomard, D., Steunou, N., Livage, J., Dupré, N., Grey, C.P.** *Synthesis of $Li_{1+\alpha}V_3O_8$ via a Gel Precursor: Part II, from Xerogel to the Anhydrous Material*
Chem. Mater., 18, 3, 629 - 636, 2006

2006-26. **Filinchuk, Y.E., Sheptyakov, D., Yvon, K.** *Directional metal-hydrogen bonding in interstitial hydrides II. Structural study of $HoNi_3D_x$ (x = 0, 1.3, 1.8)* J. Alloys and Compounds, **413**, 1-2, 106-113, 2006

2006-27. **Filinchuk, Y.E., Yvon, K.** *Directional metal–hydrogen bonding in interstitial hydrides III: Structural study of $ErCo_3D_x$ (0<=x<=4.3)*
J. Solid State Chemistry, **179**, 4, 1041-1052, 2006

2006-28. **Fossum, J.O., Méheust, Y., Palmar, K.P.S., Knudsen, K.D., Måloy, K.J., Fonseca, D.M.** *Itercalation-enhanced electric polarization and chain formation of nano-layered particles*
Europhysics Letters, **74**, 3, 438-444, 2006

2006-29. **Friese, K., Krüger, H., Kahlenberg, V ., Balic-Zunic, T ., Emerich, H ., Gesland, J-Y., Grzechnik, A .** *Study of the temperature dependence of the structure of KY_3F_{10}*
J. Phys.: Condens. Matter **18**, 2677-2687, 2006

2006-30. **Grzechnik, A., Balic-Zunic, T., Makovicky, E., Gesland, J.-Y., Friese, K.** *The compressibility mechanism of $Li_3Na_3In_2F_{12}$ garnet*
J. Phys.: Condens. Matter, **18**, 2915-2924, 2006

2006-31. **Gualtieri, A.F., Aprea, P.** *The structure of K-hydrosodalite*
Microp.& Mesop. Mater., **96**, 1-3, 276-286, 2006

2006-32. **Gualtieri, A. F., Ferrari, S., Galli, E., Di Renzo, F., Van Beek, W**. *Rietveld structure refinement of Zeolite ECR-1*
Chem. Mater., **18,** 1, 76 -84, 2006

2006-33. **Helland, R., Larsen, A. N., Smalås, A. O., Willassen, N. P.** *The 1.8 Å crystal structure of a proteinase K-like enzyme from a psychrotroph Serratia species*
FEBS J., **273**, 61-71, 2006

2006-34. **Hernandez, O., Knight, K.S., Van Beek, W., Boucekkine, A., Boudjada, A. , Paulus, W., Meinnel, J.** *Phases II and IV of 1,3,5-trichloro-2,4,6-trimethylbenzene: Ab initio crystal structure determination by high-resolution powder diffraction*
J. Molecular Structure, **791**, 1-3 , 41-52, 2006

2006-35. **Hersleth, H.-P., Ryde,U., Rydberg, P., Görbitz, C.H., Andersson, K.K.** *Structures of the high-valent metal-ion haem-oxygen intermediates in peroxidases, oxygenases and catalases*
J. Inorg.Biochemistry, **100**, 4, 460-476, 2006

2006-36. **Huber, F., Yu, Zh., Lögdberg, S., Rønning, M., Chen, D., Venvik, H., Holmen, A.** *Remarks on the passivation of reduced Cu-, Ni-, Fe-, Co-based catalysts*
Catalysis Letters, **110**, 3-4, 2006

2006-37. **Kantor, A. P., Kantor, I. Yu., Dubrovinsky, L. S., Krisch, M., Bossak, A., Dmitriev, V. P., Urusov, V. S.** *Measuring the speed of sound in an iron-nickel alloy at high pressure by inelastic X-ray scattering*
Doklady Physics, **51**,11, 584-587, 2006

2006-38. **Krivovichev, S.V., Chernyshov, D.Y., Döbelin, N., Armbruster, Th., Kahlenberg, V., Kaindl, R., Ferraris, G., Tessadri, R., Kaltenhauser, G.** *Crystal chemistry and polytypism of tyrolite*
American Mineralogist, **91**, 1378-1384, 2006

2006-39. **Kurnosov, A., Dubrovinsky, L., Kuznetsov, A., Dmitriev, V.** *High-pressure / High-temperature behavior of the methane-ammonia-water system up to 3 GPa*
Z. Naturforschung B, **61**, 12, 1573-1579, 2006

2006-40. **Kuznetsov, A., Pereira, A., Shiryaev, A., Haines, J., Dubrovinsky, L., Dmitriev, V., Pattison, P., Guignot, N.** *Pressure-Induced chemical decomposition and structural changes of Boric Acid*
J. Phys. Chem. B, **110**, 28, 13858 -13865, 2006

2006-41. **Leinekugel-le-Cocq, A.Y., Deniard, P., Jobic, S., Cerny, R., Bart, F., Emerich, H.** *Synthesis and characterization of hollandite-type material intended for the specific containment of radioactive cesium*
J. Solid State Chemistry, **179**, 10, 3196-3208, 2006

2006-42. **Le Toquin, R., Paulus, W., Cousson, A., Prestipino, C., Lamberti, C.** *Time-resolved in situ studies of oxygen intercalation into $SrCoO_{2.5}$, performed by neutron diffraction and X-ray absorption spectroscopy*
J. Am. Chem. Soc., **128**, 40, 13161-13174, 2006

2006-43. **Llewellyn, Ph.L., Bourrelly, S., Serre, Ch., Filinchuk, Y., Férey, G.** *How hydration drastically improves adsorption selectivity for CO2 over CH4 in the Flexible Chromium Terephthalate MIL-53*
Angew. Chem. Int., **45**, 46, 7751 - 7754, 2006

2006-44. **Luechinger, M., Kienhöfer, A., Pirngruber, G. D.** *Immobilized complexes of metals with Amino Acid Ligands - a first step toward the development of new biomimetic catalysts*
Chem. Mater., **18**, 5, 1330 -1336, 2006

2006-45. **Machon, D., McMillan, P. F., Xu, B., Dong, J.** *High-pressure study of the β-to-α transition in Ga_2O_3*
Phys. Rev. B, **73**, 094125, 2006

2006-46. **Marichal, C., Chézeau, J. M., Roux, M., Patarin, J., Jordá, J. L., McCusker, L. B., Baerlocher, Ch., Pattison, Ph.** *Synthesis and structure of Mu-33, a new layered aluminophosphate $|((CH_3)_3CNH_3^+)_{16}(H_2O)_4|[Al_{16}P_{24}O_{88}(OH)_8]$*
Microp. & Mesop. Materials, **90**, 1-3, 5-15, 2006

2006-47. **Méheust, Y., Knudsen, K.D., Fossum, J.O.** *Inferring orientation distributions in anisotropic powders of nano-layered crystallites froma single two-dimensional WAXS image*
J.Applied Cryst., **39**, 5, 661-670, 2006

2006-48. **Mentzen, B. F., Bergeret, G., Emerich, H., Weber, H.-P.** *Dehydrated and Cs^+-exchanged MFI Zeolites: location and population of Cs^+ from in situ diffraction data as a function of temperature and degree of exchange*
J. Phys. Chem., **110**, 1, 97 -106, 2006

2006-49. **Mentzen, B. F., Bergeret, G., Emerich, H., Weber, H.-P.** *Hydrated Cs^+-exchanged MFI Zeolites: location and population of Cs^+ cations and water molecules in hydrated $Cs_{6.6}$MFI from in and ex situ powder X-ray diffraction data as a function of temperature and other experimental conditions*
J. Phys. Chem. B, **110**, 28, 13741 -13752, 2006

2006-50. **Mentzen, B. F., Tuel, A., Bayard, F.** *Location of the tripropylbenzylammonium ion (P3BZY) in the as-synthesized zeolite ZSM-5 (Si/Al = 28): A study by solid-state NMR, computer simulations and X-ray synchrotron powder diffraction*
Microp.& Mesop. Mat., **93**, 171-179, 2006

2006-51. **Moe, E., Leiros, I., Smalås, A.O., McSweeney, S.** *The crystal structure of mismatch-specific Uracil-DNA glycosylase (MUG) from Deinococcus radiodurans reveals a novel catalytic residue and broad substrate specificity*
J. Biol. Chem., **281**, 1, 569-577, 2006

2006-52. **Nakamura, Y., Fossdal, A., Brinks, H.W., Hauback, B.C.** *Characterization of Al–Ti phases in cycled TiF_3-enhanced Na_2LiAlH_6*
J. Alloys and Compounds, **416**, 1-2, 274-278, 2006

2006-53. **Nazaralya, M., Wallez, G., Chanéac, C., Tronc, E., Ribot, F., Quarton, M., Jolivet, J. -P.** *Synthesis and characterization of $Ce^{IV}(PO_4)(HPO_4)_{0.5}(H_2O)_{0.5}$*
J. Physics & Chemistry of Solids, **67**, 5-6, 1075-1078, 2006

2006-54. **Petukhov, A. V., Thijssen, J. H. J., 't Hart, D. C., Imhof, A., Van Blaaderen, A., Dolbnya, I. P., Snigirev, A., Moussaïd, A., Snigireva, I**. *Microradian X-ray diffraction in colloidal photonic crystals*
J. Appl. Cryst. **39**, 137-144, 2006

2006-55. **Plazanet, M., Dean, M., Merlini, M., Huller, A., Emerich, H., Meneghini,C., Johnson, M.R., Trommsdorff, H.P**. *Crystallization on heating and complex phase behavior of α-cyclodextrin solutions*
J. Chem. Phys. **125**, 154504-154510, 2006

2006-56. **Poulsen, R.D., Bentien, A., Christensen, M., Iversen, B.B.** *Solvothermal synthesis, multi-temperature crystal structures and physical properties of isostructural coordination polymers, $2C_4H_{12}N^+$-$[M_3(C_8H_4O_4)_4]^{2-}$·$3C_5H_{11}NO$, M = Co, Zn*
Acta Cryst., **B62**, 245-254, 2006

2006-57. **P. Ravindran, R. Vidya, A. Kjekshus, and H. Fjellvåg, O. Eriksson** *Theoretical investigation of magnetoelectric behavior in $BiFeO_3$*
Phys. Rev. B, **74**, 224412-224430, 2006

2006-58. **Reehuis, M., Ulrich, C., Pattison, P., Ouladdiaf, B., Rheinstädter, M. C., Ohl, M., Regnault, L. P. & al.** *Neutron diffraction study of YVO_3, $NdVO_3$, and $TbVO_3$*
Phys. Rev. B, **73**, 094440, 2006

2006-59. **Reehuis, M., Ulrich, C., Proke, K., Gozar, A., Blumberg, G., Komiya, S., Ando, Y., Pattison, P., Keimer, B.** *Crystal structure and high-field magnetism of La_2CuO_4*
Phys. Rev. B, **73**, 144513, 2006

2006-60. **Riise, E. K., Lorentzen, M. S., Helland, R., Willassen, N. P.** *Crystallization and preliminary X-ray diffraction analysis of a cold-adapted catalase from Vibrio salmonicida*
Acta Cryst. F, **62**, 77-79, 2006

2006-61. **Scheidegger, A.M., Vespa, M., Grolimund, D., Wieland, E., Harfouche, M., Bonhoure, I., Dähn, R.** *The use of (micro)-X-ray absorption spectroscopy in cement research*
Waste Management, **26,** 7, 699-705 , 2006

2006-62. **Serre, Ch., Millange, F., Devic, Th., Audebrand, N., Van Beek, W.** *Synthesis and structure determination of new open-framework chromium carboxylate MIL-105 or $Cr^{III}(OH)$·{O_2C-$C_6(CH_3)_4$-CO_2}·nH_2O*
Material Res. Bulletin, **41**, 8, 1550-1557, 2006

2006-63. **Shustova, N., Chernyshev, D., Troyanov, S.** *Crystal structure of $C_{60}Cl_6$ prepared by a reaction of C_{60} with $POCl_3$*
Mendeleev Comm., 209-210, 2006

2006-64. **Søgaard, M., Hendriksen, P.V., Mogensen, M., Poulsen, F.W., Skou, E.** *Oxygen nonstoichiometry and transport properties of strontium substituted lanthanum cobaltite*
Solid State Ionics, **177**, 37-38, 3285-3296, 2006

2006-65. **Sørby, M.H., Brinks, H.W., Fossdal, A., Thorshaug, K., Hauback, B.C.** *The crystal structure and stability of K_2NaAlH_6*
J. Alloys and Compounds, **415**, 1-2, 284-287, 2006

2006-66.**Swamy, V., Menzies, D., Muddle, B.C., Kuznetsov, A., Dubrovinsky, L., Dai, Q., Dmitriev, V.** *Nonlinear size dependence of anatase TiO_2 lattice parameters*
Appl. Phys. Lett. **88**, 243103, 2006

2006-67. **Thorkildsen, G., Larsen, H. B., Beukes, J. A.** *Angle calculations for a three-circle goniostat*
J. Appl. Cryst., **39**, 151-157, 2006

2006-68. **Tkalcec, I., Mari, D., Benoit, W.** *Correlation between internal friction background and the concentration of carbon in solid solution in a martensitic steel*
Mater. Science & Engineering: A, **442**, 1-2, 471-475, 2006

2006-69. **Tokaychuka, Ya.O., Bodak, O.I., Gorelenko, Yu, K., Yvon, K.** *Structural and magnetic properties of iron-rich compounds in the Yb–Fe–Ga system* J. Alloys and Compounds, **415**, 1-2, 8-10, 2006

2006-70. **Törnroos, K.W., Hostettler, M., Chernyshov, D., Vangdal, B., Bürgi, H.-B.** *Interplay of spin conversion and structural phase transformations: reentrant phase transitions in the 2-Propanol Solvate of Tris(2-picolylamine)iron(II) Dichloride*
Chem. Eur.J., **12**, 24, 6207 - 6215 , 2006

2006-71. **Van Mechelen, J. B., Peschar, R., Schenk, H.** *Structures of mono-unsaturated triacylglycerols. I. The β2 polymorph*
Acta Cryst., **B62**, 1121-1130, 2006

2006-72. **Van Mechelen, J. B., Peschar, R., Schenk, H.** *Structures of mono-unsaturated triacylglycerols. II. The β2 polymorph*
Acta Cryst., **B62**, 1131-1138, 2006

2006-73. **Vespa, M., Dähn, R., Gallucci, E., Grolimund, E., Wieland, E., Scheidegger, A.M.** *Microscale investigations of Ni uptake by cement using a combination of scanning electron microscopy and synchrotron-based techniques*

Environ. Sci. Technol., **40**, 7702-7709, 2006

2006-74. **Vespa, M., Dähn, R., Grolimund, D., Harfouche, M., Wieland, E., Scheidegger, A. M. E.** *Speciation of heavy metals in cement-stabilized waste forms: a micro-spectroscopic study*
J. Geochem. Exploration, **88**, 1-3, 77-80, 2006

2006-75. **Vespa, M., Dähn, R., Grolimund, D., Wieland, E., Scheidegger, A. M.** *Spectroscopic investigation of Ni speciation in hardened cement paste*
Environ. Sci. Technol., **40**, 7, 2275 -2282, 2006

2006-76. **Vespa, M., Dähn, R., Wieland, E., Grolimund, D., Scheidegger, A. M.** *The influence of hydration time on the Ni uptake by cement*
Czechoslovak J. Physics, **56**, suppl. D, 2006

2006-77. **Vrålstad, T., Glomm, W.R., Ronning, M., Dathe, H., Jentys, A., Lercher, J.A., Øye, G., Stöcker, M., Sjöblom, J.** *Spectroscopic characterization of cobalt-containing mesoporous materials*
J. Phys. Chem. B, **110**, 11, 5386 -5394, 2006

2006-78. **Wallez, G., Clavier, N., Dacheux, N., Quarton, M., Van Beek, W**. *From thorium phosphate hydrogenphosphate hydrate to ß-thorium phosphate diphosphate: Structural evolution to a radwaste storage ceramic*
J. Solid State Chemistry, **179**,10, 3007-3016, 2006

2006-79. **Weber, Th., Kobas, M., Steurer, W**. *Phasonic disorder in decagonal Al–Co–Ni*
Philosophical Magazine, **86**, 3-5, 537 - 542, 2006

2006-80. **Weiher, N., Bus, E., Delannoy, L., Louis, C., Ramaker, D.E., Miller, J.T., Van Bokhoven, J.A.** *Structure and oxidation state of gold on different supports under various CO oxidation conditions*
J. Catalysis, **240**, 2, 100-107, 2006

2006-81. **Zanardi, S., Carati, A., Cruciani, G., Bellussi, G., Millini, R., Rizzo, C.** *Synthesis, characterization and crystal structure of new microporous bismuth silicates*
Microp.& Mesop. Mater., **97**, 1-3, 34-41, 2006

2006-82. **Zbinden, K. G., Banner, D. W., Hilpert, K., Himber, J., Lavé, Th., Riederer, M. et al.** *Dose-dependent antithrombotic activity of an orally active tissue factor/factor VIIa inhibitor without concomitant enhancement of bleeding propensity*
Bioorganic & Medicinal Chemistry, **14**,15, 5357-5369, 2006

2007

2007-1. **Arakcheeva, A., Pattison, Ph., Meisser, N., Chapuis, G., Pekov, I., Thélin, Ph.** *New insight into the pectolite – serandite series: a single crystal diffraction study of* $Na(Ca_{1.73}Mn_{0.27})[HSi_3O_9]$ *at 293 and 100 K*
Z. Kristallographie, **222**, 12, 696-704, 2007

2007-2. **Arod, F., Pattison, Ph., Schenk, K.J., Chapuis, G.** *Polymorphism in N-Salicylideneaniline Reconsidered*
Crystal Growth & Design, **7**, 9, 1679-1685, 2007

2007-3. **Baerlocher, Ch., Gramm, F., Massüger, L., McCusker, L.B., He, Zh., Hovmöller, S., Zou, X.** *Structure of the polycrystalline zeolite catalyst IM-5 solved by enhanced charge flipping*
Science, **315**, 5815, 1113 - 1116, 2007

2007-4. **Baerlocher, Ch., McCusker, L.B., Palatinus, L.** *Charge flipping combined with histogram matching to solve complex crystal structures from powder diffraction data*
Z. Kristallographie, **222**, 02, 047-053, 2007

2007-5. **Besnard, C., Camus, F., Fleurant, M., Dahlström, A., Wright, J.P., Margiolaki, I., Pattison, P., Schiltz, M.** *Exploiting X-ray induced anisotropic lattice changes to improve intensity extraction in protein powder diffraction: Application to heavy atom detection*
Z. Kristallog., **Suppl.26**, 39-44, 2007

2007-6. **Betti, C. Fois, E., Mazzucato, E., Medici, C., Quartieri, S., Tabacchi, G., Vezzalini, G., Dmitriev, V.** *Gismondine under HP: deformation mechanism and re-organization of the extra-framework species*
Microp. & Mesop. Mater., **103**, 1-3, 190-209 , 2007

2007-7. **Beukes, J. A. , Mo, F., Van Beek, W.** *X-ray induced radiation damage in taurine - A combined X-ray diffraction and Raman study*
J. Phys. Chem. Chem. Phys., **9**, 4609-4724, 2007

2007-8. **Borg, Ø., Rønning, M., Storsæter, S., Van Beek, W., Holmen, A.** *Identification of cobalt species during temperature programmed reduction of Fischer-Tropsch catalysts*
Stud. Surf. Sci. Catal., **163**, 255, 2007

2007-9. **Boccaleri, E., Milanesio, M., Carniato, F., Croce, G., Viterbo, D., Van Beek, W., Emerich, H.** *In situ simultaneous Raman/High-Resolution X-ray Powder Diffraction study of transformations occurring in materials at non-ambient conditions*
J .Appl.Cryst., **40**, 684-693, 2007

2007-10. **Boldyreva, E.** *High-Pressure Polymorphs of Molecular Solids: When Are They Formed, and When Are They Not? Some Examples of the Role of Kinetic Control*
Crystal Growth & Design, **7,** 9, 1662 -1668, 2007

2007-11. **Bourrelly, S., Serre, S., Vimont, A., Ramsahye, N.A., Maurin, G., Daturi, M., Filinchuk, Y. et al.** *A multidisciplary approach to understanding sorption induced breathing in the metal organic framework MIL53(Cr)*
Stud. Surf. Sci. Catal., **170**, 1, 1008-1014, 2007

2007-12. **Brinks, H.W., Brown, C., Jensen, C., Graetz, J., Reilly, J., Hauback, B.C.** *The crystal structure of γ-AlD_3*
J. Alloys & Compounds, **441**, 1-2, 364-367, 2007

2007-13. **Brinks, H.W., Langley, W., Jensen, C.M., Graetz, J., Reilly, J.J., Hauback, B.C.** *Synthesis and crystal structure of ß-AlD_3*
J. Alloys & Compounds, **433**, 1-2, 180-183, 2007

2007-14. **Brugger, J., Etschmann, B., Liu, W., Testemale, D., Hazemann, J.L., Emerich, H. , Van Beek, W. , Proux, O.** *An XAS study of the structure and thermodynamics of Cu(I) chloride complexes in brines up to high temperature (400°C, 600 bars)*
Geochimica et Cosmochimica Acta, **71**, 4920-4941, 2007

2007-15. **Bus, E., Prins, R., Van Bokhoven, J.A.** *Time-resolved in situ XAS study of the preparation of supported gold clusters*
Phys. Chem. Chem. Phys., **9**, 3312 - 3320, 2007

2007-16. **Bus, E., Van Bokhoven, J.A.** *Electronic and Geometric Structures of Supported Platinum, Gold, and Platinum-Gold*
Catalysts Phys. Chem. C, **111**, 27, 9761 -9768, 2007

2007-17. **Caignaert, V., Satya Kishore, M., Pralong, V., Raveau, B., Creon, N., Fjellvåg, H.** *From a 3D protonic conductor $VO(H_2PO_4)_2$ to a 2D cationic conductor $Li_4VO(PO_4)_2$ through lithium exchange*
J. Solid State Chem., **180**, 9, 2437-2442, 2007

2007-18. **Cardoso, M.B., Putaux, J.-L., Nishiyama, Y., Helbert, W., Hytch, M., Silveira, N.P., Chanzy, H.** *Single Crystals of V-Amylose Complexed with -Naphthol*
Biomacromolecules, **8**, 4, 1319 -1326, 2007

2007-19. **Casapu, M., Grunwaldt, J.-D., Maciejewski, M., Baiker, A., Eckhoff, S., Göbel, U., Wittrock, M.** *The fate of platinum in $Pt/Ba/CeO_2$ and $Pt/Ba/Al_2O_3$ catalysts during thermal aging*
J. Catalysis, **251**, 1, 28-38, 2007

2007-20. **Cerny, R., Filinchuk, Y., Hagemann, H., Yvon, K.** *Magnesium borohydride: synthesis and crystal structure*
Ang.Chemie Int. Ed.,**46**, 30 , 5765 - 5767, 2007

2007-21. **Chernyshov, D., Kinduhov, N., Törnroos, K.W., Hostettler, M., Vangdal, B., Bürgi, H. B.** *Coupling between spin conversion and solvent disorder in spin crossover solids*
Phys. Rev. B, **76**, 014406-014413, 2007

2007-22. **Chiarello, G.L., Grunwaldt, J.-D., Ferri, D., Krumeich, F., Oliva, C., Forni, L., Baiker, A.** *Flame-synthesized LaCoO3-supported Pd 1. Structure, thermal stability and reducibility*
J. Catalysis, **252**, 2, 127-136 , 2007

2007-23. **Chiarello, G.L., Ferri, D., Grunwaldt, J.-D.,Forni, L., Baiker, A.** *Flame-synthesized $LaCoO_3$-supported Pd 2. Catalytic behavior in the reduction of NO by H_2 under lean conditions*
J.Catalysis, **252**, 2, 137-147, 2007

2007-24. **Courcot, B. , Firley, D., Fraisse, B. , Becker, P., Gillet, J.-M., Pattison, P., Chernyshov, D. et al.** *Crystal and Electronic Structures of Magnesium(II), Copper(II), and Mixed Magnesium(II)-Copper(II) Complexes of the Quinoline Half of Styrylquinoline-Type HIV-1 Integrase Inhibitors*
J. Phys. Chem. B, **111,** 21, 6042 -6050, 2007

2007-25. **Cowan-Jacob, S. W., Fendrich, G., Floersheimer, A., Furet, P., Liebetanz, J., Rummel, G., Rheinberger, P., Centeleghe, M., D. Fabbro, Manley, P. W.** *Structural biology contributions to the discovery of drugs to treat chronic myelogenous leukaemia*
Acta Cryst. D **63**, 80-93, 2007

2007-26. **Cunha-Silva, L., Mafra, L., Ananias, D., Carlos, L.D., Rocha, J.,Almeida Paz, F.A.** *Photoluminescent Lanthanide-Organic 2D Networks: A Combined Synchrotron Powder X-ray Diffraction and Solid-State NMR Study*
Chem. Mater., **19**, 14, 3527-3538, 2007

2007-27. **Deledda, S., Hauback, B.C., Fjellvåg, H.** *H-sorption behaviour of mechanically activated Mg–Zn powders*
J. Alloys & Compounds, **446-447**, 173-177, 2007

2007-28. **Denys, R.V., Riabov, B., Yartys, V.A., Delaplane, R.G., Sato, M.** *Hydrogen storage properties and structure of $La_{1-x}Mg_x(Ni_{1-y}Mn_y)_3$ intermetallics and their hydrides*
J. Alloys & Compounds, **446-447**, 166-172, 2007

2007-29. **Denys, R.V., Yartys, V.A., Sato, M., Riabov, A.B., Delaplane, R.G.** *Crystal chemistry and thermodynamic properties of anisotropic $Ce_2Ni_7H_{4.7}$ hydride*
J. Solid State Chem., **180**, 9, 2566-2576, 2007

2007-30. **Dmitriev, V., Chernyshov, D., Filinchuk, Y., Degtyareva, V.** *Antiisostructural phases and anomalous thermoelasticity in In-based alloys: Synchrotron x-ray diffraction experiments and unified phenomenological model*
Phys. Rev. B, **75**, 024111-024119, 2007

2007-31. **Dong, J., Liu, L., Li, J., Li, Y., Baerlocher, Ch., McCusker, L.B.** *Synthesis, characterization and crystal structure analysis of an open-framework zirconium phosphate*
Microp.& Mesop. Mater., **104**, 1-3, 185-191, 2007

2007-32. **Dorokhov, A. V., Chernyshov, D. Y., Burlov, A. S., Garnovskii, A. D., Ivanova, I. S. , Pyatova, E. N. , Tsivadze, A. Y., Aslanov, L. A., Chernyshev, V. V.** *Synchrotron powder diffraction in a systematic study of 4'-[2-(tosylamino)benzylideneamino]-2,3-benzo-15-crown-5 complexes*
Acta Cryst., **B63**, 402-410, 2007

2007-33. **Dragan, F., Bratu, I., Borodi, Gh., Toma, M., Hernanz, A., Simon, S., Cristea, Gh., Peschar, R.** *Spectroscopic investigation of ß-cyclodextrin -metoprolol tartrate inclusion complexes*
J. Incl. Phenom. Macrocyclic Chem., **59**, 1-2, 125-130 , 2007

2007-34. **Dubrovinskaia, N., Solozhenko, V., Miyajima, N., Dmitriev, V., Kurakevych, O., Dubrovinsky, L.** *Superhard nanocomposite of dense polymorphs of boron nitride: Noncarbon material has reached diamond hardness*
Appl. Phys. Lett., **90**, 101912-101915, 2007

2007-35. **Dubrovinsky, L., Dubrovinskaia, N., Crichton, W.A., Mikhaylushkin,S.I., et al.** *Noblest of all metals is structurally unstable at high pressure*
Phys. Rev. Lett. **98**, 045503, 2007

2007-36. **Dyrbeck, H., Hammer, N., Rønning, M., Blekkan, E.A.** *Catalytic oxidation of hydrogen over Au/TiO_2 catalysts*
Topics in Catalysis, **45**, 1-4, 21-24, 2007

2007-37. **Feuerbacher M. et al.** *The Samson phase, ß-Mg_2Al_3, revisited*
Z. Kristallographie, **222**, 6, 259-288 , 2007

2007-38. **Filinchuk, Y., Talyzin, A. V., Chernyshov, D., Dmitriev, V.** *High-pressure phase of $NaBH_4$: Crystal structure from synchrotron powder diffraction data*
Phys. Rev. B, **76**, 092104-092107, 2007

2007-39. **Filinchuk, Y.E., Yvon, K.** *Deuterium site occupancies in $Ce_2Ni_7D_{\sim 4}$ and Comparison with $CeNi_3D_{2.8}$*
J. Alloys & Compounds, **446-447**, 3-5, 2007

2007-40. **Filinchuk, Y., Yvon, K., Emerich, H.** *Tetrahedral D atom coordination of Nickel and evidence for anti-isostructural phase transition in orthorhombic $Ce_2Ni_7D_{\sim 4}$*

Inorg. Chem., **46**, 2914-2920, 2007

2007-41. **Frunz, L., Prins, R., Pirngruber, G.D.** *Mimicking the Active Center of Methane-monooxygenase by Metal-Peptide Complexes Immobilized on Mesoporous Silica*
Chem. Mater., **19**, 17, 4357 -4366, 2007

2007-42. **Giannici, F. , Longo, A., Deganello, F., Balerna, A., Arico, A.S., Martorana, A.** *Local environment of Barium, Cerium and Yttrium in $BaCe_{1-x}Y_xO_{3-\delta}$ ceramic protonic conductors*
Solid State Ionics, **178**, 7-10, 587-591, 2007

2007-43. **Gieck, C., Bisio, C., Marchese, L., Filinchuk, Y., Da Silva, C.E., Pastore, H.O.** *Layered Assembly of Organic Molecules and Host-Guest Interactions in a CAL-1 Chabasite-Type Precursor of H-SAPO-34 Catalysts*
Angew. Chem. Int. Ed., **46**, 8895 - 8897, 2007

2007-44. **Grove, H., Sørby, M.H., Brinks, H.W., Hauback, B.C.** *In Situ Synchrotron Powder X-ray Diffraction Studies of the Thermal Decomposition of β- and γ-AlD_3* J. Phys. Chem. C, **111**, 44, 16693 -16699, 2007

2007-45. **Grunwaldt, J.-D., Van Vegten, N., Baiker, A.** *Insight into the structure of supported palladium catalysts during the total oxidation of methane*
Chem. Commun., 4635-4637, 2007

2007-46. **Grzechnik, A., Gesland, J.-Y., Friese, K.** *High-pressure behaviour of Li_2CaHfF_8 scheelite*
J. Phys.: Condens. Matter, **19**, 096215-0962225, 2007

2007-47. **Gu, Q.F., Krauss, G., Grin, Yu., Steurer, W.** *Comparative high-pressure study and chemical bonding analy sis of Rh_3Bi_{14} and isostructural $Rh_3Bi_{12}Br_2$*
J. Solid State Chem., **180**, 933-941, 2007

2007-48. **Haas, S., Batlogg, B., Besnard, C., Schiltz, M., Kloc, C., Siegrist, T.** *Large uniaxial negative thermal expansion in pentacene due to steric hindrance*
Phys. Rev. B **76,** 205203-205208, 2007

2007-49. **Hafizovic, J., Krivokapic, A., Szeto, K.C., Jakobsen, S. et al.** *Tailoring the Dimensionality of Metal–Organic Frameworks Incorporating Pt and Pd. From Molecular Complexes to 3D Networks*
Cryst. Growth Des., **7**, 11, 2302–2304, 2007

2007-50. **Hammer, N., Kvande, I., Chen, D., Rønning, M.** *Au–TiO_2 catalysts stabilised by carbon nanofibres*
Catalysis Today, **122**, 3-4, 365-369, 2007

2007-51. **Hammer, N., Kvande, I., Chen, D., Van Beek, W., Rønning, M.** *Identification of valence shifts in Au during the water-gas shift reaction*
Topics in Catalysis, **45**, 1-4 , 2007

2007-52. **Hammer, N., Kvande, I., Xu, X., Gunnarsson, V., Tøtdal, B., Chen, D., Rønning, M.** *Au–TiO_2 catalysts on carbon nanofibres prepared by deposition-precipitation and from colloid solutions*
Catalysis Today, **123**, 1-4, 245-256 , 2007

2007-53. **Hannemann, S., Casapu, M., Grunwaldt, J.-D., Haider, P., Trüssel, P., Baiker, A. , Welter, E.** *A versatile in situ spectroscopic cell for fluorescence/transmission EXAFS and X-ray diffraction of heterogeneous catalysts in gas and liquid phase*
J. Synchrotron Rad., **14**, 345-354, 2007

2007-54. **Helmholdt, R. B., Sonneveld, Ed J., Vande Velde, Ch. M. L., Blockhuys, F., Lenstra, A. T. H., Geise, H. J., Peschar, R.** *Structures of tetrabromothiophene and tetrabromoselenophene: the influence of the heteroatom on the heterophene packing*
Acta Cryst. B **63**, 5, 783-790

2007-55. **Hensen, E.J.M., Van der Meer, Y., Van Veen, J.A.R., Niemantsverdriet, J.W.** *Insight into the formation of the active phases in supported NiW hydrotreating catalysts*
Appl. Catalysis A: Gen., **322**, 16-32, 2007

2007-56. **Hersleth, H.-P., Uchida, T., Røhr, Å. K.,Teschner, Th., Schünemann, V., Kitagawa, T. et al.** *Crystallographic and spectroscopical studies of peroxide-derived myoglobin compound II - Occurrence of Protonated Fe(IV)O*
J. Biol. Chem., **278**, 23372 – 23386, 2007

2007-57. **Hong, S. B., Min, H.-K., Shin, Ch.-H., Cox, P.A., Warrender, S.J., Wright, P.A.** *Synthesis, Crystal Structure, Characterization, and Catalytic Properties of TNU-9*
J. Am. Chem. Soc., **129**, 35, 10870 -10885, 2007

2007-58. **Janáková, S., Salavcová, L., Renaudin, G., Filinchuk, Y., Boyer, D., Boutinaud, Ph.** *Preparation and structural investigations of sol–gel derived Eu^{3+}-doped $CaAl_2O_4$*
J. Phys. & Chem. of Solids, **68**, 5-6, 1147-1151, 2007

2007-59. **Joubert, J.-M., Cerný, R., Emerich, H.** *Mixed site occupancies in μ-Zr-Nb-Al by resonant powder diffraction*
Z. Kristallog., **Suppl.26**, 311-316, 2007

2007-60. **Kalisz, M., Novak, M.A., Pinheiro, C.B., Florencio, A.S., Chapuis, G., Caneschi, A., Vaz, M.G.F.** *Synthesis, Structural and Magnetic Characterization of a New Copper(II)-Nitronyl Nitroxide Radical Complex*
J. Brazilian Chem. Soc., **18**, 5, 916-923, 2007

2007-61. **Kantor, A., Kantor, I., Kurnosov, A., Kuznetsov, A., Dubrovinskaia, N., Krisch, M., Bossak, A., Dmitriev, V. et. al.** *Sound wave velocities of fcc Fe-Ni alloy at high pressure and temperature by mean of inelastic X-ray scattering*
Phys. Earth & Planetary Inter., **164**, 1-2, 83-89, 2007

2007-62. **Karau, F. W., Seyfarth, L., Oeckler, O., Senker, J., Landskron, K., Schnick, W.** *The Stuffed Framework Structure of SrP_2N_4: Challenges to Synthesis and Crystal Structure Determination*
Chem. - A Eur. J., **13**, 24 , 6841 - 6852, 2007

2007-63. **Karen, P., Gustafsson, K., Lindén, J.** *$EuBaFe_2O_{5+\omega}$: Valence mixing and charge ordering are two separate cooperative phenomena*
J. Solid State Chem., **180**, 1, 148-157, 2007

2007-64. **Kimmerle, B., Grunwaldt, J.-D., Baiker, A.** *Gold catalysed selective oxidation of alcohols in supercritical carbon dioxide*
Topics in Catalysis, **44**, 1-2, 285-292, 2007

2007-65. **Knudsen, K.D., Hemmingsen, P.V., Mo, F.** *Temperature-induced structural changes in some random ethylene/1-hexene copolymers*
Polymer , **48**, 11, 3148-3161, 2007

2007-66. **Krauss, G., Gu, Q.F., Katrych, S., Steurer, W.** *In situ study of icosahedral Zn–Mg–Dy and Co-rich decagonal Al–Co–Ni at high pressures and high temperatures*
J. Phys.: Condens. Matter., **19**, 116203-116214, 2007

2007-67. **Krstic, V., Rikken, G.L.J.A., Kaempgen, M., Roth, S., Beukes, J.A.** *Effects of geometry of nano-structured materials on their thermal expansion: tellurium nanocylinders as model sysyem*
Int. J. Materials and Structural Integrity, **1**, 1/2/3, 2007

2007-68. **Krstic, V., Rikken, G.L.J.A., Kaempgen, M., Roth, S., Beukes, J.A.** *Tellurium Nanocylinders under Pressure: Effects of the Geometry of Nanostructures*
Advanced Materials, **19**, 8 , 1101 - 1104, 2007

2007-69. **Kuznetsov, A. Yu. , Dmitriev, V., Volkova, Y., Kurnosov, A., Dubrovinskaia, N., Dubrovinsky, L.** *In-situ combined X-ray diffraction and electrical resistance measurements at high pressures and temperatures in diamond anvil cells*
High Pressure Research, **27**, 2, 213 - 222, 2007

2007-70. **Laufek, F., Pazout, R. , Makovicky, E.** *Crystal structure of owyheeite, $Ag_{1.5}\ Pb_{4.43}\ Sb_{6.07}\ S_{14}$: refinement from powder synchrotron X-ray diffraction*
Eur. J. Mineralogy, **19**, 4, 557-566(10), 2007

2007-71. **Legrand, V., Pillet, S., Weber, H.-P., Souhassou, M. , Létard, J.-F., Guionneau, P., Lecomte, C.** *On the precision and accuracy of structural analysis of light-induced metastable states*
J. Appl. Cryst., **40**, 1076-1088, 2007

2007-72. **Leiros, H.-K. S., Pey, A. L.,Innselset, M., Moe, E., Leiros, I., Steen, I. H., Martinez, A.** *Structure of phenylalanine hydroxylase from Colwellia psychrerythraea 34H; a monomeric cold active enzyme with local flexibility around the active site and high overall stability*
J. Biol. Chem, **282**, 30, 21973-21986, 2007

2007-73. **Maehlen, J.P., Yartys, V.A., Denys, R.V.,Fichtner, M. , Frommen, Ch., Bulychev, B.M., Pattison, P., Emerich, H., Filinchuk, Y.E., Chernyshov, D.** *Thermal decomposition of AlH_3 studied by in situ synchrotron X-ray diffraction and thermal desorption spectroscopy*
J. Alloys & Compounds, **446-447**, 280-289, 2007

2007-74. **Maehlen, J.P., Yartys, V.A., Riabov, A.B., Budziak, A., Figiel, H., Zukrowski, J.** *Synchrotron X-ray diffraction study of $ErMn_2D_2$*
J. Alloys & Compounds, **437**, 1-2, 140-145, 2007

2007-75. **Malcherek, Th.** *A structural phase transition in NaTaOGeO4 and its relation to phase transitions in titanite*
Acta Cryst. B, **63**, 4, 545-550, 2007

2007-76. **Marchal, C., Filinchuk, Y., Imbert, D., Bünzli, J.-C. G., Mazzanti, M.** *Toward the Rational Design of Lanthanide Coordination Polymers: a New Topological Approach*
Inorg. Chem., **46**, 16, 6242 -6244, 2007

2007-77. **Margiolaki, I., Wright, J.P., Fitch, A.N., Fox, G.C. et al.** *Powder diffraction studies on proteins: An overview of data collection approaches*
Z. Kristallog., **Suppl.26**, 1-13, 2007

2007-78. **Martinelli, A., Roberta, M.** *Cimberle Evolution of the structure, microstructure and physical properties of $RuSr_2GdCu_2O_8$ as a function of the thermal treatment*
Z. Kristallogr., **222**, 9, 459-465, 2007

2007-79. **Massüger, L., Baerlocher, Ch., McCusker, L.B., Zwijnenburg, M.A.** *Synthesis and structure analysis of the layer silicate DLM-2*
Microp. & Mesop. Mater., **105**, 1-2, 75-81, 2007

2007-80. **Meisser, N., Schenk, K., Berlepsch, P., Brugger, J., Bonin, M., Criddle, A., Thélin, P., Bussy, F.** *Pizgrischite, $(Cu,Fe)Cu_{14}PbBi_{17}S_{35}$, a new sulfosalt from the Swiss Alps: description, crystal structure and occurrence*
Canadian mineralogist, **45**, 1229-1245, 2007

2007-81. **Mentzen, B.F.** *Crystallographic Determination of the Positions of the Monovalent H, Li, Na, K, Rb, and Tl Cations in Fully Dehydrated MFI Type Zeolites*
J. Phys. Chem. C, **111**,51, 18932 -18941, 2007

2007-82. **Mentzen, B.F., Bergeret, G.** *Crystallographic Determination of the Positions of the Copper Cations in Zeolite MFI*
J. Phys. Chem. C, **111**, 34, 12512 -12516, 2007

2007-83. **Mørkved, E.H., Beukes, J.A., Mo, F.** *o-Quinonoid Heterocycles: Synthesis and Crystal Structure of 2,3-Dicyano-5,7-bismethylthieno[3,4-b]pyrazine*
Molecules, **12**, 1623-1631, 2007

2007-84. **Nilsen, M.H., Antonakou, E., Bouzga, A., Lappas, A., Mathisen, K., Stöcker, M.** *Investigation of the effect of metal sites in Me–Al-MCM-41 (Me = Fe, Cu or Zn) on the catalytic behavior during the pyrolysis of wooden based biomass*
Microp. & Mesop. Mat., **105**, 1-2, 189-203, 2007

2007-85. **Nilsen, M., Nordhei, C., Ramstad, A.L., Nicholson, D., Poliakoff, M., Cabañas, A.** *XAS (XANES and EXAFS) investigations of Nanoparticulate Ferrites synthesized continuously in near critical and supercritical water*
J. Phys. Chem. C, **111**, 17, 6252 - 6262, 2007

2007-86. **Oksanen, E., Ahonen, A.-K., Tuominen, H., Tuominen, V., Lahti, R., Goldman, A., Heikinheimo, P.** *A complete structural description of the catalytic cycle of Yeast Pyrophosphatase*
Biochemistry, **46**, 5, 1228 -1239, 2007

2007-87. **Oliéric, V., Ennifar, E., Meents, A., Fleurant, M., Besnard, C., Pattison, P., Schiltz, M. et al.** *Using X-ray absorption spectra to monitor specific radiation damage to anomalously scattering atoms in macromolecular crystallography*
Acta Cryst., D**63**, 759-768, 2007

2007-88. **Opalka, S.M., Lvvik, O.M., Brinks, H.W., Saxe, P.W., Hauback, B.C.** *Integrated experimental-theoretical investigation of the Na-Li-Al-H system*
Inorg. Chem., **46,** 4, 1401 - 1409, 2007

2007-89. **Palin, L., Brunelli, M., Pattison, Ph., Fitch, A.N.** *A structural investigation of the four phases of 7-oxabicyclo [2.2.1] heptane*
Z. Kristallographie, **222**, 9, 487-491, 2007

2007-90. **Pastore, H., De Oliveira, E., Superti, G., Gatti, G., Marchese, L.** *Reaction at interfaces: the silicoaluminophosphate molecular sieve CAL-1*
J. Phys. Chem. C, **111**, 3116-3129, 2007

2007-91. **Pouchon, M.A., Chen, J.C., Degueldre, C., Froideval, A., Emerich, H., Van Beek, W.** *EXAFS Study on Irradiated ODS Ferritic Steel PRICM 6*
Materials Science Forum, **561**, 1761-1764, 2007

2007-92. **Rabe, S., Nachtegaal, M., Vogel, F.** *Catalytic partial oxidation of methane to synthesis gas over a ruthenium catalyst: the role of the oxidation state*
Phys. Chem. Chem. Phys., **9**, 1461 - 1468, 2007

2007-93. **Renaudin, G., Mapemba, E., El-Ghozzi, M., Dubois, M., Avignant, D., Cerný, R.** *Combined high resolution powder and single-crystal diffraction to determine the structure of* $Li_{1+x}Ce^{III}_{x}Ce^{IV}_{6-x}F_{25}$
Z. Kristallog., **Suppl.26**, 455-460, 2007

2007-94. **Rieder, M., Crelling, J.C., Šustai,O., Drábek, M., Weiss, Z., Klementová, M.** *Arsenic in iron disulfides in a brown coal from the North Bohemian Basin, Czech Republic*
Int. J. Coal Geology , **71**, 2-3, 115-121, 2007

2007-95. **Riise, E.K., Lorentzen, M.S., Helland, R., Smalås, A.O., Leiros, H.-K.S., Willassen, N.P.** *The first structure of a cold-active catalase from Vibrio salmonicida at 1.96 Å reveals structural aspects of cold adaptation*
Acta Cryst., D**63**, 135-148, 2007

2007-96. **Riktor, M. D., Sørby, M. H., Chopek, K., Fichtner, M., Buchter, F., Züttel, A., Hauback, B. C.** *In situ synchrotron diffraction studies of phase transitions and thermal decomposition of* $Mg(BH_4)_2$ *and* $Ca(BH_4)_2$
J. Mater. Chem., **17,** 4939 - 4942, 2007

2007-97. **Sanishvili, R., Besnard, C., Camus, F., Fleurant, M., Pattison, P., Bricogne, G., Schiltz, M.** *Polarization-dependence of anomalous scattering in brominated DNA and RNA molecules, and importance of crystal orientation in single- and multiple-wavelength anomalous diffraction phasing*
J. Appl. Cryst., **40**, 552-558, 2007

2007-98. **Schaub, P., Weber, T., Steurer, W.** *Exploring local disorder in single crystals by means of the three-dimensional pair distribution function*
Philosophical Mag., **87**, 2781 - 2787 , 2007

2007-99. **Serre, Ch., Bourrelly, S., Vimont, A., Ramsahye, N., Maurin, G., Llewellyn, Ph., Daturi, M., Filinchuk, Y. et al.** *An explanation for the very large breathing effect of a metal-organic framework during* CO_2 *absorption*
Adv. Materials, **19**, 17, 2246-2251, 2007

2007-100. **Serre, C., Mellot-Draznieks, C., Surblé, S., Audebrand, N., Filinchuk, Y., Férey, G.** *Role of solvent-host interactions that lead to very large swelling of hybrid frameworks* Science, **315**, 5820, 1828 - 1831, 2007

2007-101. **Siegrist, T., Besnard, C., Haas, S., Schiltz, M., Pattison, P., Chernyshov, D., Batlogg, B., Kloc, C.** *A Polymorph Lost and Found: The High-Temperature Crystal Structure of Pentacene*
Adv. Materials, **19,** 16, 2078-2082, 2007

2007-102. **Sikorski, P., Mo, F., Skjåk-Bræk, G., Stokke, B.T.** *Evidence for Egg-Box-Compatible Interactions in Calcium-Alginate Gels from Fiber X-ray Diffraction*
Biomacromolecules, **8,** 7, 2098 -2103, 2007

2007-103. **Sørby, M.H., Nakamura, Y., Brinks, H.W., Ichikawa, T., Hino, S., Fujii, S., Hauback, B.C.** *The crystal structure of* $LiND_2$ *and* $Mg(ND_2)_2$
J. Alloys & Compounds, **428**, 1-2 , 297-301, 2007

2007-104. **Van der Maelen, J. F., Gutiérrez-Puebla, E., Monge, Á., García-Granda, S., Resa, I., Carmona, E., Fernández-Díaz, M. T., McIntyre, G. J., Pattison, P., Weber, H.-P.** *Experimental and theoretical characterization of the Zn-Zn bond in* $[Zn_2(\cdot 2\text{-}C_5Me_5)_2]$
Acta Cryst., B**63**, 862-868, 2007

2007-105. **Van Mechelen, J. B., Peschar, R., Schenk, H.** *The crystal structures of the ß1 and ß2 polymorphs of mono-unsaturated triacylglycerols and cocoa butter determined from high resolution powder diffraction data*
Z. Kristallogr. **Suppl. 26**, 599-604, 2007

2007-106. **Vespa, M., Dähn, R., Grolimund, D., Wieland, E., Scheidegger, A. M.** *Co speciation in hardened cement paste: a macro- and micro-spectroscopic investigation*
Environ. Sci. Technol., **41**, 6, 1902 -1908, 2007

2007-107. **Vespa, M., Wieland, E., Dähn, R., Grolimund, D., Scheidegger, A.M.** *Determination of the elemental distribution and chemical speciation in highly heterogeneous cementitious materials using synchrotron-based micro-spectroscopic techniques*
Cement & Concrete Res., **37**, 11, 1473-1482 , 2007

2007-108. **Vrålstad, T., Øye, G., Stöcker, M., Sjöblom, J.** *Synthesis of comparable Co-MCM-48 and Co-MCM-41 materials containing high cobalt contents*
Microp. & Mesop. Mater., **104**, 1-3, 10-17, 2007

2007-109. **Weiher N., Beesley A.M., Tsapatsaris N., Louis C., Delannoy L., Van Bokhoven J.A., Schroeder S.L.M.** I*n situ XAS studies on the structure of the active site of supported gold catalysts*
AIP Conference Proceedings **882**, 600-602, 2007 In: "X-RAY ABSORPTION FINE STRUCTURE - XAFS13: 13th International Conference" - Stanford, California,USA

2007-110. **Yartys, V.A., Denys, R.V., Maehlen, J.P., Frommen, Ch., Fichtner, M., Bulychev, B.M., Emerich, H.** *Double-Bridge Bonding of Aluminium and Hydrogen in the Crystal Structure of gamma-AlH_3*
Inorg. Chem., **46**, 4, 1051 - 1055, 2007

2007-111. **Yvon, K., Rapin, J.-Ph., Penin, N., Ma, Zhu, Chou, M.Y.** *LaMg2PdH7, a new complex metal hydride containing tetrahedral $[PdH_4]^{4-}$ anions*
J. Alloys & Compounds, **446-447**, 34-38, 2007

2007-112. **Zanardi, S., Cruciani, G., Carluccio, L.C., Bellussi, G., Perego, C., Millini, R.** *Synthesis and framework topology of the new disordered ERS-10 zeolite*
J. Porous Mater.,**14**, 3 , 315-323, 2007

2008

2008-1. **Albertsen, J., Grong, Ø., Walmsley, J., Mathiesen, R., Van Beek, W.** *A Model for High-Temperature Pitting Corrosion in Nickel-Based Alloys Involving Internal Precipitation of Carbides, Oxides, and Graphite*
Metallur. & Mater. Transac. A, **39A**, 6, 1258-1276, 2008

2008-2. **Arakcheeva, A., Pattison, P., Chapuis, G., Rossell, M., Filaretov, A. et al.** *$KSm(MoO_4)_2$, an incommensurately modulated and partially disordered scheelite-like structur*e
Acta Cryst., B**64**, 160-171, 2008

2008-3. **Baerlocher, Ch., Xie, D., McCusker, L., Hwang, S.-J., Chan, I., Ong, K. et al.** *Zones Ordered silicon vacancies in the framework structure of the zeolite catalyst SSZ-74*
Nature Materials, in press, 2008

2008-4. **Blanchard, D., Lem, A., Øvergaard, S., Brinks, H., Hauback, B.** *$LiAlD_4$ with VCl_3 additives: influence of ball-milling energies*
J. Alloys & Compounds, **458**, 1-2, 467-473, 2008

2008-5. **Boldyreva, E., Sowa, H., Ahsbahs, H., Goryainov, S., Chernyshev, D., Dmitriev, V. et al.** *Pressure-induced phase transitions in organic molecular crystals: a combination of x-ray single-crystal and powder diffraction, raman and IR-spectroscopy*
J. Phys.: Conf. Ser. **121**, 022023 , 2008

2008-6. **Borodi, G., Bratu, I., Dragan, F., Peschar, R., Helmholdt, R.B., Hernanz, A.** *Spectroscopic investigations and crystal structure from synchrotron powder data of the inclusion complex of ß-cyclodextrin with atenolol Spectrochim*
Acta Part A: Mol. Biomol. Spectrosc., **70**, 1041-1048, 2008

2008-7. **Bosak, A., Chernyshov, D.** *Model-free reconstruction of lattice dynamics from thermal diffuse scattering*
Acta Cryst., A **64**, 598-600, 2008

2008-8. **Brinks, H., Fossdal, A., Hauback, B.** *Adjustment of the Stability of Complex Hydrides by Anion Substitution*
J. Phys. Chem., C **112**, 14, 5658 -5661, 2008

2008-9. **Brodski, V., Peschar, R., Schenk, H., Brinkmann, A., Van Eck, E., Kentgens, A.** *Structure of Tetrakis(melaminium) Bis(dihydrogenphosphate) Monohydrogenphosphate Trihydrate from X-ray Powder Diffraction and Solid-State NMR Spectroscopy*
J. Phys. Chem. C, **112**, 32, 12515–12523, 2008

2008-10. **Buchter, F., Lodziana, Z., Remhof, A., Friedrichs, O., Borgschulte, A. et al**. *Structure of $Ca(BD_4)_2$ beta-Phase from Combined Neutron and Synchrotron X-ray Powder Diffraction Data and Density Functional Calculations*
J. Phys. Chem. B, **112**, 27, 8042–8048, 2008

2008-11. **Casapu, M., Grunwaldt, J.-D., Maciejewski, M., Krumeich, F., Baiker, A. et al.** *Comparative study of structural properties and NO_x storage-reduction behavior of $Pt/Ba/CeO_2$ and $Pt/Ba/Al_2O_3$*
Appl. Catalysis B: Environmental, **78**, 3-4, 288-300, 2008

2008-12. **Chen, X.-Y., Marchal, C., Filinchuk, Y., Imbert, D., Mazzanti, M.** *A flexible tripodal ligand linking octametallic terbium rings into luminescent polymeric chains*
Chem. Commun., 3378 - 3380, 2008

2008-13. **Chernyshov, D., Dmitriev, V., Pomjakushina, E., Conder, K., Stingaciu, M. et al.** *Superstructure formation at the metal-insulator transition in $RBaCo_2O_{5.5}$ (R=Nd,Tb) as seen from reciprocal space mapping*
Phys. Rev., B **78**, 024105-024112, 2008

2008-14. **Crosignani, S., Page, P., Missotten, M., Colovray, V., Cleva, Ch. et al.** *Discovery of a New Class of Potent, Selective, and Orally Bioavailable CRTH2 (DP2) Receptor Antagonists for the Treatment of Allergic Inflammatory Diseases#*
J. Med. Chem., **51**, 7, 2227–2243, 2008

2008-15. **Denys, R.V., Riabov, A.B., Yartys, V.A., Sato, M., Delaplane, R.G**. *Mg substitution effect on the hydrogenation behaviour, thermodynamic and structural properties of the La_2Ni_7–$H(D)_2$ system*
J. Solid State Chem., **181**, 4, 812-821, 2008

2008-16. **Dietzel, P. D. C., Johnsen, R. E., Blom, R., Fjellvåg, H.** *Structural Changes and Coordinatively Unsaturated Metal Atoms on Dehydration of Honeycomb Analogous Microporous Metal-Organic Frameworks*
Chem. - A Eur. J., **14**, 8, 2389 - 2397, 2008

2008-17. **Dmitriev, V., Filinchuk, Y., Chernyshov, D., Talyzin, A.V., Dzwilevski, A. et al.** *Pressure-temperature phase diagram of $LiBH_4$: Synchrotron x-ray diffraction experiments and theoretical analysis*
Phys. Rev. B **77**, 174112-174123, 2008

2008-18. **Dondi, M., Matteucci, F., Baldi, D., Barzanti, A., Cruciani, G., Zama, I., Bianchi, C.L.** *Gray–blue Al_2O_3–MoO_x ceramic pigments: Crystal structure, colouring mechanism and performance*
Dyes & Pigments , **76**, 1, 179-186, 2008

2008-19. **Dubarry, M., Gaubicher, J., Guyomard, D., Wallez, G., Quarton, M., Baehtz, C**. *Uncommon potential hysteresis in the $Li/Li_{2x}VO(H_{2-x}PO_4)_2$ ($0 \leq x \leq 2$) system*
Electrochimica Acta, **53**, 13, 4564-4572, 2008

2008-20. **Filinchuk, Y., Chernyshov, D., Cerny, R.** *Lightest Borohydride Probed by Synchrotron X-ray Diffraction: Experiment Calls for a New Theoretical Revision*
J. Phys. Chem. C, **112**, 28, 10579–10584, 2008

2008-21. **Filinchuk, Y., Chernyshov, D., Nevidomskyy, A., Dmitriev, V.** *High-Pressure Polymorphism as a Step towards Destabilization of $LiBH_4$*
Angew. Chem. Int. Ed., **47**, 3, 529 - 532, 2008

2008-22. **Filinchuk, Y., Hagemann, H.** *Structure and Properties of $NaBH_4 \cdot 2H_2O$ and $NaBH_4$*
Eur. J. Inorg. Chem., **20**, 3127 - 3133, 2008

2008-23. **Filinchuk, Y., Lisnyak, V.V., Stratiichuk, D.A., Stus, N.V.** *Crystal structure of $Nax(MoO)_5(P_2O_7)_4$ studied by synchrotron X-ray diffraction*
J. Alloys & Compounds, **463**, 1-2, 124-128, 2008

2008-24. **Fois, E., Gamba, A., Medici, C., Tabacchi, G., Quartieri, S., Mazzucato, E., Arletti, R., Vezzalini, G., Dmitriev, V.** *High pressure deformation mechanism of Li-ABW: Synchrotron XRPD study and ab initio molecular dynamics simulations*
Microp. & Mesop. Mat., **115**, 267-280, 2008

2008-25. **Galli, E., Gualtieri, A.F.** *Direnzoite, $[NaK_6MgCa_2(Al_{13}Si_{47}O_{120}) \cdot 36H_2O]$, a new zeolite from Massif Central (France): Description and crystal structure*
Am. Mineralogist, **93**, 95-102, 2008

2008-26. **Gao, T., Glerup, M., Krumeich, F., Nesper, R., Fjellvåg, H., Norby, P.** *Microstructures and Spectroscopic Properties of Cryptomelane-type Manganese Dioxide Nanofibers*
J. Phys. Chem. C, **112,** 34, 13134–13140, 2008

2008-27. **Grove, H., Brinks, H., Heyn, R., Wu, F.-J., Opalka, S. et al.** *The structure of $LiMg(AlD_4)_3$*
J. Alloys & Compounds, **455**, 1-2, 249-254, 2008

2008-28. **Grove, H., Brinks, H., Løvvik, O., Heyn, R., Hauback, B.** *The crystal structure of $LiMgAlD_6$ from combined neutron and synchrotron X-ray powder diffraction*
J. Alloys & Compounds, **460**, 1-2, 64-68, 2008

2008-29. **Gualtieri, A., Ferrari, S., Leoni, M., Grathoff, G., Hugo, R. et al.** *Structural characterization of the clay mineral illite-1M*
Applied Crystal., **41**, 2, 402-415, 2008

2008-30. **Hagemann, H., Longhini, M., Kaminski, J., Wesolowski, T. et al.** *$LiSc(BH_4)_4$: A Novel Salt of Li+ and Discrete $Sc(BH_4)_4$ - Complex Anions*
J. Phys. Chem. A, **112**, 33, 7551–7555, 2008

2008-31. **Hamacek, J., Bernardinelli, G., Filinchuk, Y.** *Tetrahedral Assembly with Lanthanides: Toward Discrete Polynuclear Complexes*
Eur. J. Inorg. Chem., **22**, 3419 - 3422, 2008

2008-32. **Helland, R., Fjellbirkeland, A., Karlsen, O., Ve, Th., Lillehaug, J., Jensen, H.** *An Oxidized Tryptophan Facilitates Copper Binding in Methylococcus capsulatus-secreted Protein MopE**
J. Biol. Chem., **283**, 20, 13897-13904, 2008

2008-33. **Hersleth, H.-P., Hsiao, Y.-W., Ryde, U., Gorbitz, C.H., Andersson, K.** *The crystal structure of peroxymyoglobin generated through cryoradiolytic reduction of myoglobin compound III during data collection*
Biochem. J., **412**, 257–264, 2008

2008-34. **Hersleth, H.-P., Varnier, A., Harbitz, E., Røhr, Å., Schmidt, P., Sørlie, M. et al.** *Reactive complexes in myoglobin and nitric oxide synthase Inorganica*
Chimica Acta, **361**, 4, 831-843, 2008

2008-35. **Horcajada, P., Serre, Ch., Maurin, G., Ramsahye, N., Balas, F., Vallet-Regí, M. et al.** *Flexible Porous Metal-Organic Frameworks for a Controlled Drug Delivery*
J. Am. Chem. Soc., **130**, 21, 6774–6780, 2008

2008-36. **Huber, F., Venvik, H., Rønning, M. Walmsley, J., Holmen, A.** *Preparation and characterization of nanocrystalline, high-surface area CuCeZr mixed oxide catalysts from homogeneous co-precipitation* Chem. Eng. J., **137**, 3, 686-702, 2008

2008-37. **Hušák, M., Jegorov, A., Brus, J., Van Beek, W., Pattison, P. et al.** *Metergoline II: structure solution from powder diffraction data with preferred orientation and from microcrystal*
Struct. Chem., **19**, 3, 512-525, 2008

2008-38. **Kiebach, R., Pienack, N., Bensch, W., Grunwaldt, J.-D. et al.** *Hydrothermal Formation of W/Mo-Oxides: A Multidisciplinary Study of Growth and Shape*
Chem. Mater., **20**, 9, 3022–3033, 2008

2008-39. **Kowalchuk, C., Paz, F., Ananias, D., Pattison, Ph., Carlos, L., Rocha, J.** *Photoluminescent Microporous Lanthanide Silicate AV-21 Frameworks*
Chem. - A Eur. J., in press, 2008

2008-40. **Lambert, J., Wallez, G., Quarton, M., Le Mercier, T., Van Beek, W.** *Searching for the dopant ion in Eu^{2+}-activated $BaMgAl_{10}O_{17}$ phosphor with synchrotron diffraction*
J. Luminescence, **128**, 366-372, 2008

2008-41. **Llewellyn, Ph., Maurin, G., Devic, Th., Loera-Serna, S., Rosenbach, N. et al.** *Prediction of the Conditions for Breathing of Metal Organic Framework Materials Using a Combination of X-ray Powder Diffraction, Microcalorimetry, and Molecular Simulation*
J. Am. Chem. Soc., in press, 2008

2008-42. **Mantion, A., Massüger, L., Rabu, P., Palivan, C., McCusker, L., Taubert, A.** *Metal-Peptide Frameworks (MPFs): "Bioinspired" Metal Organic Frameworks*
J. Am. Chem. Soc., **130**, 8, 2517-2526, 2008

2008-43. **Millange, F., Serre, Ch., Guillou, N., Férey, G., Walton, R.I.** *Structural Effects of Solvents on the Breathing of Metal-Organic Frameworks: An In Situ Diffraction Study*
Angew. Chem. Int. Ed., **47**, 22 , 4100 - 4105, 2008

2008-44. **Nakamura, Y., Hino, S., Ichikawa, T., Fujii, H., Brinks, H., Hauback, B.** *Dehydrogenation reaction of Li-Mg-N-H systems studied by in situ synchrotron powder X-ray diffraction and powder neutron diffraction*
J. Alloys & Compounds, **457**, 1-2, 362-367, 2008

2008-45. **Nielsen, R., Kongshaug, K., Fjellvåg, H.** *Delamination, synthesis, crystal structure and thermal properties of the layered metal-organic compound $Zn(C_{12}H_{14}O_4)$*

J. Mater. Chem., 2008, **18**, 1002 - 1007

2008-46. **Nordhei, C., Ramstad, A., Nicholson, D.** *Nanophase cobalt, nickel and zinc ferrites: synchrotron XAS study on the crystallite size dependence of metal distribution*
Phys. Chem. Chem. Phys., **10**, 1053-1066, 2008

2008-47. **Ori, S., Quartieri, S., Vezzalini, G., Dmitriev, V.** *Pressure-induced structural deformation and elastic behavior of wairakite*
Am. Mineralogist, **93**, 53-62, 2008

2008-48. **Palacios, L., Cabeza, A., Bruque, S., García-Granda, S., Aranda, M.** *Structure and Electrons in Mayenite*
Electrides Inorg. Chem., **47**, 7, 2661–2667, 2008

2008-49. **Pillet, S., Legrand, V., Weber, H.-P., Souhassou, M., Létard, J.-F., Guionneau, Ph., Lecomte, C.** *Out-of-equilibrium charge density distribution of spin crossover complexes from steady-state photocrystallographic measurements: experimental methodology and results*
Z. Kristallogr., **223**, 4-5, 235-249, 2008

2008-50. **Pitt, M., Vullum, P., Sørby, M., Sulicc, M., Jensen, C. et al.** *Structural properties of the nanoscopic Al_{85} Ti_{15} solid solution observed in the hydrogen-cycled $NaAlH_4$ + $0.1TiCl_3$ system*
Acta Materialia, in press, 2008

2008-51. **Renaudin, G., Laquerrière, P., Filinchuk, Y., Jallot, E., Nedelec, J.M**. *Structural characterization of sol–gel derived Sr-substituted calcium phosphates with anti-osteoporotic and anti-inflammatory properties*
J. Mater. Chem., **18**, 3593 - 3600, 2008

2008-52. **Remmerie, B., Vandenbroucke, K., De Smet, L., Carpentier, W. et al.** *Expression, purification, crystallization and structure determination of two glutathione S-transferase-like proteins from Shewanella oneidensis*
Acta Cryst., F **64**, 6, 548-553, 2008

2008-53. **Rouquette, J., Kantor, I., McCammon, C., Dmitriev, V., Dubrovinsky, L.** *High-Pressure Studies of $(Mg_{0.9}Fe_{0.1})2SiO_4$Olivine Using Raman Spectroscopy, X-ray Diffraction, and Mössbauer Spectroscopy*
Inorg. Chem., **47**, 7, 2661–2667, 2008

2008-54. **Sartori, S., Opalka, S., Løvvik, O., Guzik, M., Tang, X., Hauback, B.** *Experimental studies of alpha-AlD_3 and alpha'-AlD_3 versus first-principles modelling of the alane isomorphs*
J. Mater. Chem., **18**, 2361 - 2370, 2008

2008-55. **Schiltz, M., Bricogne, G.** *Exploiting the anisotropy of anomalous scattering boosts the phasing power of SAD and MAD experiments*
Acta Cryst., D **64**, 7, 711-729, 2008

2008-56. **Sereda, O., Neels, A., Stoeckli, F., Stoeckli-Evans, H., Filinchuk, Y.** *Sponge-like Reversible Transformation of a Bimetallic Cyanometallate Polymer*
Cryst. Growth Des., **8**, 7, 2307–2311, 2008

2008-57. **Serre, C., Surblé, S., Mellot-Draznieks, C., Filinchuk, Y., Férey, G.** *Evidence of flexibility in the nanoporous iron(III) carboxylate MIL-89*
Dalton Trans., in press, 2008

2008-58. **Talysin, A., Solozhenko, V., Kurakevych, O., Szabo, T., Dekany, I., Kurnosov, A., Dmitriev, V.** *Pressure-Induced Lattice Expansion of Graphite Oxide in the Presence of Water*
Angewandte Chem. Int. Ed, **47**, in press, 2008

2008-59. **Tokaychuk, Y., Filinchuk, Y., Sheptyakov, D., Yvon, K.** *Hydrogen Absorption in Transition Metal Silicides: La3Pd5Si-Hydrogen System*
Inorg. Chem., in press, 2008

2008-60. **Tonti, D., Mohammed, M., Al-Salman, A., Pattison, Ph., Chergui, M**. *Multimodal Distribution of Quantum Confinement in Ripened CdSe Nanocrystals*
Chem. Mater., **20**, 4, 1331–1339, 2008

2008-61. **Van Mechelen, J., Peschar, R., Schenk, H.** *Structures of mono-unsaturated triacylglycerols. III. The beta-2 polymorphs of trans-mono-unsaturated triacylglycerols and related fully saturated triacylglycerols*
Acta Cryst., B **64**, 240-248, 2008

2008-62. **Van Mechelen, J., Peschar, R., Schenk, H.** *Structures of mono-unsaturated triacylglycerols. IV. The highest melting beta'-2 polymorphs of trans-mono-unsaturated triacylglycerols and related saturated TAGs and their polymorphic stability*
Acta Cryst., B **64**, 249-259, 2008

2008-63. **Veen, S., Roy, S., Filinchuk, Y., Chernyshov, D., Petukhov, A. et al.** *Extended Structure Design with Simple Molybdenum Oxide Building Blocks and Urea As a Directing Agent*
Inorg. Chem., **47**, 15, 6863–6866, 2008

2008-64. **Vorobiev, A., Chernyshov, D., Godeev, G., Orlova, D.** *Non-destructive characterization of ferrofluids by wide-angle synchrotron light diffraction: crystalline structure and size distribution of colloidal nanoparticles*
Acta Cryst. C, in press, 2008

2008-65. **Winne, J., De Clercq, P., Milanesio, M., Pattison, Ph., Viterbo, D**. *Nonenzymic polycyclisation of analogues of oxidosqualene with a preformed C-ring*
Org. Biomol. Chem., 2008, **6**, 1918 - 1925

2008-66. **Wieland, E., Tits, J., Kunz, D., Dähn, R.** *Strontium Uptake by Cementitious*
Materials Environ. Sci. Technol., **42**, 2, 403–409, 2008

2008-67. **Wright, J., Besnard, C., Margiolaki, I., Basso, S., Camus, F., Fitch, F. et al.** *Molecular envelopes derived from protein powder diffraction data*
J.Appl.Cryst., **41**, 329-339, 2008

2008-68. **Yu, Zh., Chen, D., Rønning, M., Vrålstad, T., Ochoa-Fernández, E., Holmen, A.** *Large-scale synthesis of carbon nanofibers on Ni–Fe–Al hydrotalcite derived catalysts I. Preparation and characterization of the Ni–Fe–Al hydrotalcites and their derived catalysts*
Appl. Catalysis A: General, **338,** 1-2, 136-146, 2008

2008-69. **Yu, Zh., Chen, D., Rønning, M., Vrålstad, T., Ochoa-Fernández, E., Holmen, A.** *Large-scale synthesis of carbon nanofibers on Ni-Fe-Al hydrotalcite derived catalysts II: Effect of Ni/Fe composition on CNF synthesis from ethylene and carbon monoxide*
Appl. Catalysis A: General, **338**, 1-2, 147-158, 2008

2008-70. **Zaharko, O., Mesot, J., Salguero, L., Valentí R., Zbiri, M., Johnson, M., Filinchuk, Y. et al.** *Tetrahedra system $Cu_4OCl_6daca_4$: High-temperature manifold of molecular configurations governing low-temperature properties*
Phys. Rev. B **77**, 224408-224419, 2008

APPENDIX B

PhD Theses: 2005-2007
(based in part on data from SNBL)

Albertsen J.Z.
NTNU Trondheim (Norway), 2007
Experimental and theoretical investigations of metal dusting corrosion in plant exposed nickel-based alloys.

Brodski V.
University of Amsterdam (the Netherlands), 2005
Structure determination of melamine phosphates from powder diffraction data with a new direct-spase approach.

Bus E.
ETH Zürich (Switzerland), 2007
Characterization of supported gold, platinum-gold, and platinum catalysts for hydrogenation reactions.

Fagot S.
Universite Paris 7-Denis Diderot (France), 2005
Etude structurale de $BaVS_3$ un conducteur quasi-1D à électrons fortement corrélés.

Gramm F.
ETH Zürich (Switzerland), 2007
Kombination von Transmissionselektronenmikroskopie und Pulverbeugungsdaten zur Losung von komplexen Zeolithstrukturen.

Haas S.
ETH Zürich (Switzerland), 2006
Crystal structure analysis and trap spectroscopy in organic semiconducting crystals.

Hersleth, H.-P.
University of Oslo (Norway), 2007
Strutural studies of hydrogen peroxide derived myoglobin complexes.

Larsen A.N.
University of Tromso (Norway), 2005
Identification, characterization and structural determination of proteinase K like enzyme from a psychrotrophic *Serratia* sp.

Marshall A.
NTNU Trondheim (Norway), 2005
Electrocatalysts for the oxygen evolution electrode in water electrolysers using proton exchange membranes: synthesis and characterisation.

Mathisen K.
NTNU Trondheim (Norway), 2005
X-ray absorption spectroscopic studies on active metal sites in zeotypes during the selective catalytic reduction of NO_x with propene in an oxygen-rich atmosphere.

Ramin M.O.
ETH Zürich (Switzerland), 2006
Heterogeneously catalyzed synthesis of propylene carbonate using carbon dioxide.

Rohr M.
ETH Zürich (Switzerland), 2005
Ruthenium-catalyzed formylations using carbon dioxide as carbon source and solvent.

Vespa M.
ETH Zürich (Switzerland), 2006
Influence of the inherent heterogeneity of cement on the uptake mechanisms of Ni and Co: a micro-spectroscopic study.

Vraalstad T.
NTNU Trondheim (Norway), 2005
Synthesis and characterisation of cobalt-containing mesoporous model catalysts.

Zhixin Yu.
NTNU Trondheim (Norway), 2005
Synthesis of carbon nanofibers and carbon nanotubes.

APPENDIX C

List of Abbreviations

ASNG	Assosiation Swiss-Norwegian Grenoble (Grenoble, France)
BL	Beam Line
DUBBLE	Dutch-Belgium Beam Lines at ESRF (Grenoble, France)
EMPA	Swiss Federal Laboratories for Materials Testing and Research (Dübendorf, Switzerland)
EPFL	Ecole Polytechnique Fédérale de Lausanne (Switzerland)
ETHZ	Eidgenössische Technische Hochschule Zürich (Switzerland)
EXAFS	Extended X-ray Absorption Fine Structure
HRPD	High-Resolution Powder Diffraction
IFE	Institute for Energy Technology (Kjeller, Norway)
NSR	Research Council of Norway
NTNU	Norwegian University of Science and Technology (Trondheim, Norway)
PSI	Paul Scherrer Institute (Villigen, Switzerland)
SER	State Secretariat for Education and Research (Bern, Switzerland)
SLS	Swiss Light Source (Villigen, Switzerland)
SN	Swiss-Norwegian
SNBL	Swiss-Norwegian Beam Lines at ESRF
SNX	Swiss-Norwegian Foundation for Research with X-rays
SR	Synchrotron Radiation
UiB	University of Bergen (Norway)
UiO	University of Oslo (Norway)
UiS	University of Stavanger (Norway)
UiT	University of Tromsø (Norway)
UniB	University of Bern (Switzerland)
UniGE	University of Geneva (Switzerland)
UniNE	University of Neuchatel (Switzerland)
XAFS	X-ray Absorption Fine Structure